

Deliverable 2.2

Assessment of applicable renewable energy generation technologies on NRA land and assets



Supporting the implementation by NRAs of renewable energy technologies in the road infrastructure



Deliverable 2.2

Assessment of applicable renewable energy generation technologies on NRA land and assets

Deliverable no.:	2.2
Work Package no.:	2
Status	Submitted
Version:	01
Author:	SINTEF Energi AS
Date:	24.06.2022
Dissemination level:	Public

Disclaimer: ENROAD has received funding from the CEDR Transnational Road Research Program – Call 2019. This document reflects only the author’s views. The Conference of European Directors of Roads (CEDR) is not responsible for any use that may be made of the information contained therein.

Deliverable 2.2

Assessment of applicable renewable energy generation technologies on NRA land and assets



List of AUTHORS		
Rene A. Barrera-Cardenas	SINTEF Energy AS	Rene.barrera-cardenas@sintef.no
Jon Are Suul	SINTEF Energy AS	Jon.A.Suul@sintef.no

List of REVIEWERS		
Bendik Nybakk Torsæter	SINTEF Energy AS	Bendik.torsater@sintef.no
Hrefna Run Vignisdottir	SINTEF AS	Hrefna.vignisdottir@sintef.no
Pablo Pascual Muñoz	Universidad de Cantabria	pablo.pascualm@unican.es

TABLE OF CONTENTS

1	Introduction	9
1.1	<i>Objective and scope</i>	9
1.1	<i>Methodology</i>	10
1.2	<i>RET Database</i>	11
2	Distributed Energy Generation Systems	14
2.1	<i>Integration of DEGS to the Electrical power system.</i>	14
2.1.1	Integration to the local road power system	17
2.2	<i>Selected DEGS alternatives for Locations in NRA land/assets</i>	19
2.2.1	Installations in open roadSide areas	19
2.2.2	Along the road or integrated with other infrastructure	21
3	Studied Renewable Energy Generation Technologies	24
3.1	<i>Overview of the Considered Renewable Energy Technologies</i>	24
3.1.1	Wind Turbines	26
3.1.1.1	Horizontal Axis Wind Turbines (HAWT)	26
3.1.1.2	Savonius - VAWT	27
3.1.1.3	Darrious - VAWT	28
3.1.2	Photovoltaic modules	30
3.1.2.1	Silicon Monocrystalline	30
3.1.2.2	Silicon Polycrystalline	31
3.2	<i>Characterization of Renewable Energy Sources</i>	32
3.2.1	Wind source characterization	32
3.2.2	Solar Radiation charaterization	37
3.3	<i>Modelling and parametrization of wind turbines</i>	44
3.3.1	Power curve model	44
3.3.2	Total Capital Cost	50
3.3.3	Expected Lifetime and Warranty period	51
3.4	<i>Modelling and parametrization of Photovoltaic modules</i>	51
3.4.1	PV Model and characteristic curve	51
3.4.2	Total Capital Cost	59
3.4.3	Expected Lifetime and Warranty period	59
3.5	<i>Modelling of Other components in DEGS</i>	60

Deliverable 2.2

Assessment of applicable renewable energy generation technologies on
NRA land and assets



3.5.1	DC/AC Converter	60
3.5.2	Power Transformer	63
3.6	<i>Wind Farms Modelling and Evaluation</i>	65
3.7	<i>Solar PV Farms Modelling and Evaluation</i>	69
4	RET Trends and Performance comparison	75
4.1	<i>Wind Turbines Meta-parametrization</i>	75
4.2	<i>PV Module Meta-Parametrization</i>	91
4.3	<i>Case study: Roadside location</i>	97
4.3.1	Small scale wind	98
4.3.2	Solar PV farms	101
5	Conclusion	104
6	List of references	106
Annex 1: Study of energy storage technologies (BESS)		109

Deliverable 2.2

Assessment of applicable renewable energy generation technologies on NRA land and assets



LIST OF TABLES

Table 1 Summary of the initial reviewed RETs within project ENROAD, Deliverable 2.1: Report of main renewable energy technologies (RETs) for the road infrastructure (University of Cantabria, 2021)	25
Table 2 Typical values of surface roughness length for various types of terrain.	34
Table 3 Example of PV Module typical datasheet information for Monocrystalline modules series NeON R from LG manufacturer	54
Table 4 VSC Power Loss Model parameters	61
Table 5 Small Scale Wind Turbine Metaparameters.....	79
Table 6 Large Scale Wind Turbine Metaparameters.....	85
Table 7 Silicon PV Module Crystalline Metaparameters.....	95
Table 8 Terrain characteristics for roadside case study.....	98

LIST OF FIGURES

Figure 1-1 Evaluation of Renewable Energy Generation Technologies	11
Figure 2-1 Generic power system configuration where the grid interconnection of a wind farm associated with the road infrastructure is independent from the AC-distribution system along the road	16
Figure 2-2 Generic power system configuration with small-scale DEGS consisting of few wind turbines or medium size PV installations connected to the road-side AC-distribution system	18
Figure 2-3 Generic power system configuration including local power hubs with internal DC distribution for integrating small-scale generation and road-side DC-loads with an EV charging station	18
Figure 2-4 Assumed layout of a wind farm on limited land area associated with a road	20
Figure 2-5 Assumed layout of a PV farm on a limited land area associated with a road	21
Figure 2-6 Overview of general layout for a road with noise barriers and light poles that can be utilized for mounting small scale DEGS installations	22
Figure 3-1 Basic comparative illustration of the considered wind turbine technologies.	26
Figure 3-2 a) HAWT main common components; b) 1.5MW HAWT (V63) from Vestas Manufacturer (source: https://en.wind-turbine-models.com/); c) 300W five-bladed HAWT from Rexco manufacturer (source: https://www.bestwindsolar.com/).....	27
Figure 3-3 Savonius VAWT: a) Main components schematic; b) ATLAS2.0 Savonius straight bucket type turbine from TESUP manufacturer (source: https://www.tesup-norge.com/); c) Four savonius helical bucket WS-4B turbines installed in a radar station China (source: https://windside.com/products/).....	28
Figure 3-4 Darrius VAWT: a) Main components schematic troposkien-type; b) QR6 quiet revolution, a 7kW helical-type darrius turbine from VWT Power manufacturer (source: https://vwtpower.com/); c) Ropatec Maxi 6kW straight-type darrius turbine from Ropatec manufacturer (source: www.ropatec.it).....	29
Figure 3-5 Silicon crystalline modules appearance: Monocrystalline (left); Polycrystalline (right)	30
Figure 3-6 Weibull PDF for different values of the shape factor and mean wind speed.	34
Figure 3-7 Simulated Wind speed map for central Europe at 100m height. (source: https://globalwindatlas.info/)..	35
Figure 3-8 Example of wind speed statistics as reported in (CENER; ERA-Net Plus NEWA 2019) for a place located at (43.342° latitude, -4.145° longitude) with 50mx50m scale. a) wind speed distribution at 50m with fitted Weibull PDF ($V_w = 6.4m/s$, $k_w = 1.8$); b) wind rose at 50m.....	36
Figure 3-9 Example of seasonal and hourly wind speed profile (Jake Badger 2021). Left: location example 9km ² area at southern Denmark (55.22°Lat, 9.05°Long) with mean wind speed of 8.42[m/s]. Right: (top) Seasonal wind speed profile as wind speed index (variation from mean wind speed), (bottom) Hourly wind speed profile. (Source: https://globalwindatlas.info/).....	37
Figure 3-10 Example of seasonal variation on daily insolation and solar irradiance (source: https://www.alternative-energy-tutorials.com/solar-power/solar-irradiance.html).....	38
Figure 3-11 Example of Global Solar Atlas (World Bank Group 2021), (top) Direct normal irradiation and (bottom) global horizontal irradiation (source: https://globalsolaratlas.info/download).....	39
Figure 3-12 Example of TMY data obtained from PVGIS tool (European Commission - EU Science Hub 2020) for a specific location at 43.342° Latitude and -4.145° Longitude.....	41
Figure 3-13 PV module tilt and azimuth angle definition (source: https://solar-design-guide.com/solar-panel-tilt-and-azimuth/).....	42
Figure 3-14 Mean annual total PV irradiance as function of module tilt and module azimuth for the TMY data plotted in Figure 3-12. Location: 43.342° Latitude and -4.145° Longitude	43
Figure 3-15 Comparison of typical wind turbine power curves: Pitch-regulated versus Stall-regulated	45
Figure 3-16 Considered power curve model for large scale wind turbines	46
Figure 3-17 Power coefficient comparison for the considered wind turbine technologies	47
Figure 3-18 Considered combined generator and power electronic converter nominal efficiency for large scale wind turbines.	48
Figure 3-19 Considered power curve model for small scale wind turbines.....	49
Figure 3-20 Illustration of PV cell characteristic curve, Maximum Power Point (MPP), short circuit current and Open circuit voltage. (Figure from (S.G.Bowden 2019)).....	52
Figure 3-21 Equivalent circuit of a photovoltaic cell using the single exponential model (Dezso Sera 2007).	52

Deliverable 2.2

Assessment of applicable renewable energy generation technologies on
NRA land and assets



Figure 3-22 Example of obtained VI curves with cell temperature of 25°C and for monocrystalline PV module LG375Q1C-V5 with datasheet parameters as shown in Table 3.....	56
Figure 3-23 Example of obtained output power and module temperature as function of irradiance and ambient temperature for monocrystalline PV module LG375Q1C-V5 with datasheet parameters as shown in Table 3.....	58
Figure 3-24 Considered DC/AC Converter topogoloy	60
Figure 3-25 Main parameter definitions for the considred wind farm layout	66
Figure 3-26 Geometric problem definition for determination of number of wind turbine rows parallel to prevalent wind direction.....	68
Figure 3-27 Main parameter definitions for the considered solar PV farm layout	69
Figure 3-28 Geometric problem definition for determination of number of PV Module rows perpendicular to the module azimuth orientation.....	70
Figure 3-29 Self-shading and shadow angle definition (figure adapted from (Energy 2016)).....	73
Figure 4-1 Sizing parameterization definition for the considered wind turbine technologies.....	76
Figure 4-2 Small scale wind turbine parameters trends (part 1).....	80
Figure 4-3 Small scale wind turbine parameters trends (part 2).....	81
Figure 4-4 Small scale wind turbine Tower cost model.....	82
Figure 4-5 Calculated power curve parameters for small scale wind turbine technologies.....	83
Figure 4-6 Example of calculated power curves for small scale virtual wind turbines (part 1): Top: Darrieus technology; Bottom: HAWT technology.	84
Figure 4-7 Example of calculated power curves for small scale virtual wind turbines (part 2): (Top) Savonious technology; (Bottom) Hybrid (Savonious&Darrieus) technology.....	84
Figure 4-8 Large scale wind turbine parameters trends	87
Figure 4-9 Example of calculated power curves for large scale virtual wind turbines.....	88
Figure 4-10 Warranty period and Lifetime of small scale wind turbines.	89
Figure 4-11 PV module parameters trends (part 1)	92
Figure 4-12 PV module parameters trends (part 2)	93
Figure 4-13 PV module parameters trends (part 3)	94
Figure 4-14 Guaranty - Linear Output Degradation for analyzed PV modules.....	96
Figure 4-15 Considered roadside area (marked in blue colour) for roadside application case. Location Latitud: 43°20'41.31"N ; Longitude: 4°8'41.74"W	97
Figure 4-16 Performance Comparison of small scale wind technologies for roadside case study	99
Figure 4-17 Performance Comparison of PV solar technologies for roadside case study	102

Deliverable 2.2

Assessment of applicable renewable energy generation technologies on
NRA land and assets



LIST OF ACRONYMS

DEGS Distributed Energy Generation System

NRA National Road Administration

RET Renewable Energy Technology

1 INTRODUCTION

1.1 OBJECTIVE AND SCOPE

The main objective of this work is to perform an assessment of applicable renewable energy generation technologies on NRA land and assets. To fulfil with this objective, the following sub-tasks have been performed and compiled in this document:

- Different aspects regarding the integration of distributed energy generation systems have been reviewed and compiled in chapter 2. Also, the characterization of focussed application cases for the NRA land and assets as well as definition of main input/required data and parameters for DEGS evaluation has been presented, so the optimal integration of distributed energy resources with existing power systems and road infrastructure can be analysed in future steps.
- A methodology for the performance evaluation and comparison of renewable energy generation systems based on different technologies has been introduced. The performance evaluation has been focused on evaluation of the potential energy production per unit area and the total capital cost of the preselected RETs in report D.2.1 with ENROAD project (University of Cantabria 2021). Methods and models for the design and evaluation of wind farms and solar PV farms have been reviewed, proposed, and compiled in chapter 3.
- A methodology for the general performance comparison of RETs has been introduced, which is based on the technology trends of relevant parameters of the generation devices. Representative meta-parameters for different wind turbines technologies and solar PV modules have been obtained based on compiled/collected RET data available in the market. Then, a general comparison of the considered RETs has been performed for a specific case example to show the application of the proposed/reviewed methods and potential of the proposed approach when comparing different technologies. Chapter 4 reports the calculated meta-parameters and technology trends for small- and large-scale wind turbines as well as solar PV modules based on Silicon crystalline technologies.

Deliverable 2.2

Assessment of applicable renewable energy generation technologies on NRA land and assets



1.1 METHODOLOGY

The proposed methodology identifies relevant RET parameters and bring an overview of parameters trends based on current products in the market. The methodology allows to perform a comprehensive/general comparison of RETs using the technology trends but not limiting to the discrete selection of renewable generation devices in the market.

The following actions have been performed within this work:

- Database creation: Collection of relevant data/parameters for different wind turbine technologies and solar PV modules has been done. The data has been compiled in an excel file, which can be used for future reference.
- Identification of relevant parameters for RETs performance (focus on potential energy production).
- Analysis of renewable energy generation devices based on same RET with similar parameter trends and identification of technology meta-parameters. Meta-parameters allow to predict the RET parameters as function of main inputs (Definition of the NRA land/assets).

Figure 1-1 introduces the correlation between the different modules involved in the potential performance evaluation of the different renewable energy generation technologies, which depends on:

- Definition of the NRA land/assets and characterization of focus application cases: definition of input data and relevant parameters for DEGS evaluation.
- Characterization of the Renewable Energy Source in the specific location.
- Renewable Energy Generation device performance, which is quantified in the generation device parameters and/or the technology meta-parameters.

Deliverable 2.2

Assessment of applicable renewable energy generation technologies on NRA land and assets

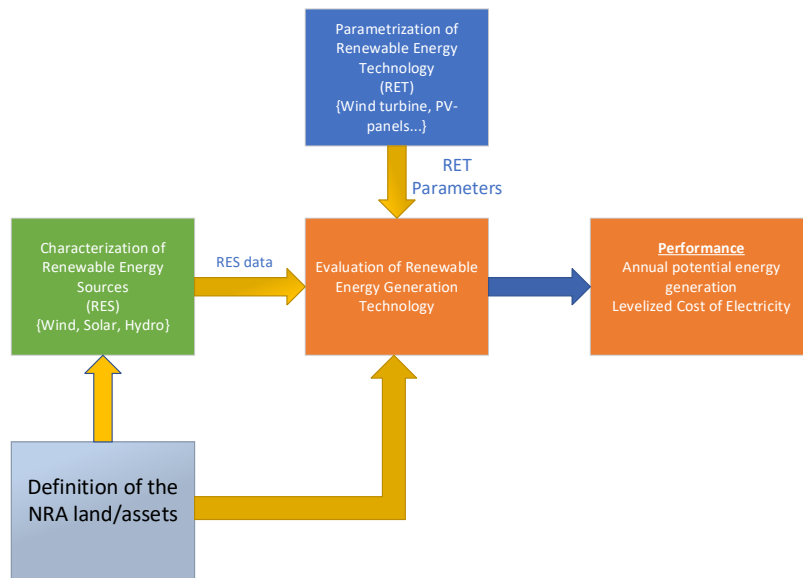


Figure 1-1 Evaluation of Renewable Energy Generation Technologies

1.2 RET DATABASE

To characterize the different considered RETs, a database has been created, which compiles collected data of small-scale wind turbines and Photovoltaic modules in an excel file format. Relevant data and parameters for a total of 224 wind turbines and around 90 PV modules have been included in the database.

The compiled data for wind turbines is list as follows:

- Wind turbine type: Darrieus, Savonius, HAWT, hybrid (combining Savonius and Darrieus rotor architecture)
- Wind turbine Sub-type: classification within the rotor architecture.
- Manufacturer
- Reference/name
- Nominal Power
- Peak Power
- Swept Area
- Rotor Diameter

Deliverable 2.2

Assessment of applicable renewable energy generation technologies on NRA land and assets



- Rotor height/length
- Hub height
- Maximum and minimum available tower height
- Turbine Base height
- Total height
- Nominal wind speed
- Wind speed at peak power
- Cut-in and cut-out wind speed
- Turbine Weight
- Turbine cost
- Power coefficient
- Number of blades
- Warranty
- Expected lifetime
- Reference for technical data
- Reference for wind turbine price

The compiled data for solar PV modules is list as follows:

- Manufacturer
- Product family/series
- Module reference name
- Cell type (Monocrystalline vs polycrystalline)
- Subtype (N-type vs P-type cell)
- Price
- Reference for price
- Number of cells per module
- Module dimensions: Length, width, and height
- Cell dimension: Length, width
- Module weight

Deliverable 2.2

Assessment of applicable renewable energy generation technologies on NRA land and assets



- Glass type/description
- Frame type/description
- Maximum system voltage
- Number of bypass diodes
- Product warranty
- Performance guarantee
- Linear output degradation
- Initial performance
- Performance at end of warranty
- Electrical properties at standard test conditions:
 - Maximum power
 - MPP voltage
 - MPP current
 - Open circuit voltage
 - Short circuit current
 - Module efficiency
- Electrical properties at Nominal module operating temperature:
 - Maximum power
 - MPP voltage
 - MPP current
 - Open circuit voltage
 - Short circuit current

Deliverable 2.2

Assessment of applicable renewable energy generation technologies on NRA land and assets



2 DISTRIBUTED ENERGY GENERATION SYSTEMS

2.1 INTEGRATION OF DEGS TO THE ELECTRICAL POWER SYSTEM.

The most suitable approach for power system integration of DEGS associated with road infrastructures will depend on the scale and location of the installations. For large systems with high generation capacity, the most relevant approach can be a traditional connection to the high voltage distribution or transmission system. However, for geographically distributed installations at lower power levels, a direct integration with the roadside power system could be beneficial. In this case integration of DEGS with the loads associated with the road infrastructure could potentially provide key benefits to the local roadside electric power distribution system as follows:

- Reduce/eliminate power consumption from main power grid caused by the electric loads associated with the road infrastructure.
- Reduce local transmission losses and limit the maximum required capacity for power supply to the road infrastructure from the main grid.
- Provide/enhance coordination with energy storage and/or EV charging infrastructure for supporting the electrification of transport.
- Become an active player in the energy market system providing flexibility to the main power system.

The optimal utilization of energy storage and distributed generation units for supporting EV charging and/or for operating in the energy market requires further attention to the energy management and power control within the system beyond the scope of this report. However, a brief overview of some relevant configurations and topologies for power system integration of diverse types and scales of DEGS is presented in the following.

Deliverable 2.2

Assessment of applicable renewable energy generation technologies on NRA land and assets



2.1.1 INTEGRATION TO THE MAIN POWER SYSTEM

For large-scale DEGS installations, the power system integration is likely to be designed independently from the distribution system and loads associated with the road installations. Such cases might be most relevant for relatively large wind farms installed close to the roads, containing multiple turbines in the MW range. A typical schematic for this case is shown in Figure 2-1, where the wind farm has a dedicated transformer station for interconnection to the high voltage transmission system. The wind farm itself will then have an internal collection grid, typically at a voltage level of 33 kV, and a dedicated transformer for each turbine will then be used for connecting the low voltage generation system to the collection grid. A similar configuration could be used for a large-scale PV installation.

The single line diagram in Figure 2-1 also shows how the roadside AC distribution system, typically at 11 or 22 kV, can be supplied from the same busbar of the regional transmission grid at the same busbar as the wind farm. However, the road-side power distribution will typically be supplied by a transformer station that can also feed multiple other distribution lines.

It can be noted that the configuration in Figure 2-1 does not provide any close integration between the DEGS and the road-side distribution system. Thus, any support to the roadside loads or utilization of flexibility to the benefit of the road-side power system would in this case be mainly relevant as indirect contributions via system-wide market mechanisms.

It does not give any close integration between the DEGS and the road-side distribution system. Thus, any support to the roadside loads or utilization of flexibility to the benefit of the road-side power system would in this case be mainly relevant as indirect contributions via system-wide market mechanisms.

Deliverable 2.2

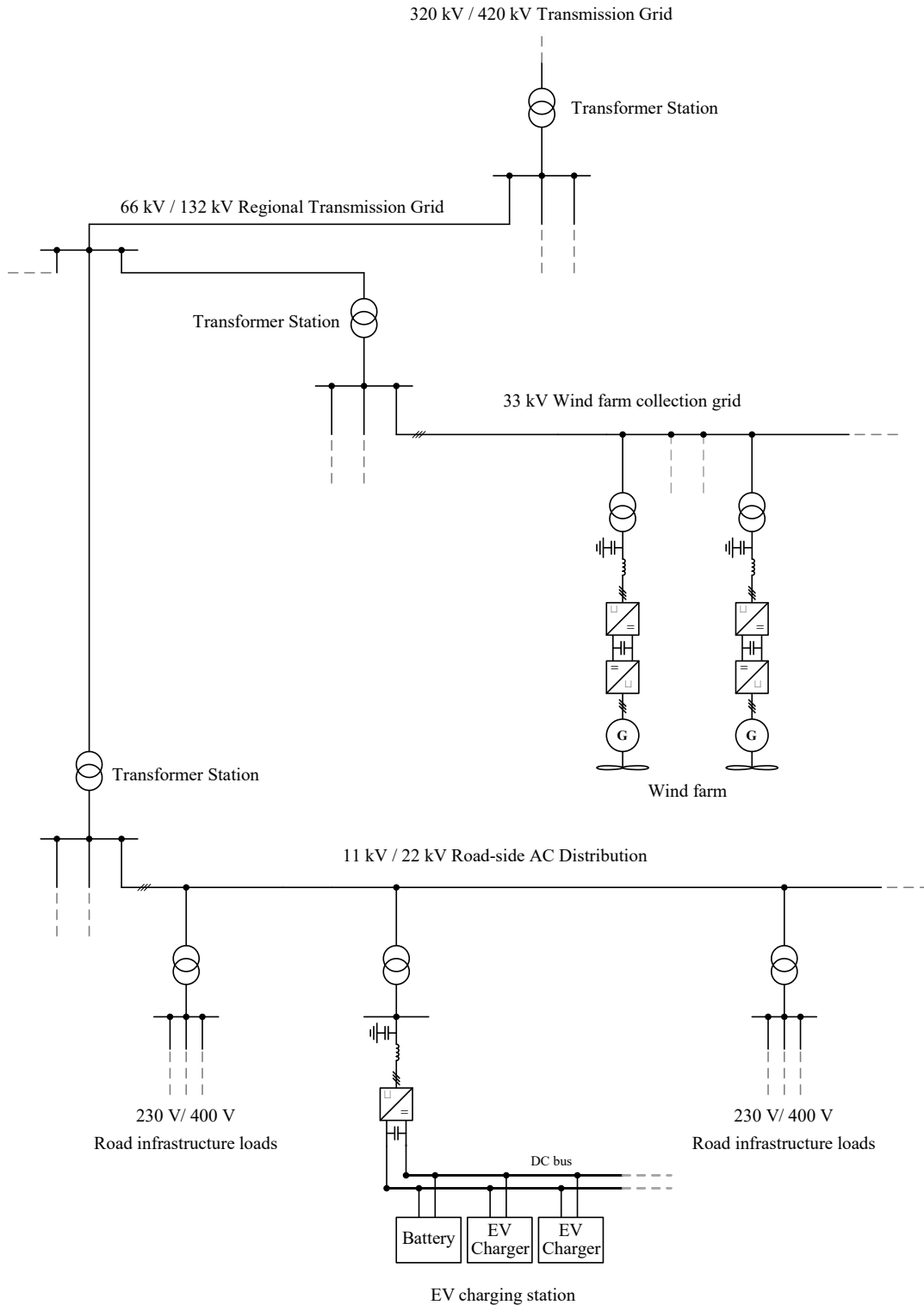


Figure 2-1 Generic power system configuration where the grid interconnection of a wind farm associated with the road infrastructure is independent from the AC-distribution system along the road

Deliverable 2.2

Assessment of applicable renewable energy generation technologies on NRA land and assets



2.1.2 INTEGRATION TO THE LOCAL ROAD POWER SYSTEM

For DEGS installations with lower total power rating, direct integration with the local road-side power system can be relevant and provide several benefits. Especially, having local production close to the load will reduce the need for long distance transmission, and can also help to alleviate capacity constraints on the local power distribution system. An example of a generic system configuration that could be directly utilized is shown in Figure 2-2, where different medium or small-scale DEGS installation are connected directly to the road-side high voltage distribution line. Furthermore, the figure shows how the same distribution line also can supply an EV charging station, which could potentially include local battery energy storage. In this case, the battery can be utilized to support the operation of the EV charging station as well as to support the utilization of the local DEGS installations.

The configuration in Figure 2-2 is still based on the assumption that each DEGS installation is relatively large (i.e. has a power level in the range from around 100 kW to a few MW), and is connected to the road-side AC distribution line by a dedicated transformer. Thus, the local power consumption supported by the DEGS installation will be always transferred via the local high voltage line. For smaller DEGS installations, the integration directly with the local low voltage system can also be relevant, as indicated by the structure shown in Figure 2-3. This integration at low voltage could be on the AC-side, as indicated for small-scale wind turbines in the figure, but could also be with a DC-distribution system as shown by extending the DC-busbar of the EV charging station. In such a system configuration, flexibility could be provided a several levels of complexity, where the simplest would be to have a management system for a dedicated dc busbar which could include both generation, storage, and loads (including EV charging but also other DC-connected loads). However, by also including AC generation supplied by the same transformer for interfacing to the high voltage distribution line, the combined system including both local generation, storage and load could be considered as a local power hub.

Deliverable 2.2

Assessment of applicable renewable energy generation technologies on NRA land and assets

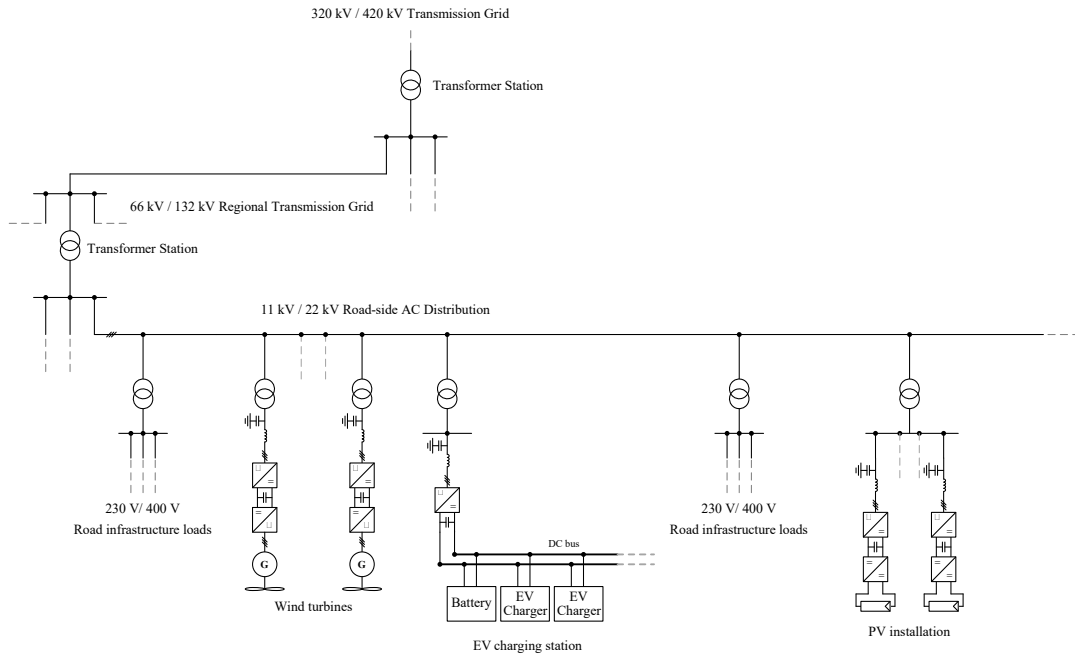


Figure 2-2 Generic power system configuration with small-scale DEGS consisting of few wind turbines or medium size PV installations connected to the road-side AC-distribution system

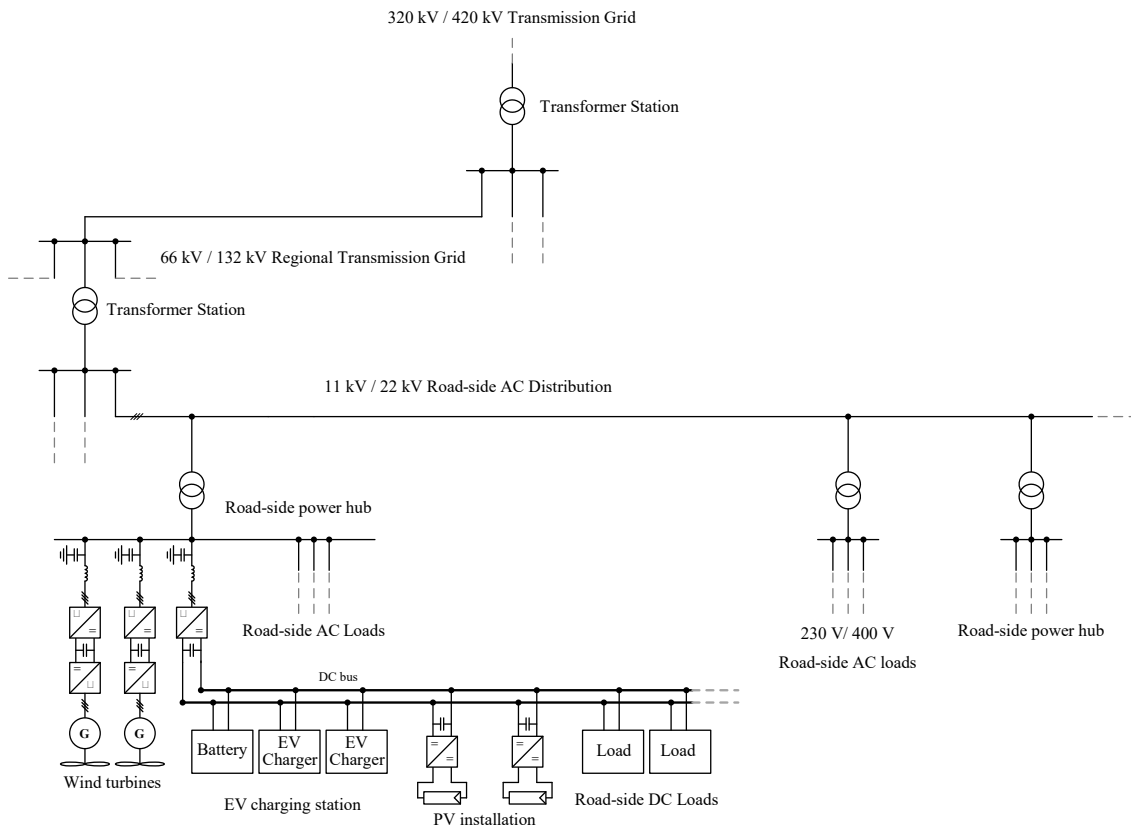


Figure 2-3 Generic power system configuration including local power hubs with internal DC distribution for integrating small-scale generation and road-side DC-loads with an EV charging station

Deliverable 2.2

Assessment of applicable renewable energy generation technologies on NRA land and assets



2.2 SELECTED DEGS ALTERNATIVES FOR LOCATIONS IN NRA LAND/ASSETS

A range of DEGS technologies that can be relevant for utilizing available land and assets owned by NRAs are identified and surveyed in Deliverable D 2.1 within ENROAD project (University of Cantabria 2021). For the more detailed assessment presented in this report, only a subset of the most relevant and scalable technologies is considered. The main alternatives considered for detailed assessment can be considered in two groups, depending on whether they can be installed in open areas related to the road or if they will be directly integrated with the road or the road-side infrastructure. This also gives a natural distinction in terms of scale and power levels, as the DEGS that can be relevant for integration into the infrastructure will be mainly smaller distributed units, while utilization of larger areas in vicinity of the road can allow for installation of larger systems with higher power rating of the individual units.

2.2.1 INSTALLATIONS IN OPEN ROADSIDE AREAS

For utilizing relatively large open areas in vicinity of roads, two main DEGS options are considered:

- Large- or small-scale wind turbines (Large vs small scale against on proximity to road and urban areas)
- PV farms

For such installations with many individual wind turbines or PV panels, the main parameters providing the basis for optimizing the utilization of the area will be:

- Occupied area (footprint) of each unit
- The spacing between the wind turbines or PV-panels
- Safety distance to the road and to urban areas
- Minimum available roadside area/width

These main parameters are illustrated for a wind farm in Figure 2-4 and Figure 2-5, respectively. As seen in the figures, the required safety distance to the road is denoted as *Dsafe*, while a simple layout is

Deliverable 2.2

assumed with the individual units placed in a grid structure aligned with the road, and with the same *spacing* between the units both in the direction along the road and perpendicular to the road. These generic installation layouts could be applied for regular large-scale wind turbines but could be equally applicable for small-scale turbines depending on the size, shape, and wind conditions of the available areas. Similarly, the presented parameters can be utilized to represent any regular size of PV panels.

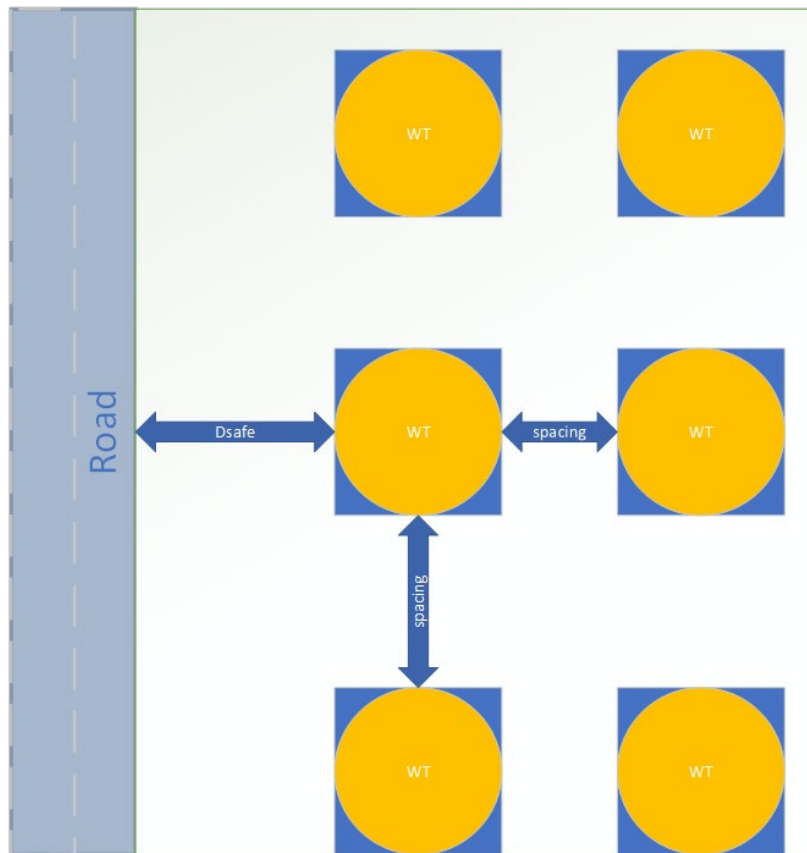


Figure 2-4 Assumed layout of a wind farm on limited land area associated with a road

Deliverable 2.2

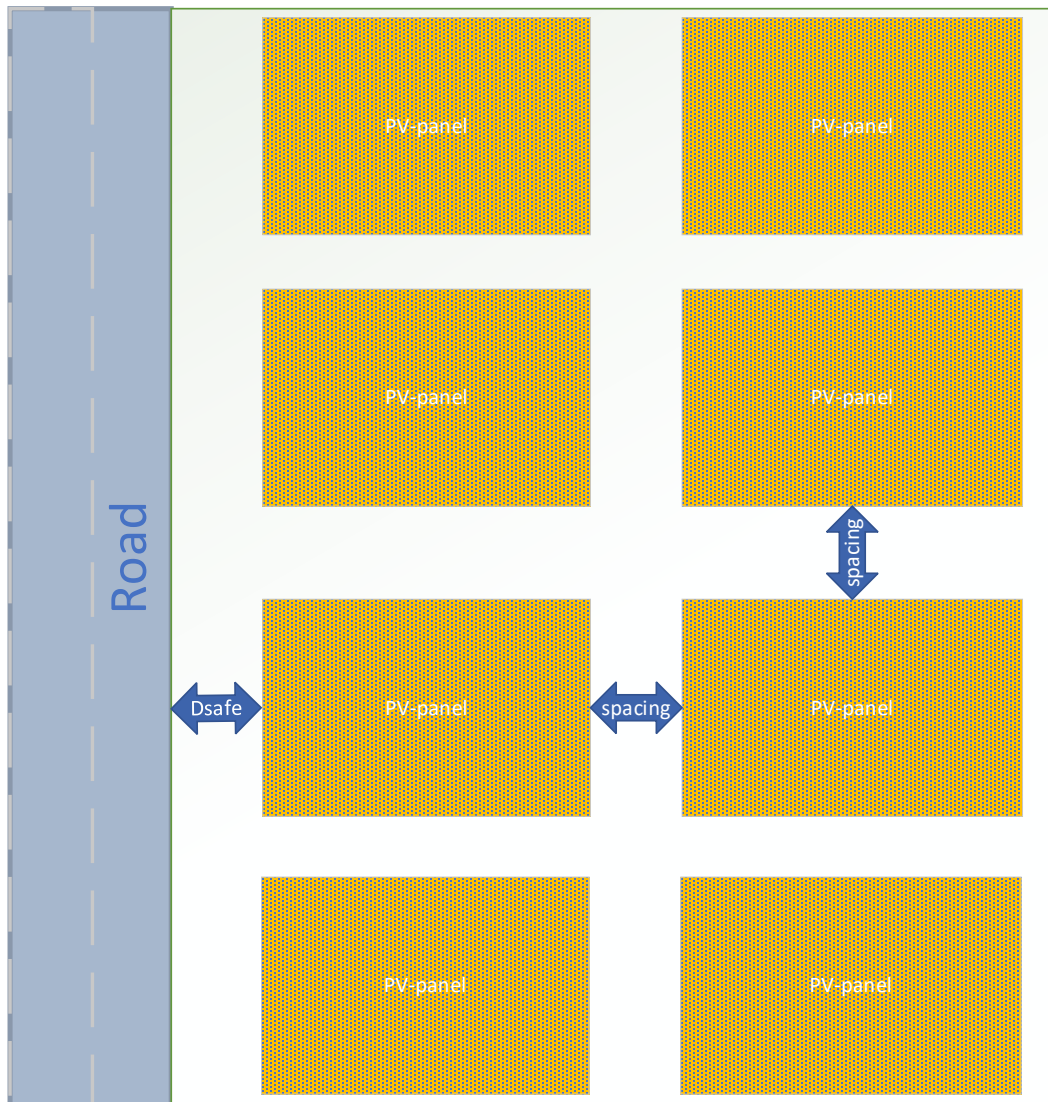


Figure 2-5 Assumed layout of a PV farm on a limited land area associated with a road

2.2.2 ALONG THE ROAD OR INTEGRATED WITH OTHER INFRASTRUCTURE

For small-scale DEGS installations along the road the following two main options are considered

- Small- or micro-scale wind turbines that can be integrated with light poles or traffic lights, or mounted on any other available structures along the road

Deliverable 2.2

- Small-scale PV panels that can be installed on noise barriers or integrated with any other available structures, including roofs or carports for EV charging and/or parking areas

A general overview of a road section with noise barriers and light poles is shown in Figure 2-6 to indicate how PV panels, and possibly micro-scale wind turbines, can be integrated with the road infrastructure.

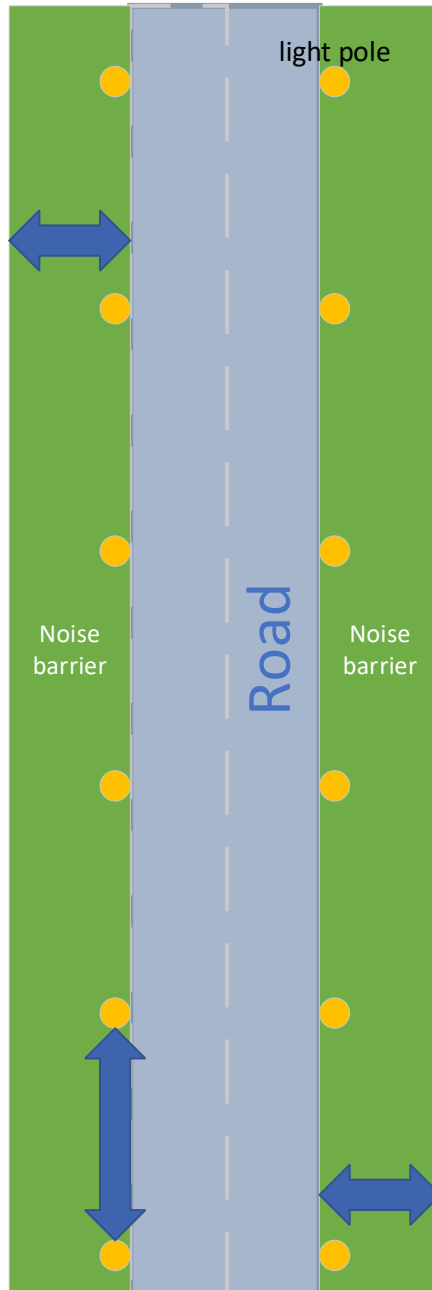


Figure 2-6 Overview of general layout for a road with noise barriers and light poles that can be utilized for mounting small scale DEGS installations

Deliverable 2.2

Assessment of applicable renewable energy generation technologies on NRA land and assets



For such installations, it will be necessary to consider the local conditions of wind speed and/or irradiation to evaluate how a DEGS installation can be designed to maximize the utilization for the available area and/or infrastructure. Further details on methods for parameterization of the DEGS units and for assessment of the potential energy generation capacity will be discussed later.

The use of micro hydro turbines for generating power from the rainfall gathered by the road infrastructure or the associated buildings or other constructions has also been identified as a relevant DEGS technology in (University of Cantabria 2021). However, design of such systems will be highly case dependent, with local topography, specific conditions of the nearby buildings or the hydrotechnical installations along the road as well as the rainfall conditions determining what will be the most suitable technology and configuration of the DEGS. Thus, such systems cannot be easily parameterized and evaluated in generic configurations in the same ways as wind turbine or PV panel installations. Thus, micro hydro installations are not further evaluated in this report.

Deliverable 2.2

Assessment of applicable renewable energy generation technologies on NRA land and assets



3 STUDIED RENEWABLE ENERGY GENERATION TECHNOLOGIES

3.1 OVERVIEW OF THE CONSIDERED RENEWABLE ENERGY TECHNOLOGIES

Identification and first screening of the renewable energy technologies with the highest potential for their application on the main topologies of NRA's assets has been conducted within Task 2.1 of the ENROAD project and has been reported by the Deliverable 2.1: *Report of main renewable energy technologies (RETs) for the road infrastructure* (University of Cantabria 2021). (University of Cantabria 2021) has been used as starting point to select the RETs suitable for NRA land and assets that have been analyzed in further detail in this report. Table 1 summarizes the initial reviewed RETs within project ENROAD, reported in Deliverable 2.1 (University of Cantabria 2021)

As indicated in section 2, the scope of this analysis is in general limited to wind turbines and PV systems. The specific RETs studied in this report have been selected based on the results and suggestions regarding the Technology Readiness Level (TRL) and Market Readiness Levels (MRL) of the reviewed RETs reported in Deliverable 2.1 (University of Cantabria 2021). Only RETs with TRL and MRL at least seven have been considered. A summary of the considered RETs in this report is presented in the next subsections.

Deliverable 2.2

Assessment of applicable renewable energy generation technologies on NRA land and assets



Table 1 Summary of the initial reviewed RETs within project ENROAD, Deliverable 2.1: Report of main renewable energy technologies (RETs) for the road infrastructure (University of Cantabria, 2021)

		RETs		TRL	MRL	
ROADSIDE	Wind Turbines	Large Scale	HAWT	Three blade	9	9
			HAWT	Three blade		
		Small Scale	VAWT	Savonius	8	7
				Darrieus		
				Venturi		
	Vortex	5		1		
	Photovoltaic Cells	Silicon Crystalline	Monocrystalline	9	9	
			Polycrystalline			
		Thin film	Amorphous	8	6	
			CdTe			
			GaAs			
			CIGS			
		Multijunction	Two junction cells	5	2	
			Three junction cells			
			Four junction cells			
		Emerging	Organic cells	5	2	
	Perovskite		--	--		
	Dye sensitized					
Quantum dot cells						
Mini-hydro turbines	Action turbines	Pelton Wheel	9	9		
		Ossberger turbine	9	8		
	Turgo turbine	9	9			
Reaction turbines	Francis turbine					
Micro-scale Biomass	Primary conversion	Direct combustion	8-9	5-6		
		Gasification				
		Pyrolysis				
		Anaerobic digestion				
	Secondary conversion	Steam turbine	8-9	5-6		
		Gas turbine				
Stirling engine						
BUILT IN	Solar harvesting	PVs into	Road Pavement	8-9	2-3	
			Noise barriers		7-9	
	Thermoelectricity	Ceramic-based	Cementitious mixes	3	1-2	
						Piezoelectric
	Piezoceramics					
	Polymers					
	Mechanical harvesting	Electromagnetic	Hydraulic	3-4	1-2	
Pneumatic						
Electro-mechanical						

3.1.1 WIND TURBINES

The Venturi and Vortex Vertical Axis Wind Turbines (VAWTs) have been excluded from this analysis because the ENROAD project is focused on high TRL technologies and medium to high MRL market status. Large-scale and small-scale wind turbines are analyzed in this document. Figure 3-1 shows a basic comparative illustration of the four considered wind turbine technologies, which differ on the rotor axis position (horizontal vs. vertical axis), aerodynamic force exploited (drag vs. lift forces) and the wind turbine blade architecture (with or without airfoil profile). A brief description of each considered technology is presented below.

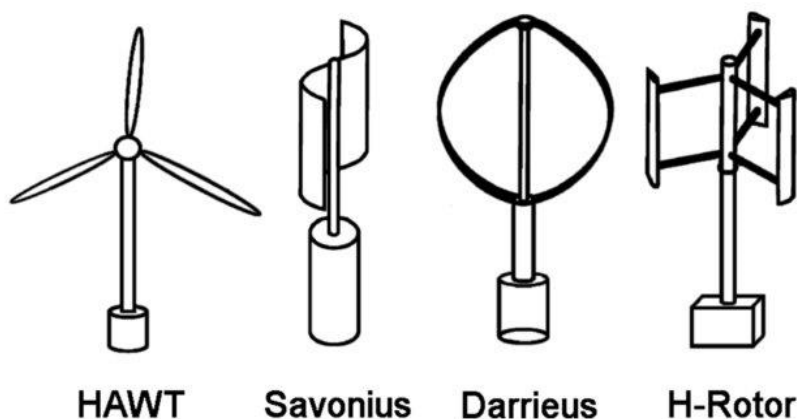


Figure 3-1 Basic comparative illustration of the considered wind turbine technologies.

Source: (Mehrpooya 2014)

3.1.1.1 Horizontal Axis Wind Turbines (HAWT)

This type of turbine is the most used technology for wind generation. Figure 3-2a) shows the main components of the HAWT, common in large- and small-scale turbines. However, compared with the small scale HAWT, the large scale HAWTs include more complex system components within the turbine nacelle, e.g., the orientation systems (yaw and pitch systems), the electrical interface between generator and electric grid (power converter and sometimes the transformer). Large scale HAWTs are normally constructed based on three-blade architecture (around 99% of installed wind turbines (University of Cantabria 2021)), however small scale HAWTs can be found with different number of blades (two, three, five or six as most common). Figure 3-2b) shows the V63 wind turbine, a 1.5MW

Deliverable 2.2

Assessment of applicable renewable energy generation technologies on NRA land and assets

three-bladed HAWT from Vestas Wind Systems A/S Manufacturer, while Figure 3-2c) shows a 300W five-bladed HAWT from Rexco manufacturer. Small scale HAWTs normally include a passive yaw system (a tail blade orients the turbine in the direction of the wind and is a cost-effective solution), but do not include a pitch system (to adjust the blade angle), so they normally apply brakes and completely stop at high wind speeds.

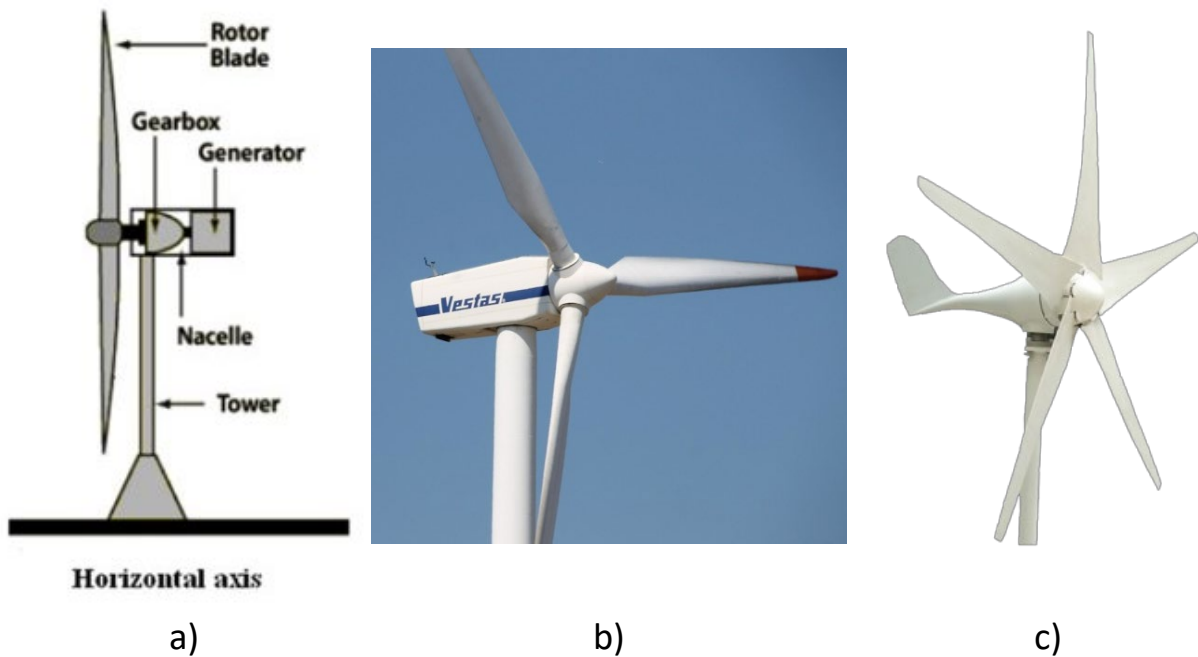


Figure 3-2 a) HAWT main common components; b) 1.5MW HAWT (V63) from Vestas Manufacturer (source: <https://en.wind-turbine-models.com/>); c) 300W five-bladed HAWT from Rexco manufacturer (source: <https://www.bestwindsolar.com/>)

3.1.1.2 Savonius - VAWT

Savonius turbines are drag force based and can generate power in turbulent and low wind speed prevalent in the built-up area. (Kumar 2019). These turbines consisting of two to three scoops. These turbines have an 'S' shaped cross section when looked from above. As they move along the wind, they experience lesser drag and this difference in drag helps these turbines to spin. Due to the drag, the efficiency of these turbines is less when compared to other types of turbines (Tummala, et al. 2016). There are two main types of Savonius turbine in the market, based on the architecture of the bucket/blades, the straight

Deliverable 2.2

bucket type and the helical bucket type. Figure 3-3a) shows a standard Savonius helical bucket type turbine along with their main components, gearbox and generator are placed in the lower part of the turbine. Figure 3-3b) shows the 2kW Savonius straight bucket type, ATLAS 2.0 from TESUP manufacturer. Figure 3-3b) shows four savonius helical bucket type, WS-4B turbines, installed in the top of a radar station in China.

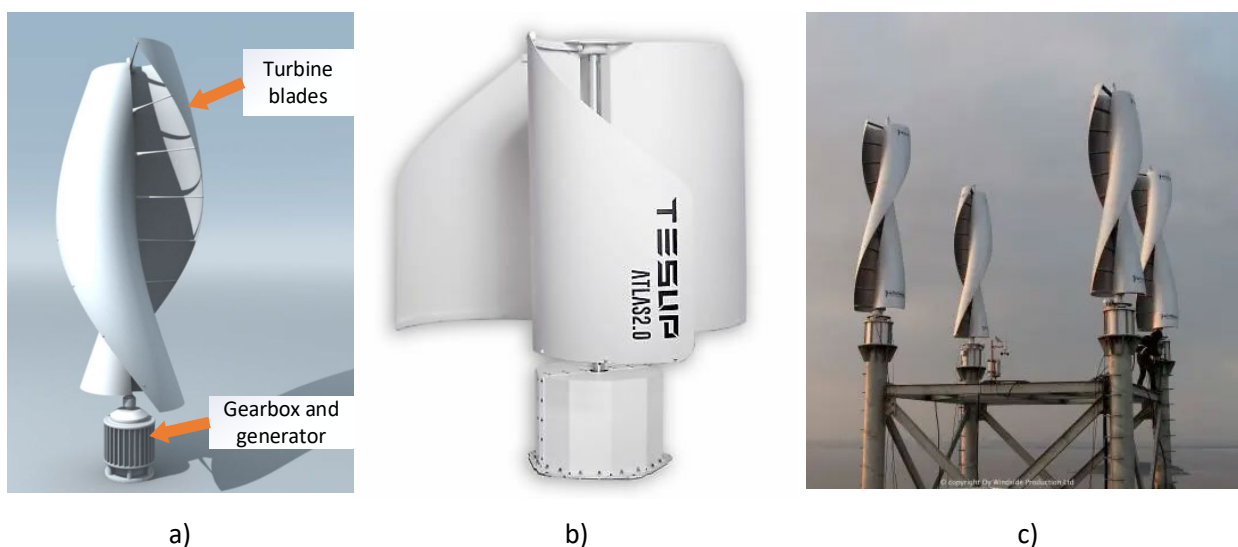


Figure 3-3 Savonius VAWT: a) Main components schematic; b) ATLAS2.0 Savonius straight bucket type turbine from TESUP manufacturer (source: <https://www.tesup-norge.com/>); c) Four savonius helical bucket WS-4B turbines installed in a radar station China (source: <https://windside.com/products/>)

3.1.1.3 Darrieus - VAWT

Darrieus turbines work from the lift forces produced during rotation. They consist of a number of blades (straight or curved) mounted on a vertical framework (Tummala, et al. 2016). Based on the architecture of their blades, they can be classified in four types: troposkien or D-type, straight or H-type (also known as giro mill), V-type and helical or Gorlov (Kharade 2019, Kumar 2019, Tummala, et al. 2016). Figure 3-4a) shows the main components and schematic of a D-type Darrieus turbine. Gearbox and generator are normally placed in the downside of the turbine for all Darrieus type turbines. Figure 3-4b) shows the

Deliverable 2.2

Assessment of applicable renewable energy generation technologies on NRA land and assets

7kW helical-type Darrieus turbine, QR6 quiet revolution from VWT power manufacturer. Figure 3-4c) shows the 6kW H-type Darrieus turbine, Ropatec-Maxi from Ropatec manufacturer.



Figure 3-4 Darrieus VAWT: a) Main components schematic troposkien-type; b) QR6 quiet revolution, a 7kW helical-type darrieus turbine from VWT Power manufacturer (source: <https://vwtpower.com/>); c) Ropatec Maxi 6kW straight-type darrieus turbine from Ropatec manufacturer (source: www.ropatec.it)

3.1.2 PHOTOVOLTAIC MODULES

The silicon crystalline photovoltaic technology has been selected as focus technology based on the fact that their TRL and MRL values are by far the highest ones compared with other photovoltaic cell technologies. Thin film technology has a good TRL value but still not enough MRL to be considered here.

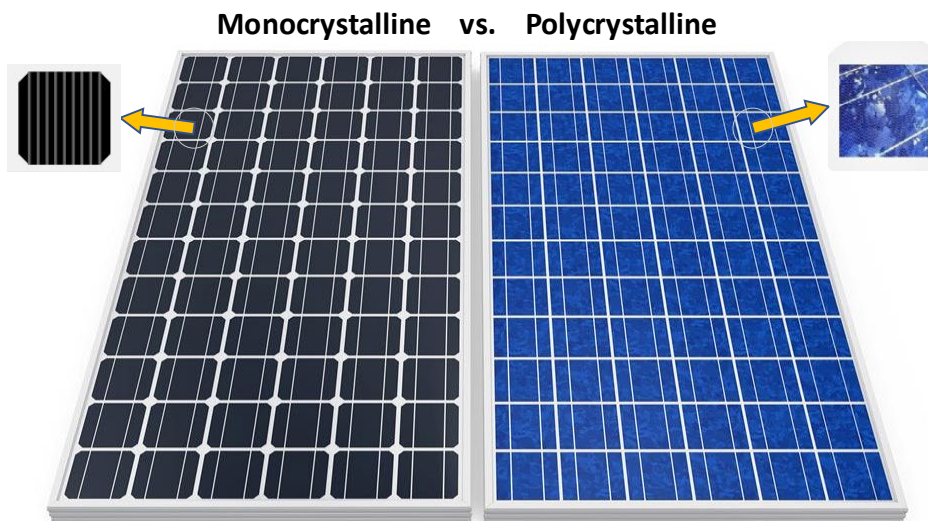


Figure 3-5 Silicon crystalline modules appearance: Monocrystalline (left); Polycrystalline (right)

3.1.2.1 Silicon Monocrystalline

Monocrystalline PV cells are produced with silicon wafers, using single-crystal silicon, and providing more space to the electron to move for a better electricity flow and therefore higher efficiency compared with polycrystalline technology (Okil, et al. 2021). Figure 3-5(left) shows the common appearance of PV modules based on monocrystalline cell technology. Due to how they are cut, monocrystalline cells form a distinct pattern of small diamonds when put together. They are also darker in appearance than polycrystalline cells.

Deliverable 2.2

Assessment of applicable renewable energy generation technologies on NRA land and assets



3.1.2.2 Silicon Polycrystalline

Polycrystalline cells are commonly manufactured by casting process, where multiple silicon crystal fragments are melted, then cast into molds and solidified into blocks. This manufacturing process allows to get solar cells with lower cost compared with monocrystalline technology, but also the impurities and crystal defects inherent to polycrystalline cell production make them more delicate and less efficient than monocrystalline cells (Okil, et al. 2021). Figure 3-5(right) shows the common appearance of PV modules based on polycrystalline cell technology.

3.2 CHARACTERIZATION OF RENEWABLE ENERGY SOURCES

3.2.1 WIND SOURCE CHARACTERIZATION

A widely used approach to characterize the wind resource is by its wind speed probability distribution function (PDF). There are many PDFs that can be used to characterize the wind resource of a given region, however the most used is the Weibull PDF, as it provides a good fit to the annual frequency wind speeds of many sites (Borunda 2020). In this study, the two-parameter family of Weibull PDFs is used, which is given by (J. F. Manwell 2009):

$$f_W(v_w) = \begin{cases} \frac{k_w}{\lambda_w} \cdot \left(\frac{v_w}{\lambda_w}\right)^{k_w-1} \cdot e^{-\left(\frac{v_w}{\lambda_w}\right)^{k_w}} & v_w \geq 0 \\ 0 & v_w < 0 \end{cases} \quad (1)$$

Where $k_w > 0$ and $\lambda_w > 0$ are the shape and scale factors of the distribution, respectively, and v_w is the wind speed. The mean wind speed (\bar{V}_w) of the Weibull PDF can be calculated by

$$\bar{V}_w = \lambda_w \cdot \Gamma\left(1 + \frac{1}{k_w}\right) \quad (2)$$

where the gamma function ($\Gamma(x)$) is defined as

$$\Gamma(x) = \int_0^{\infty} t^{x-1} \cdot e^{-t} \cdot dt \quad (3)$$

Figure 3-6 shows an example of the Weibull PDF for different values of shape factor and mean wind speed. The Weibull function factors are normally obtained by fitting the function to the measurements of wind speeds using wind masts for duration of some months to one year through 10 minutes intervals (Sedagha, et al. 2016). The wind profiles are dependent on the height above the ground, the ground's surface

Deliverable 2.2

roughness, the ground's roughness variation, the atmospheric stability, and the geographical elevation (Wass 2018). The wind speed profiles generated from wind speed measurements will be referred to as the mat's height. There are two common models to estimate/scale wind profile at any given height: the log law and the power law. Here, a simplified log wind profile is considered, and the mean wind speed (\bar{V}_w) at a height (z) above the ground is estimated by (Holmes 2015) (Wikipedia 2021)

$$\bar{V}_w = \bar{V}_{w,REF} \cdot \frac{\log\left(\frac{z - z_d}{z_0}\right)}{\log\left(\frac{z_{REF} - z_d}{z_0}\right)} \quad (4)$$

where $\bar{V}_{w,REF}$ is the mean wind speed at the reference height z_{REF} , z_d is the zero-plane displacement, and z_0 is the roughness length, which accounts for the effect of the roughness surface. The zero-plane displacement is the height above the ground at which zero wind is achieved as results of flow obstacles such as trees or buildings. It can be approximated as 2/3 to 3/4 of the average height of the obstacles (Holmes 2015). On the other hand, the value of the roughness length depends on the terrain. Table 2 introduces typical values of surface roughness length as reported by (Tony Burton 2001).

The Weibull distribution factors (λ_w , k_w) can be extrapolated at any height of the rotor (z) by using the Justus and Mikhail method (Justus, et al. 1978, Djohra Saheb 2014):

$$\lambda_w = \lambda_{wREF} \cdot \left(\frac{z}{z_{REF}}\right)^{ak} \quad (5)$$

$$ak = \frac{1}{\log\left(\frac{\sqrt{z} \cdot z_{REF}}{z_0}\right)} - 0.0881 \cdot \log\left(\frac{\lambda_{wREF}}{6}\right)$$

$$k_w = \frac{k_{wREF}}{1 - 0.088 \cdot \log\left(\frac{z}{z_{REF}}\right)} \quad (6)$$

Deliverable 2.2

Assessment of applicable renewable energy generation technologies on NRA land and assets

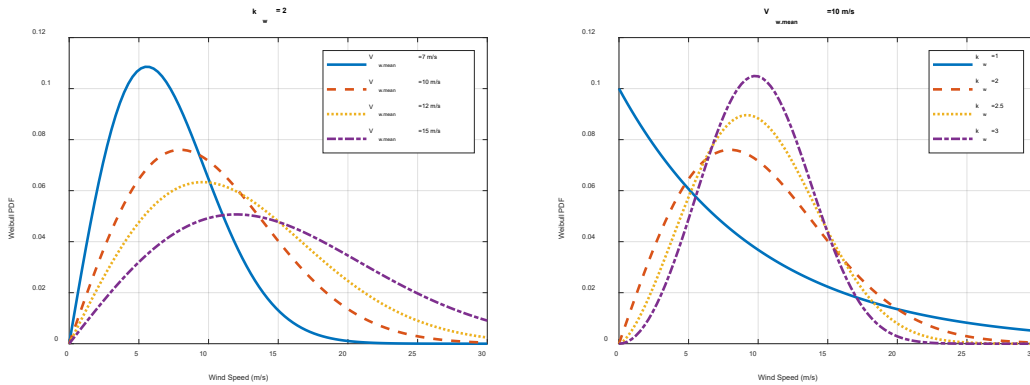


Figure 3-6 Weibull PDF for different values of the shape factor and mean wind speed.

Table 2 Typical values of surface roughness length for various types of terrain.

Type of terrain	Typical surface roughness length (z_0)	Type of terrain	Typical surface roughness length (z_0)
Mud flats, Ice	1e-5 to 3e-5	Calm Sea	2e-4 to 3e-4
Sand	2e-4 to 1e-3	Mown grass	0.001 to 0.04
Low grass	0.02 to 0.03	Fallow field	0.02 to 0.03
High grass	0.04 to 0.1	Forest and Woodland	0.1 to 1
Built up area, suburb	1 to 2	City	1 to 4

In principle, the expected energy production of a wind turbine can be estimated based on wind Weibull PDF on the target location and the turbine hub height. However, when many wind turbines are going to be placed near each other, as in a wind farm, the prevalent wind direction in the target location is also needed to determine the allocation/arrangement of the wind turbines affecting the effective available area. For a given area, this information is normally given by a wind rose chart. There are multiple data sources that can be addressed to get the wind characterization of a given area, for example a global wind atlas is available at (Jake Badger 2021), where different wind speed statistics has been extrapolated for different areas worldwide with a resolution of 9km². Figure 3-7 shows a simulated wind speed map for central Europe at 100m height as reported in (Jake Badger 2021). Besides, there are also specific wind speed data sources for each country which can also be accessed online, for example wind data source for the Iberian Peninsula can be accessed at (CENER; ERA-Net Plus NEWA 2019). Figure 3-8 shows an example

Deliverable 2.2

Assessment of applicable renewable energy generation technologies on NRA land and assets

of wind speed statistics as reported in (CENER; ERA-Net Plus NEWA 2019) for a place located at (42.64° latitude, -8.67° longitude) with 50mx50m scale.

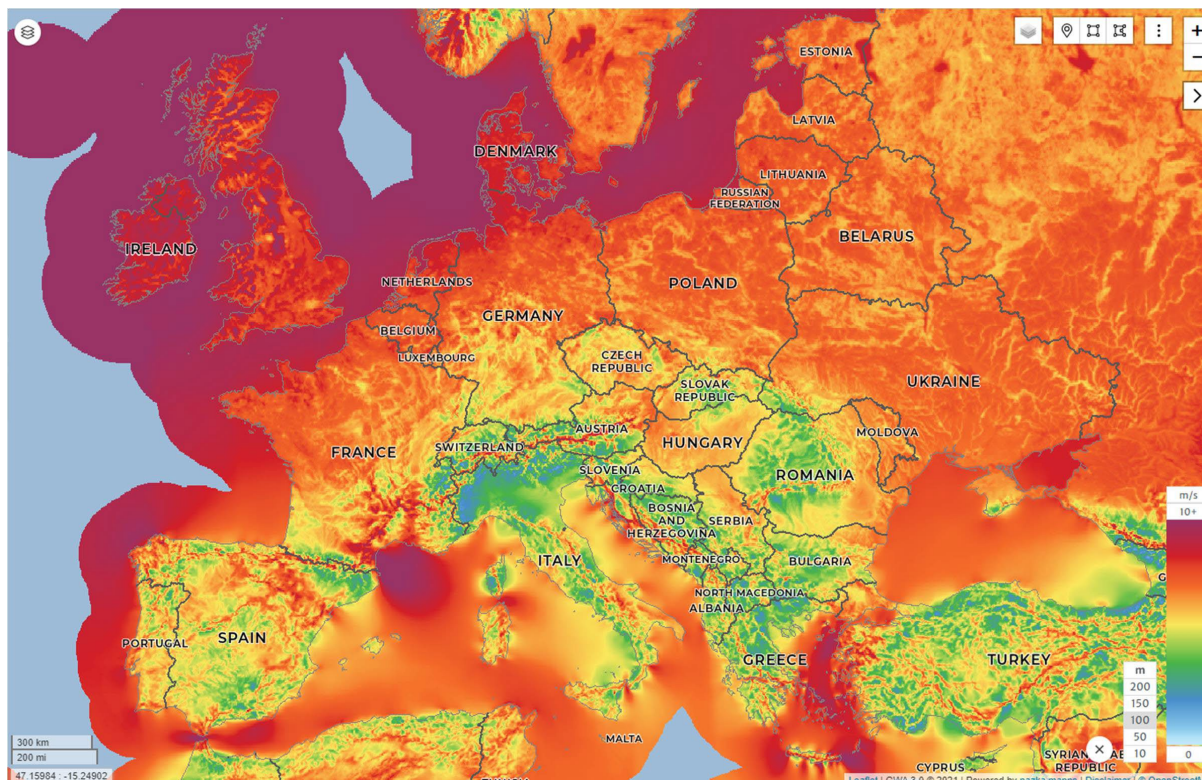


Figure 3-7 Simulated Wind speed map for central Europe at 100m height. (source: <https://globalwindatlas.info/>)

Deliverable 2.2

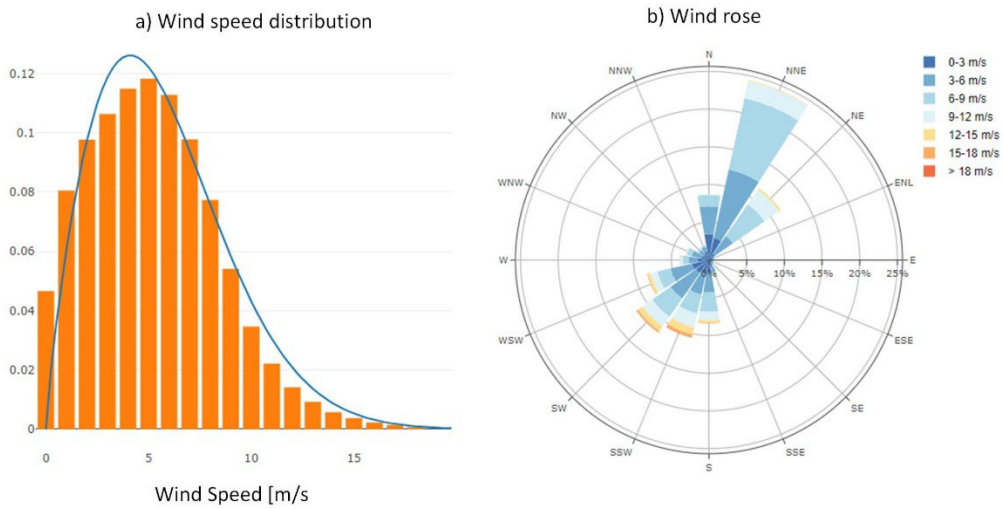


Figure 3-8 Example of wind speed statistics as reported in (CENER; ERA-Net Plus NEWA 2019) for a place located at (43.342° latitude, -4.145° longitude) with 50mx50m scale. a) wind speed distribution at 50m with fitted Weibull PDF ($\bar{V}_w = 6.4\text{m/s}$, $k_w = 1.8$); b) wind rose at 50m.

Additionally, temporal wind speed profile may be needed when wind turbine is intended to be operated in combination with Energy Storage System (ESS) to provide a given energy/power demand. In that aspect, the seasonal and hourly wind speed profiles of the area of interest can provide additional information needed so the ESS can be sized according to the expected load profile. Figure 3-9 shows an example of seasonal and hourly wind speed profiles taken from (Jake Badger 2021) for an aleatory 9km² area located at southern Denmark (55.22°Lat, 9.05°Long) with mean wind speed of 8.42[m/s]. The seasonal and hourly wind speed profiles are plotted as wind speed index, which is the relative variation from mean wind speed (8.42[m/s]).

Deliverable 2.2

Assessment of applicable renewable energy generation technologies on NRA land and assets

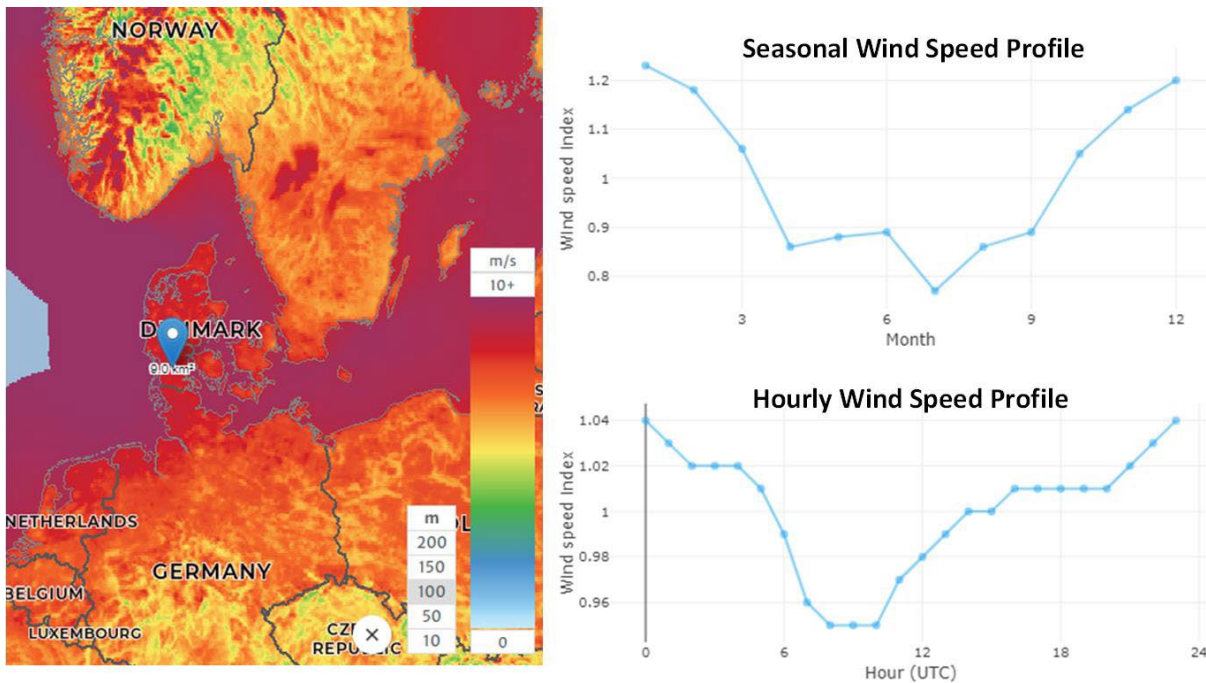


Figure 3-9 Example of seasonal and hourly wind speed profile (Jake Badger 2021). Left: location example 9km² area at southern Denmark (55.22°Lat, 9.05°Long) with mean wind speed of 8.42[m/s]. Right: (top) Seasonal wind speed profile as wind speed index (variation from mean wind speed), (bottom) Hourly wind speed profile. (Source: <https://globalwindatlas.info/>)

3.2.2 SOLAR RADIATION CHARACTERIZATION

The amount of sunlight available in each location at a given time is essential information in the design and evaluation of a photovoltaic system. The solar radiation may be characterized by the measured solar irradiance (power per area at a given moment) (or radiation) and by the solar insolation (total amount of solar energy received at a particular location during a specified period) (S.G.Bowden 2019).

Solar insolation data can be used for rough estimations in simple PV system design while solar irradiance is used in more accurate evaluation of PV system performance which calculates the system performance at each point in the day. The used methods for photovoltaic system evaluation in this document are based on solar irradiance data. Figure 3-10 shows an example of seasonal variation on daily insolation and solar irradiance.

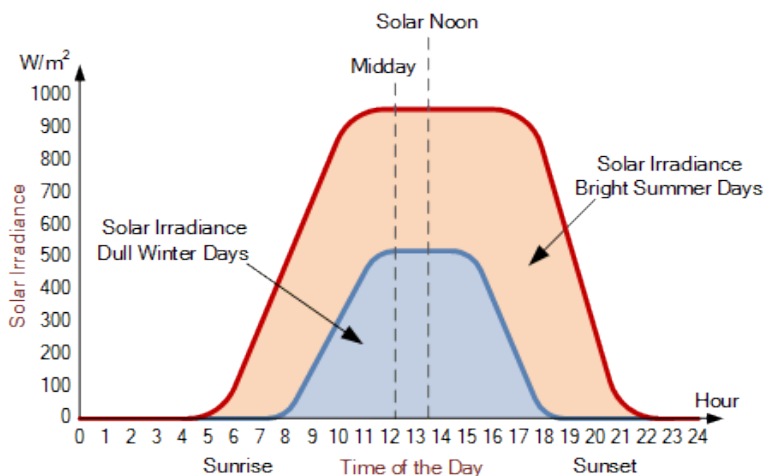


Figure 3-10 Example of seasonal variation on daily insolation and solar irradiance (source: <https://www.alternative-energy-tutorials.com/solar-power/solar-irradiance.html>)

The most common format for solar radiation data is the Typical Meteorological Year (TMY) data (S.G.Bowden 2019). In the process of estimation of the TMY data, meteorological measurements are made at hourly intervals over several years to build up a picture of the local climate. The data set is produced by choosing for each month the most "typical" month out of number of measured years of data. Typically, the variables used to select the typical month are global horizontal irradiance, air temperature, and relative humidity.

The TMY data set typically includes the following relevant quantities for PV evaluation:

- Date and time: The data is usually an average for the hour and covers ½ an hour before the sample to ½ an hour after the sample.
- Global Horizontal Irradiation (*GHI*): The amount of energy striking a horizontal surface during the hour.
- Direct Beam/Normal Irradiation (*DNI*): The irradiation striking a plate perpendicular to the sun's rays but does not include diffuse radiation.
- Diffuse Horizontal Irradiance (*DHI*): the amount of radiation received per unit area by a surface that does not arrive on a direct path from the sun but has been scattered by molecules and particles in the atmosphere.
- Temperature: Air temperature at 2 meters
- Wind Speed: total wind speed at 10 meters.

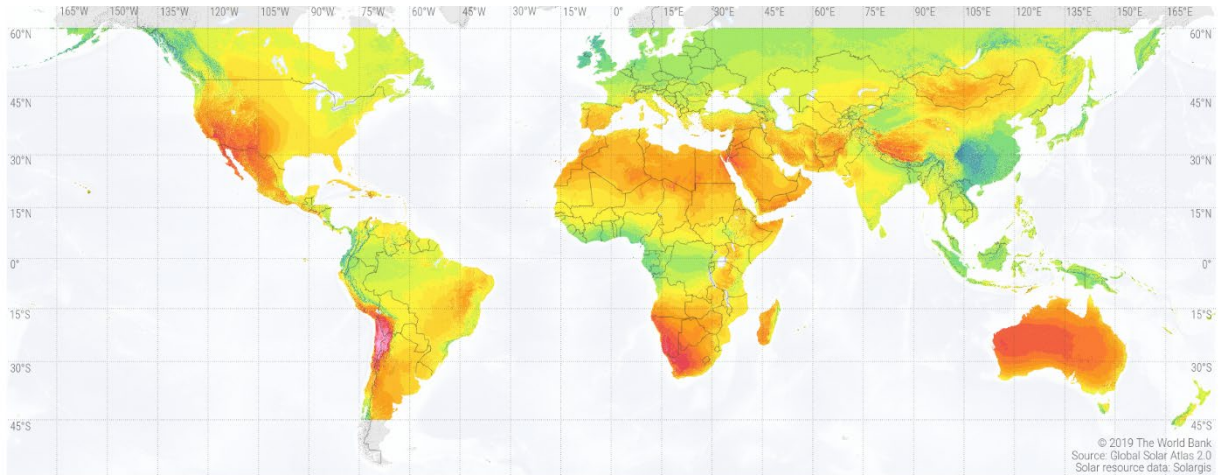
Deliverable 2.2

Assessment of applicable renewable energy generation technologies on NRA land and assets



SOLAR RESOURCE MAP

DIRECT NORMAL IRRADIATION



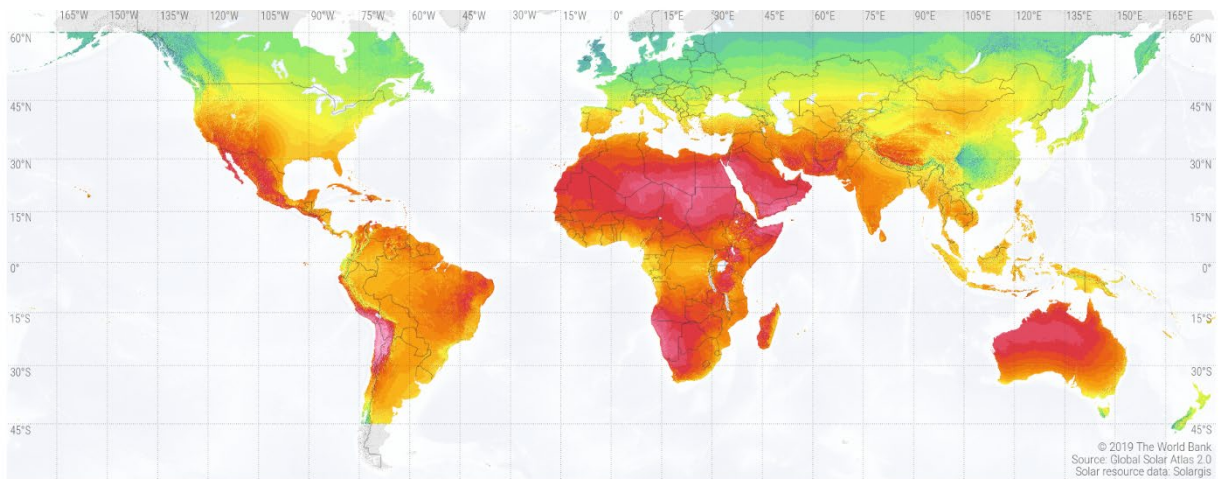
Long-term average of direct normal irradiation (DNI)

Daily totals:	1.0	2.0	3.0	4.0	5.0	6.0	7.0	8.0	9.0	10.0	
Yearly totals:	365	730	1095	1461	1826	2191	2556	2922	3287	3652	kWh/m ²

This map is published by the World Bank Group, funded by ESMAP, and prepared by Solargis. For more information and terms of use, please visit <http://globalsolaratlas.info>.

SOLAR RESOURCE MAP

GLOBAL HORIZONTAL IRRADIATION



Long-term average of global horizontal irradiation (GHI)

Daily totals:	2.2	2.6	3.0	3.4	3.8	4.2	4.6	5.0	5.4	5.8	6.2	6.6	7.0	7.4	
Yearly totals:	803	949	1095	1241	1387	1534	1680	1826	1972	2118	2264	2410	2556	2702	kWh/m ²

This map is published by the World Bank Group, funded by ESMAP, and prepared by Solargis. For more information and terms of use, please visit <http://globalsolaratlas.info>.

Figure 3-11 Example of Global Solar Atlas (World Bank Group 2021), (top) Direct normal irradiation and (bottom) global horizontal irradiation (source: <https://globalsolaratlas.info/download>)

Deliverable 2.2

Assessment of applicable renewable energy generation technologies on NRA land and assets



TMY data can be obtained from different data sources, depending on the location and availability of data. A global solar atlas (World Bank Group 2021) has been developed by the World Bank Group, and Figure 3-11 shows an example of the global map of direct normal irradiation and global horizontal irradiation provided by the global solar atlas app. Also, the National Renewable Energy Laboratory (NREL) has published a National Solar Radiation Database (NSRDB) with global irradiation datasets, which are available for download (National Renewable Energy Laboratory 2021). Also, NREL has created EnergyPlus, a free simulation software package, developed under funding from the US Department of Energy, and has published TMY data covering the period from 2006 and 2021 for about 16,000 locations globally, with most of them available at no cost from their website (NREL - EnergyPlus 2021).

On the other hand, the Photovoltaic Geographical Information System (PVGIS) (European Commission - EU Science Hub 2020) provides free and open access to information about solar radiation and photovoltaic system performance for any location in Europe and Africa, as well as a large part of Asia and America. Figure 3-12 shows an example of TMY data obtained from PVGIS tool for a specific location at 43.342° Latitude and -4.145° Longitude. The calculation of solar radiation in PVGIS uses information about the local horizon to estimate the effects of shadows from nearby hills or mountains.

The total amount of radiation received by a PV module, G_{PV} , is composed of direct (beam), B_{PV} , and diffuse, D_{PV} , components:

$$G_{PV} = B_{PV} + D_{PV}$$

The beam component is the irradiance perpendicular to the PV surface. For PV systems with 2-axis trackers, which allow adjusting themselves to face the sun (as sunflowers do), the beam component is the DNI from TMY data. However, most of the PV systems are fully/partially fixed in place and don't rotate (with few variations in their orientation/tilt angle manually done through the year), so the PV module only gets a portion of the DNI component from TMY data.

Deliverable 2.2

Assessment of applicable renewable energy generation technologies on NRA land and assets

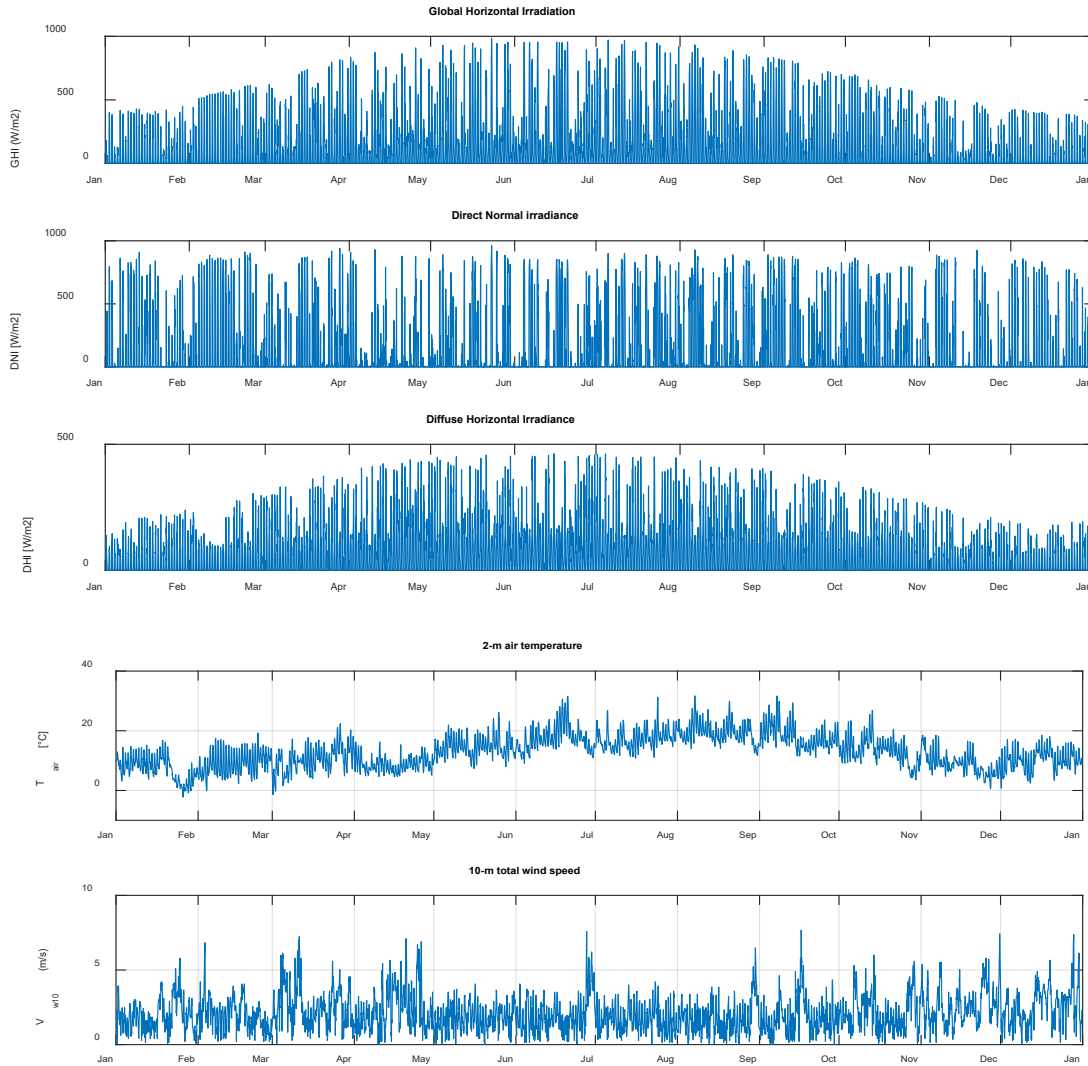


Figure 3-12 Example of TMY data obtained from PVGIS tool (European Commission - EU Science Hub 2020) for a specific location at 43.342° Latitude and -4.145° Longitude

Figure 3-13 shows the PV module tilt (β_{Mod}) and azimuth angle (ψ_{Mod}) definition, which is used in this document. The PV module beam component can be calculated by

$$\begin{aligned}
 B_{PV} = & DNI \cdot (\sin(\delta_{sun}) \cdot \sin(\varphi_{Lat}) \cdot \cos(\beta_{Mod}) \dots \\
 & - \sin(\delta_{sun}) \cdot \cos(\varphi_{Lat}) \cdot \sin(\beta_{Mod}) \cdot \cos(\psi_{Mod}) \dots \\
 & + \cos(\delta_{sun}) \cdot \cos(\varphi_{Lat}) \cdot \cos(\beta_{Mod}) \cdot \cos(HRA) \dots \\
 & + \cos(\delta_{sun}) \cdot \sin(\varphi_{Lat}) \cdot \sin(\beta_{Mod}) \cdot \cos(\psi_{Mod}) \cdot \cos(HRA) \dots \\
 & + \cos(\delta_{sun}) \cdot \sin(\psi_{Mod}) \cdot \sin(\beta_{Mod}) \cdot \sin(HRA)
 \end{aligned}$$

Deliverable 2.2

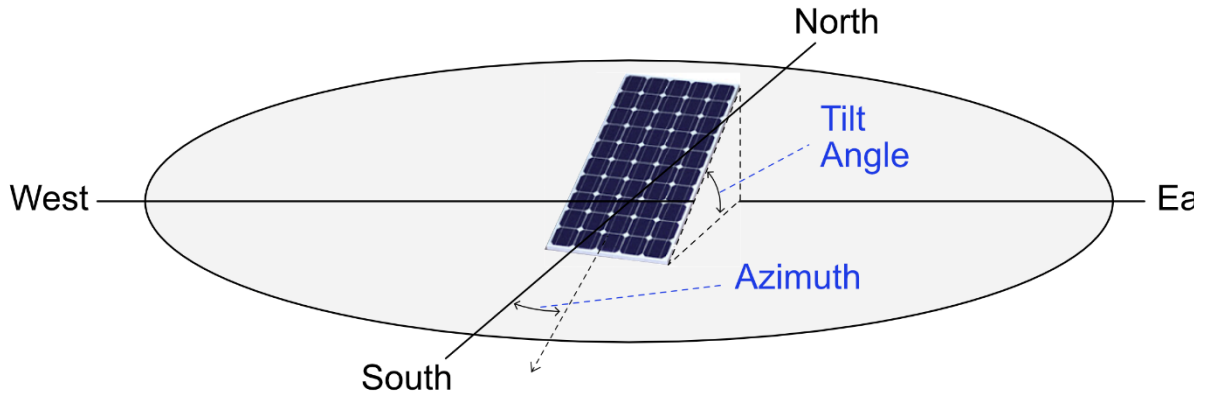


Figure 3-13 PV module tilt and azimuth angle definition (source: <https://solar designguide.com/solar-panel-tilt-and-azimuth/>)

Where, δ_{sun} is the sun declination angle, φ_{Lat} is the latitude of the location, and HRA is the solar hour angle. The sun declination angle in decimal degrees can be calculated by (Cooper 1969):

$$\delta_{sun} = -23.45^\circ \cdot \cos\left(\frac{360 \cdot (d_{year} + 10)}{365}\right)$$

Where, d_{year} is the number of days since the start of the year.

The solar hour angle in decimal degrees can be calculated by (S.G.Bowden 2019):

$$HRA = 15^\circ \cdot (LST - 12)$$

$$LST = LT + \frac{TC}{60}$$

$$TC = 4 \cdot (\lambda_{Lon} - 15^\circ \cdot \Delta T_{UTC}) + EoT$$

Where, LST is the local solar time, LT is the local time, TC is the time correction factor, λ_{Lon} is the longitude of the location in decimal degrees, ΔT_{UTC} is the difference of LT from Universal Coordinated Time (UTC) in hours, and EoT is the equation of time in minutes, which can be approximated by (Milne 1921):

Deliverable 2.2

Assessment of applicable renewable energy generation technologies on NRA land and assets

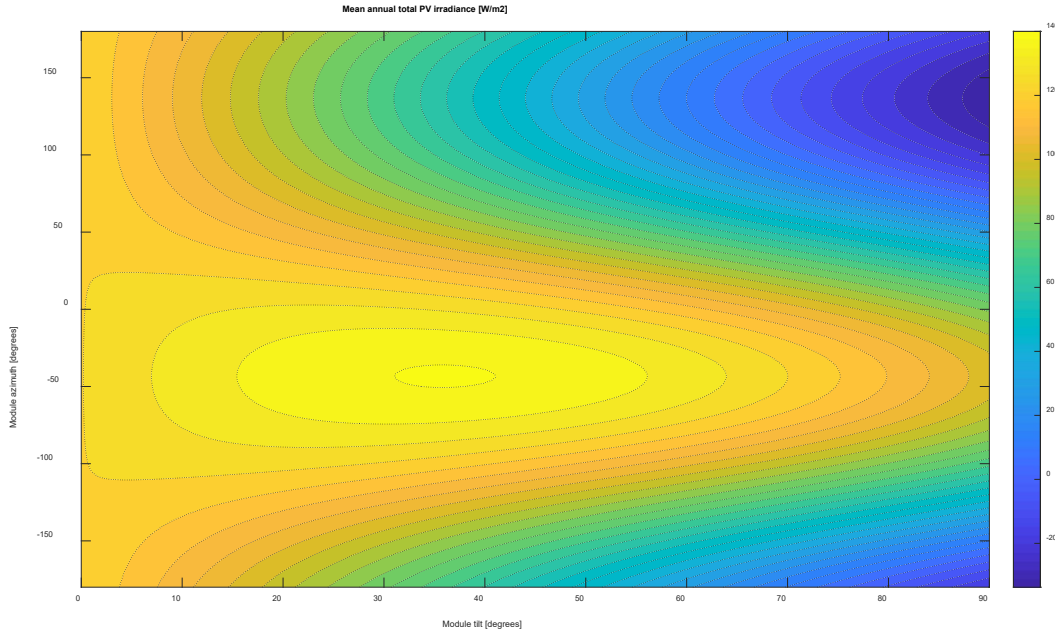


Figure 3-14 Mean annual total PV irradiance as function of module tilt and module azimuth for the TMY data plotted in Figure 3-12. Location: 43.342° Latitude and -4.145° Longitude

$$EoT = 9.87 \cdot \sin\left(\frac{720 \cdot (d_{year} - 81)}{365}\right) - 7.53 \cdot \cos\left(\frac{360 \cdot (d_{year} - 81)}{365}\right) - 1.5 \\ \cdot \sin\left(\frac{360 \cdot (d_{year} - 81)}{365}\right)$$

On the other hand, the PV module diffuse component can be approximated by (S.G.Bowden 2019) :

$$D_{PV} = DHI \cdot \frac{180^\circ - \beta_{Mod}}{180^\circ}$$

Combining the previous equations with the TMY data, it is possible to calculate the total PV irradiance for an arbitrary oriented and tilted PV module. Figure 3-14 shows the mean annual total PV irradiance as function of module tilt and module azimuth for the TMY data plotted in Figure 3-12 (location: $\varphi_{Lat} = 43.342^\circ$, $\lambda_{Lon} = -4.145^\circ$). It can be noted that there is an optimal module orientation and tilt angle that maximize the total annual average PV irradiance (for this example, the optimal values are $\beta_{Mod.OPT} = 36^\circ$ and $\psi_{Mod.OPT} = -44^\circ$).

3.3 MODELLING AND PARAMETRIZATION OF WIND TURBINES

3.3.1 POWER CURVE MODEL

In general, a wind turbine transforms the kinetic energy of the wind in rotating mechanical energy through its blades/rotor and then converts that energy in electric power using an electric generator, which is commonly interfaced by a power electronics converter and power transformer to ensure the right voltage level. For large scale wind turbines, all the previous conversion stages can be considered as part of the wind turbine device as they are normally located inside of the wind turbine nacelle, while for small scale wind turbines, the power converter and transformer are normally considered as additional components of the wind turbine.

Normally, the generated electrical power versus wind speed curve (also known as power curve) can be found in the wind turbine datasheet, which is provided by the wind turbine manufacturer to quantify the wind turbine performance. For a given wind turbine with provided power curve $P_{WT}(v_w)$, the expected annual energy production (AEP_{WT}) can be calculated by

$$AEP_{WT} = 8760 \cdot k_{WTA} \cdot \sum_{i=1}^{N_{vw}} P_{WT}(v_{wi}) \cdot f_W(v_{wi}) \quad (7)$$

where the full span of wind speeds from cut-in to cut-out wind speed has been discretized into N_{vw} wind speed bins with equal width, and the total AEP is calculated by summing all contributions of each wind speed bin, v_{wi} is the wind speed of the i -th bin at the wind turbine hub height, and f_W is the wind speed PDF of the area of interest scaled to the wind turbine hub height. The factor k_{WTA} is the wind turbine availability, so the product $8760 \cdot k_{WTA}$ estimates the annual operation hours of the wind turbine.

The wind turbine power curve is unique characteristic of the wind turbine which depends on many factors like aerodynamic blade performance, electric components (generator type, converter architecture, ...) and power control strategy, among others. However, there are two well defined power curve shapes depending on the applied control strategy for high wind speeds (beyond rated wind speed), which can be classified as pitch-regulated and stall-regulated. Figure 3-15 shows a comparative example of pitch-regulated (red curve) and stall-regulated (blue curve) wind turbine power curves.

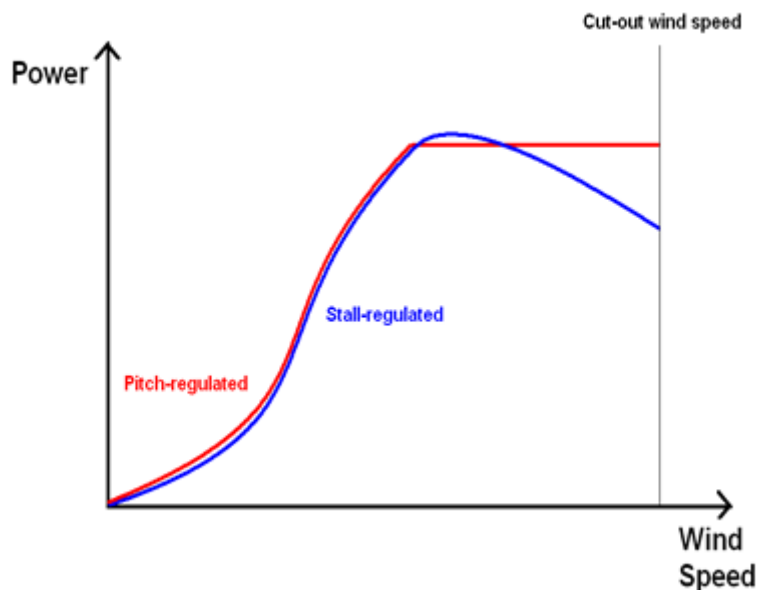


Figure 3-15 Comparison of typical wind turbine power curves: Pitch-regulated versus Stall-regulated

Pitch-regulated wind turbines have an active control system that can vary the pitch angle of the turbine blades, which allows to control/limit the turbine rotational speed, or the torque transferred to the shaft at high wind speeds. The pitch-regulated power curve is characterized by increasing power up until the rated wind speed, beyond which it keeps constant rated power up until a cut-out speed.

Stall-regulated wind turbines have their blades designed to perform in a way that at high wind speeds the rotational speed or aerodynamic torque decreases with increasing wind speed above a certain value (usually beyond the rated wind speed) to protect the wind turbine without the need for active controls.

Stall-regulated wind turbines have the benefit of lower capital cost of the turbine and a lower maintenance associated with more moving parts. However, pitch-regulated systems can deliver constant power output above rated wind speed, while stall-regulated systems are not able to keep a constant power output in high winds. Pitch-regulated control system is more commonly used for large wind turbines (MW) while stall-regulated control is always used in very small wind turbines.

Deliverable 2.2

To provide a general approach aiming to compare wind turbine technologies but not individual wind turbines, the following approach is proposed to estimate the wind turbine power curve.

Figure 3-16 shows the considered power curve model for large scale wind turbines, which is based on pitch-regulated control system. The power curve has three main regions, from the cut-in wind speed ($v_{w.in}$), the wind turbine is operated following Maximum Power Point Tracking (MPPT) algorithm, and the generated electric power increases following the wind speed up to it reaches its rated power ($P_{WT.nom}$) at the nominal wind speed ($v_{w.nom}$); then from the nominal wind speed to the cut-out wind speed ($v_{w.out}$), the output power is constant and equal to the rated power, and there is not output power for wind speeds lower than $v_{w.in}$ or higher than $v_{w.out}$ as the wind turbine is parked. Then, considering that the generated wind power is proportional to the cube of wind speed and swept area (A_{swept}), the following power function is proposed:

$$P_{WT} = \begin{cases} \frac{1}{2} \cdot k_{PWT0} \cdot \rho_{air} \cdot A_{swept} \cdot v_w^3 & v_{w.in} \leq v_w \leq v_{w.nom} \\ P_{WT.nom} & v_{w.nom} \leq v_w \leq v_{w.out} \\ 0 & v_w < v_{w.in}; v_w > v_{w.out} \end{cases}$$

where ρ_{air} is the average air density, and k_{PWT0} is the equivalent power coefficient, which accounts for the wind turbine power coefficient (C_p) and the combined generator-power converter efficiency (η_{GPE}).

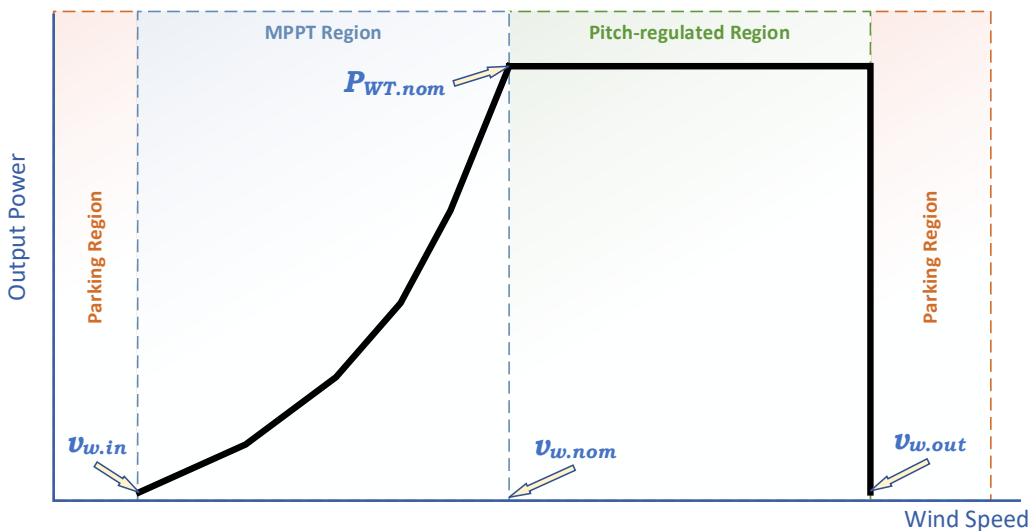


Figure 3-16 Considered power curve model for large scale wind turbines

Deliverable 2.2

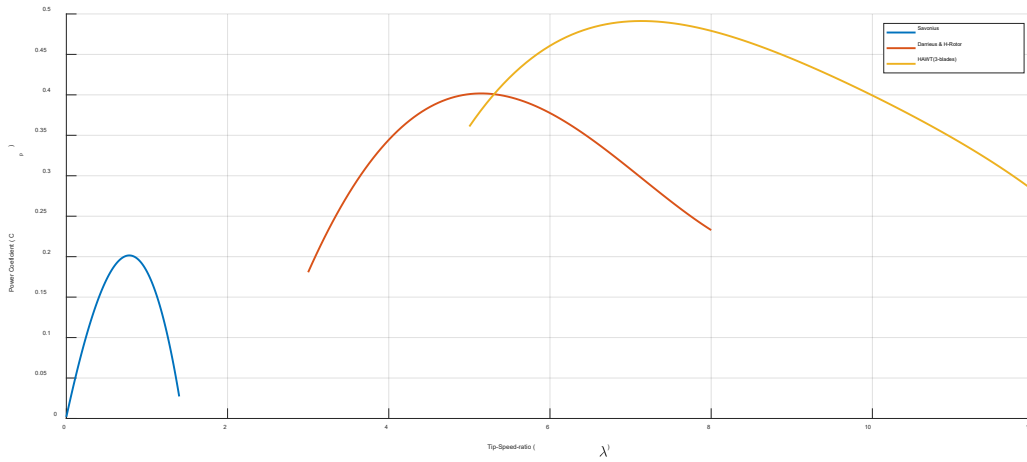


Figure 3-17 Power coefficient comparison for the considered wind turbine technologies

For comparison, Figure 3-17 shows the standard power coefficient for the considered wind turbine technologies as function of the tip-speed ratio ($\lambda = \omega_R \cdot R/v_w$), which is the ratio of the linear speed of the blades and the wind speed.

The combined generator and power electronic converter nominal efficiency has been approximated by the following equation:

$$\eta_{GPE}(P_{WT.nom}) = \eta_{GPEMX} - (\eta_{GPEMX} - \eta_{GPEMN}) \cdot \left(\frac{P_{Nref}}{P_{WT.nom} + P_{Nref}} \right)^{k_{\eta_{GPE}}}$$

$$k_{\eta_{GPE}} = \frac{\log\left(\frac{\eta_{GPEMX} - \eta_{GPEMN}}{\eta_{GPEMX} - \eta_{GPEref}}\right)}{\log(2)}$$

where η_{GPEref} is the reference efficiency at reference nominal power P_{Nref} and η_{GPEMX} , η_{GPEMN} are the maximum and minimum considered efficiencies. Figure 3-18 shows the considered combined generator and power electronic converter nominal efficiency for large scale wind turbines. The reference parameters are $\eta_{GPEref} = 0.82$, $P_{Nref} = 1MW$, $\eta_{GPEMX} = 0.92$ and $\eta_{GPEMN} = 0.6$.

Then, k_{PWT0} is calculated by

$$k_{PWT0} = C_{pMAX} \cdot \eta_{GPE}(P_{WT.nom})$$

With C_{pMAX} as the maximum power coefficient for the wind turbine technology ($C_{pMAX} = 0.5$ for HAWT and $C_{pMAX} = 0.4$ for Darrieus technologies).

Deliverable 2.2

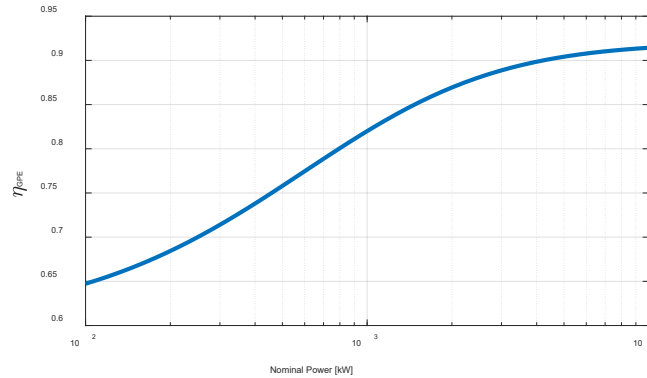


Figure 3-18 Considered combined generator and power electronic converter nominal efficiency for large scale wind turbines.

Figure 3-19 shows the considered power curve model for small scale wind turbines, which is based on stall-regulated control system. The power curve has four main regions:

- Parking region: There is not output power for wind speeds lower than $v_{w.in}$ or higher than $v_{w.out}$ as the wind turbine is parked.
- MPPT Region: The wind turbine is operated following MPPT algorithm, and the generated electric power increases following the wind speed from $v_{w.in}$ up to it reaches its $P_{WT.nom}$ at $v_{w.nom}$.
- Regulated Region 1: After wind turbine reaches its nominal wind speed, the power still increases with the wind speed but with a decreased ratio compared with the MPPT region as the generator speed is kept constant and the turbine power coefficient decreases from its maximum. This continues up to the output power reaches its peak value ($P_{WT.peak}$) at wind speed equal to $v_{w.peak}$.
- Regulated Region 2: In this region, the power decreases with increasing wind speed as the aerodynamic design of the blade is more predominant and the blades are designed to perform better at low wind speeds. The wind turbine is operated under these conditions up to the $v_{w.out}$ is reached, then it is braked to protect the equipment.

Deliverable 2.2

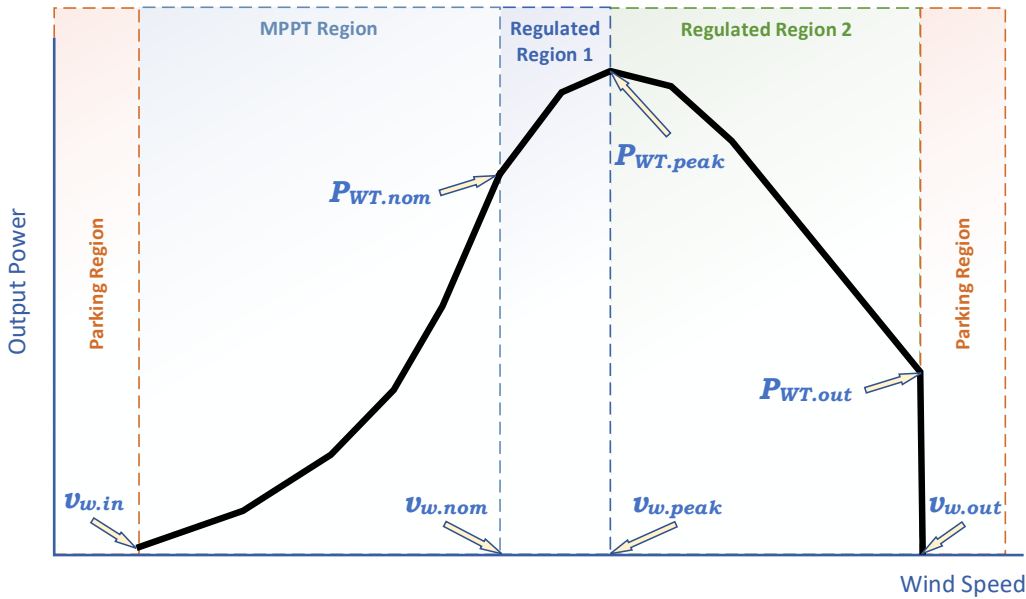


Figure 3-19 Considered power curve model for small scale wind turbines

The following power model is proposed for small wind turbines:

$$P_{WT} = \begin{cases} \frac{1}{2} \cdot k_{PWT0} \cdot \rho_{air} \cdot A_{swept} \cdot v_w^3 & v_{w.in} \leq v_w \leq v_{w.nom} \\ P_{WT.peak} - k_{PWT1} \cdot |v_w - v_{w.peak}|^{k_{PWTn}} & v_{w.nom} \leq v_w \leq v_{w.peak} \\ P_{WT.peak} - k_{PWT2} \cdot |v_w - v_{w.peak}|^{k_{PWTn}} & v_{w.peak} \leq v_w \leq v_{w.out} \\ 0 & v_w < v_{w.in}; v_w > v_{w.out} \end{cases}$$

where k_{PWT0} , k_{PWT1} , k_{PWT2} , and k_{PWTn} are the characteristic parameters of the wind turbine power curve which are fitted as function of the relation between nominal/peak power and wind speed values which varies with the turbine size. The maximum equivalent power coefficient (k_{PWT0}) is related to $v_{w.nom}$ and $P_{WT.nom}$ as follows:

$$k_{PWT0} = \frac{2 \cdot P_{WT.nom}}{\rho \cdot A_{swept} \cdot v_{w.nom}^3}$$

The parameter k_{PWT1} is estimated to fit continuity in the power curve at nominal wind speed:

$$k_{PWT1} = \begin{cases} \frac{P_{WT.peak} - P_{WT.nom}}{|v_{w.nom} - v_{w.peak}|^{k_{PWTn}}} & v_{w.nom} < v_{w.peak} \\ 0 & v_{w.nom} = v_{w.peak} \end{cases}$$

Deliverable 2.2

Assessment of applicable renewable energy generation technologies on NRA land and assets



The parameter k_{PWTn} is estimated to keep same rate of change in power curve at nominal wind speed:

$$\frac{dP_{WT}}{dv_w} \Big|_{v_{w.nom(-)}} = \frac{dP_{WT}}{dv_w} \Big|_{v_{w.nom(+)}}$$
$$k_{PWTn} = \begin{cases} \frac{3 \cdot P_{WT.nom}}{v_{w.nom}} \cdot \left(\frac{v_{w.peak} - v_{w.nom}}{P_{WT.peak} - P_{WT.nom}} \right) & P_{WT.peak} > P_{WT.nom} \\ 0 & P_{WT.peak} = P_{WT.nom} \end{cases}$$

The parameter k_{PWT2} can be estimated by

$$k_{PWT2} = \begin{cases} \frac{P_{WT.peak} - P_{WT.out}}{|v_{w.out} - v_{w.peak}|^{k_{PWTn}}} & k_{PWT1} > 0 \\ 0 & k_{PWT1} = 0 \end{cases}$$

3.3.2 TOTAL CAPITAL COST

For large scale wind turbines, the total capital cost includes the grid connection (with a cost share between 9-14%), construction (with a cost share between 4-10%), wind turbine itself (with a cost share between 64-84%) and other capital costs (normally with a cost share between 4-10%) (International Renewable Energy Agency 2016).

As reported in (International Renewable Energy Agency 2016), typical total capital cost for onshore wind is between 1280 USD and 2290 USD per kW of electricity-producing capacity. The relative cost [EUR/kW] tends to decrease as turbine size increases, also the complexity and construction of the overall farm site is greatly reduced with fewer and larger turbines.

The total capital cost for large scale wind turbines can be estimated by

$$TCC_{WT} = \frac{Cost_{WT}}{k_{SCWT}}$$

Where, $Cost_{WT}$ is the wind turbine cost and k_{SCWT} is the wind turbine share cost, assumed to be 70% for large scale wind turbines ($k_{SCWT} = 0.7$).

Once built, operation & maintenance (O&M) maintenance is an ongoing expense, which is made up of the following:

Deliverable 2.2

Assessment of applicable renewable energy generation technologies on NRA land and assets



- Insurance
- Land rent
- Service, repair, and spare parts
- Administrative tasks
- Power (it does take some electricity to run)
- Miscellaneous

An estimation of O&M cost for typical onshore installation in European is reported in (International Renewable Energy Agency 2016) with 1.3 to 2.5 cents per kilowatt-hour produced. These recurring costs are not too significant, and the turbine will significantly outproduce the maintenance costs.

The total capital cost for small scale wind turbines can be approximated by

$$TCC_{WT} = Cost_{WT} + Cost_{PEWT} + Cost_{TWT}$$

Where $Cost_{PEWT}$ is the cost of the power electronics converter and $Cost_{TWT}$ is the cost of the tower and foundation.

As for the O&M cost in small wind turbines, it is reported in (International Renewable Energy Agency 2016) that 1 to 4 cents per kilowatt-hour produced (0.01-0.04 EUR/kWh) could be expected associated with O&M.

3.3.3 EXPECTED LIFETIME AND WARRANTY PERIOD

A warranty is normally designed to protect a product from the failure of its component parts over a specific period. A typical warranty will depend on the type of installed wind turbine and can be anything from 1 to 10 years. On the other hand, the wind turbine lifetime also depends on the wind turbine technology and specific used components. An empirical model proposed based on collected data is introduced in section 4.1.

3.4 MODELLING AND PARAMETRIZATION OF PHOTOVOLTAIC MODULES

3.4.1 PV MODEL AND CHARACTERISTIC CURVE

Deliverable 2.2

The electricity generated by the photovoltaic modules/panels depends mainly on the total amount of radiation received by a PV module (G_{PV}), the presence or not of shadows in the installation place, the control method, and the performance of the PV modules, which is associated to the PV module technology.

The electrical performance of the PV module is linked to its voltage-current (V-I) characteristic. Figure 3-20 illustrates the typical PV cell/module characteristic curve along with the relevant points in the curve: the short-circuit current, the open-circuit voltage and the voltage. Current and power at maximum power point (MPP) operation. Here, it is assumed that the PV control method follows the Maximum Power Point Tracking (MPPT) algorithm (Elbarbary 2021), so the maximum power output of the solar cell can always be obtained at different conditions.

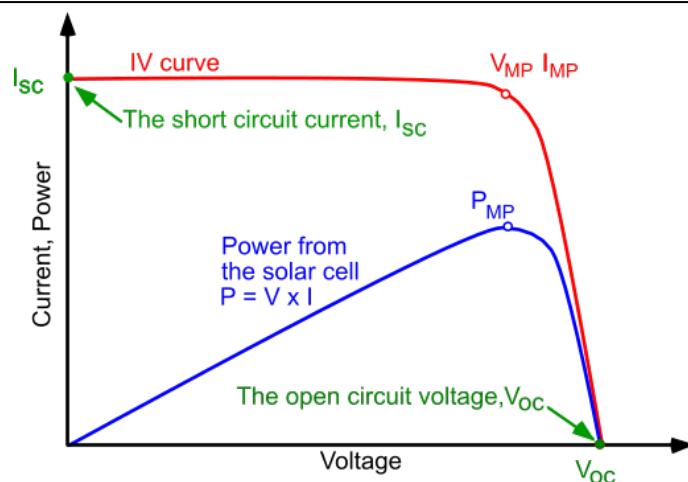


Figure 3-20 Illustration of PV cell characteristic curve, Maximum Power Point (MPP), short circuit current and Open circuit voltage. (Figure from (S.G.Bowden 2019))

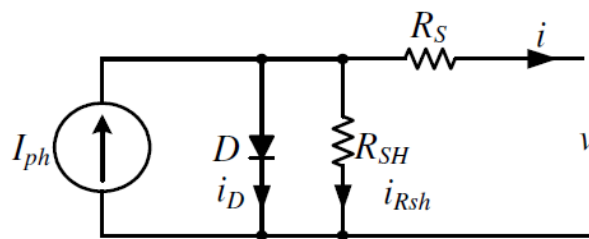


Figure 3-21 Equivalent circuit of a photovoltaic cell using the single exponential model (Dezso Sera 2007).

Deliverable 2.2

Assessment of applicable renewable energy generation technologies on NRA land and assets



The V-I characteristic of the PV module at standard test conditions (STC: Irradiance $G_{PV} = 1000 \text{ W/m}^2$ and module temperature $T_{Mod} = 25^\circ\text{C}$) can be estimated based on the equivalent circuit of a photovoltaic cell shown in Figure 3-21, and using the single exponential model as proposed in (Dezso Sera 2007):

$$i_{Mod} = I_{ph_{STC}} - I_{0_{STC}} \cdot \left(e^{\frac{v_{Mod} + i_{Mod} \cdot R_s}{n_{sMod} \cdot V_t}} - 1 \right) - \frac{v_{Mod} + i_{Mod} \cdot R_s}{R_{sh}}$$

$$V_t = A_{Mod} \cdot k \cdot \frac{T_{Mod_{STC}}}{q}$$

Where, i_{Mod} is the output module current, v_{Mod} is the module terminals voltage, k is Boltzmann's constant, q is the charge of the electron, n_{sMod} is the number of cells in the module connected in series, $T_{Mod_{STC}}$ is the temperature at STC ($T_{Mod_{STC}} = 25^\circ\text{C}$), and the five model parameters:

- $I_{ph_{STC}}$: the photo-generated current in STC,
- $I_{0_{STC}}$: the dark saturation current in STC,
- R_s : the module series resistance,
- R_{sh} : the module parallel/shunt resistance,
- A_{Mod} : the diode quality (ideality) factor.

Here, the method proposed in (Dezso Sera 2007) has been implemented to estimate the PV model parameters as function of the three key points of the V-I characteristic, normally provided in the datasheet of the PV module: the short-circuit point, the open-circuit point and the maximum power point (MPP), defined by the following values:

- $I_{SC_{STC}}$: short-circuit current in STC
- $V_{OC_{STC}}$: Open- circuit voltage in STC
- $V_{MPP_{STC}}$: Voltage at MPP in STC
- $I_{MPP_{STC}}$: Current at MPP in STC
- $P_{MPP_{STC}}$: Power at MPP in STC

Deliverable 2.2

Assessment of applicable renewable energy generation technologies on NRA land and assets



Table 3 Example of PV Module typical datasheet information for Monocrystalline modules series NeON R from LG manufacturer

Mechanical Properties

Cells	6 x 10
Cell Vendor	LG
Cell Type	Monocrystalline / N-type
Cell Dimensions	161.7 x 161.7 mm
# of Busbar	30 (Multi Ribbon Busbar)
Dimensions (L x W x H)	1,700 x 1,016 x 40 mm
Front Load*	6,000Pa
Rear Load*	5,400Pa
Weight	17.5 kg
Connector Type	MC4/MC
Junction Box	IP68 with 3 Bypass Diodes
Cables	1,000 mm x 2 ea
Glass	High Transmission Tempered Glass
Frame	Anodized Aluminium

*Manufacturer Declaration according to IEC 61215 : 2005 (Preliminary)
 *Mechanical Test Loads 5400 Pa / 4000 Pa based on IEC61215-2 : 2016
 (Test Load = Design Load x Safety Factor (1.5))

Temperature Characteristics

NMOT	[°C]	44 ± 3
Pmax	[%/°C]	-0.30
Voc	[%/°C]	-0.24
Isc	[%/°C]	0.037

Electrical Properties (STC³)

Model		LG375Q1C-V5	LG370Q1C-V5	LG365Q1C-V5	LG360Q1C-V5
Maximum Power (Pmax)	[W]	375	370	365	360
MPP Voltage (Vmpp)	[V]	37.2	37.0	36.7	36.5
MPP Current (Impp)	[A]	10,09	10,01	9,95	9,87
Open Circuit Voltage (Voc)	[V]	42,8	42,8	42,8	42,7
Short Circuit Current (Isc)	[A]	10,83	10,82	10,8	10,79
Module Efficiency	[%]	21,7	21,4	21,1	20,8
Operating Temperature	[°C]	-40 ~ +90			
Maximum System Voltage	[V]	1,000			
Maximum Series Fuse Rating	[A]	20			
Power Tolerance	[%]	0 ~ +3			

³ 1) STC (Standard Test Condition): Irradiance 1,000 W/m², module temperature 25°C, AM 1.5.

Electrical Properties (NMOT⁴)

Model		LG375Q1C-V5	LG370Q1C-V5	LG365Q1C-V5	LG360Q1C-V5
Maximum Power (Pmax)	[W]	282	279	275	270
MPP Voltage (Vmpp)	[V]	37,1	36,9	36,6	36,4
MPP Current (Impp)	[A]	7,61	7,55	7,51	7,45
Open Circuit Voltage (Voc)	[V]	40,3	40,3	40,2	40,2
Short Circuit Current (Isc)	[A]	8,72	8,71	8,7	8,69

⁴ NMOT (Nominal Module Operating Temperature): Irradiance 800 W/m², Ambient temperature 20 °C, Wind speed 1 m/s, Spectrum AM 1.5

Table 3 shows an example of typical information provided in the module datasheet, for this example the monocrystalline modules series NeON-R from LG manufacturer have been considered.

Once the PV model parameters have been estimated, then the V-I characteristic of the PV module at different conditions (G_{PV} and T_{Mod}) can be evaluated as follows:

$$i_{Mod} = I_{ph}(G_{PV}, T_{Mod}) - I_0(G_{PV}, T_{Mod}) \cdot \left(e^{\frac{v_{Mod} + i_{Mod} \cdot R_s}{n_{sMod} \cdot V_t}} \right) - \frac{v_{Mod} + i_{Mod} \cdot R_s}{R_{sh}}$$

$$V_t = A_{Mod} \cdot k \cdot \frac{T_{Mod}}{q}$$

$$I_{ph}(G_{PV}, T_{Mod}) = I_0(G_{PV}, T_{Mod}) \cdot e^{\frac{V_{OC}}{n_{sMod} \cdot V_t}} + \frac{V_{OC}}{R_{sh}}$$

$$I_0(G_{PV}, T_{Mod}) = \left(I_{SC}(G_{PV}, T_{Mod}) - \frac{V_{OC}(G_{PV}, T_{Mod}) - I_{SC}(G_{PV}, T_{Mod}) \cdot R_s}{R_{sh}} \right) \cdot e^{\frac{-V_{OC}(G_{PV}, T_{Mod})}{n_{sMod} \cdot V_t}}$$

$$I_{SC}(G_{PV}, T_{Mod}) = \frac{G_{PV}}{1000} \cdot I_{SCSTC} \cdot \left(1 + \frac{k_{iMod}}{100} \cdot (T_{Mod} - T_{ModSTC}) \right)$$

Deliverable 2.2

$$V_{OC}(G_{PV}, T_{Mod}) = n_{sMod} \cdot V_t \cdot \log\left(\frac{I_{ph*} \cdot R_{sh} - V_{OC}(G_{PV}, T_{Mod})}{I_{0T} \cdot R_{sh}}\right)$$

$$I_{ph*} = \frac{G_{PV}}{1000} \cdot \left(I_{0T} \cdot e^{\frac{V_{OCT}}{n_{sMod} \cdot V_t}} + \frac{V_{OCT}}{R_{sh}} \right)$$

$$I_{0T} = \left(I_{SC}(G_{PV}, T_{Mod}) - \frac{V_{OCT} - I_{SC}(G_{PV}, T_{Mod}) \cdot R_s}{R_{sh}} \right) \cdot e^{\frac{-V_{OCT}}{n_{sMod} \cdot V_t}}$$

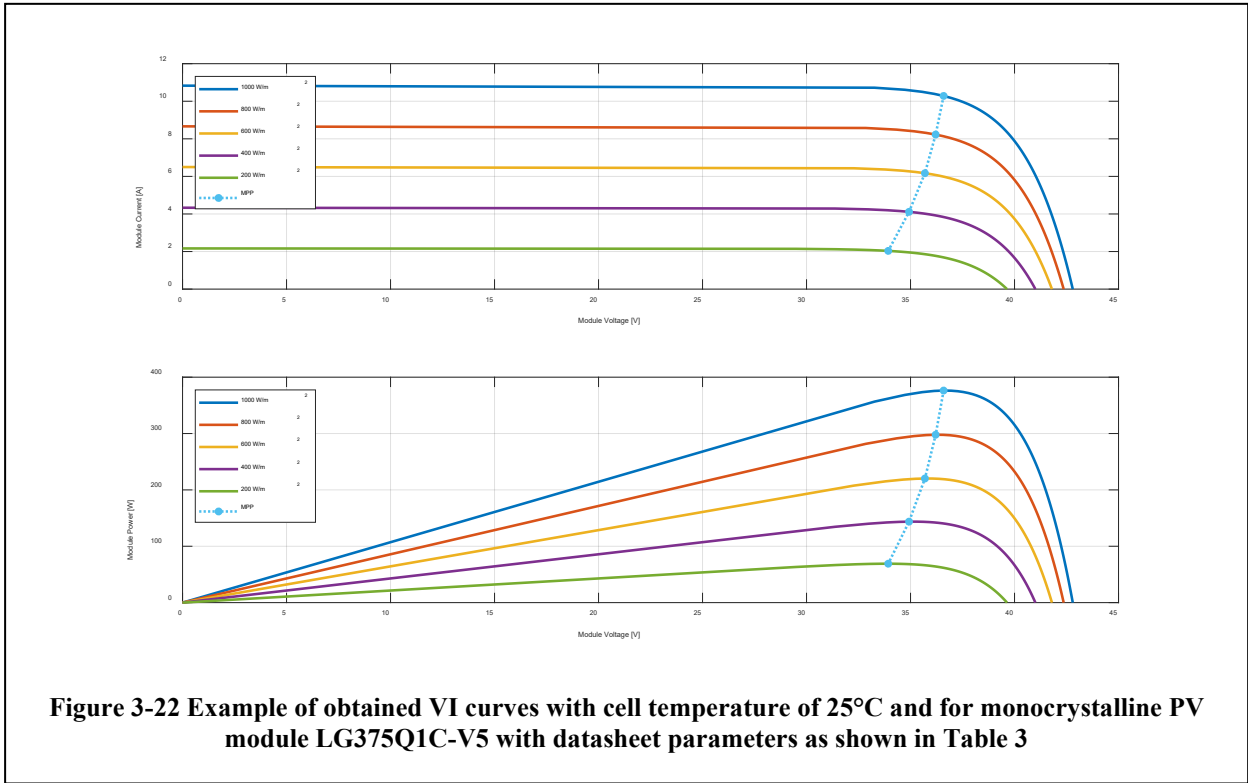
$$V_{OCT} = V_{OCSTC} \cdot \left(1 + \frac{k_{vMod}}{100} \cdot (T_{Mod} - T_{ModSTC}) \right)$$

Where, k_{iMod} and k_{vMod} are the thermal coefficients for short-circuit current (I_{SC}) and open-circuit voltage (V_{OC}), respectively, and the other variables and parameters as previously defined. Then, the MPP operating condition can be found by

$$\left. \frac{d(i_{Mod} \cdot v_{Mod})}{dv_{Mod}} \right|_{v_{Mod}=V_{MPP}} = 0$$

Figure 3-22 shows an example of obtained VI curves with cell temperature of 25°C and for monocrystalline PV module LG375Q1C-V5 with datasheet parameters as shown in Table 3.

Deliverable 2.2



Normally, the G_{PV} can be obtained from TMY data following the methodology described in section 3.2.2, however, the module temperature will depend on the PV module operating point and the amount of radiation received. The module temperature can be estimated using the steady-state thermal model for the PV module presented in (Hammami, et al. 2017), which is adapted and summarized here for the sake of completeness. First, the steady-state thermal balance equation for the PV module is:

$$G_{PV} \cdot A_{Mod} - \rho_{RPV} \cdot G_{PV} \cdot A_{Mod} - P_{MPP} - Q_{TotalPV} = 0$$

Where, A_{Mod} is the area of the PV module, the term $G_{PV} \cdot A_{Mod}$ is the total incident power, the term $\rho_{RPV} \cdot G_{PV} \cdot A_{Mod}$ is the total radiative power reflected from the PV module glass surface with reflection index $\rho_{RPV} = 0.1$, P_{MPP} is the output power generated by the PV module (assumed to be operated at MPP), and $Q_{TotalPV}$ is the total heat exchange of the PV module, which is composed by the convective heat exchange $Q_{ConvPVf}$ and the radiative heat exchange Q_{RadPVf} of the front (f) and back (b) sides of the PV module:

$$Q_{TotalPV} = Q_{ConvPVf} + Q_{RadPVf} + Q_{ConvPVb} + Q_{RadPVb}$$

Deliverable 2.2

$$Q_{RadPVf} + Q_{RadPVb} = (h_{RadPVf} + h_{RadPVb}) \cdot A_{Mod} \cdot (T_{Mod}^4 - T_{amb}^4)$$

$$Q_{ConvPVf} + Q_{ConvPVb} = h_{convPVfb} \cdot A_{Mod} \cdot (T_{Mod} - T_{amb})$$

Where, h_{RadPVf} , h_{RadPVb} are the radiative heat coefficient from front and back sides of the PV module, respectively, $h_{convPVfb}$ is the equivalent convective heat coefficient (front and back sides of the PV module) and T_{amb} is the ambient temperature. The radiative heat coefficient can be calculated by

$$h_{RadPVf} = \frac{\sigma}{1 + \frac{1 - \varepsilon_{PVf}}{\varepsilon_{PVf}} + \frac{1 - \varepsilon_{sky}}{\varepsilon_{sky}}}$$

$$h_{RadPVb} = \frac{\sigma}{1 + \frac{1 - \varepsilon_{PVb}}{\varepsilon_{PVb}} + \frac{1 - \varepsilon_{ground}}{\varepsilon_{ground}}}$$

Where ε_{PVf} and ε_{PVb} are the emissivity coefficients of the front (glass) and back (back sheet) of the PV module surfaces, respectively, ε_{sky} is the emissivity coefficient of the sky ($\varepsilon_{sky} = 0.91$ (Hammami, et al. 2017)), ε_{ground} is the emissivity coefficient of the ground ($\varepsilon_{ground} = 0.94$ (Hammami, et al. 2017)), and σ is the Stephan-Boltzmann constant ($\sigma = 5.67 \times 10^{-8} \frac{W}{m^2 \cdot K^4}$). For silicon crystalline PV modules the emission coefficient can be approximated to $\varepsilon_{PVf} = 0.91$ and $\varepsilon_{PVb} = 0.85$, and therefore a fixed value for the total radiative heat coefficient ($h_{RadPVf} + h_{RadPVb}$) can be used for all the PV module. For the considered emission coefficients:

$$h_{RadPVf} + h_{RadPVb} = 47.34 nW/m^2 K^4 + 45.72 nW/m^2 K^4 = 9.305 nW/m^2 K^4$$

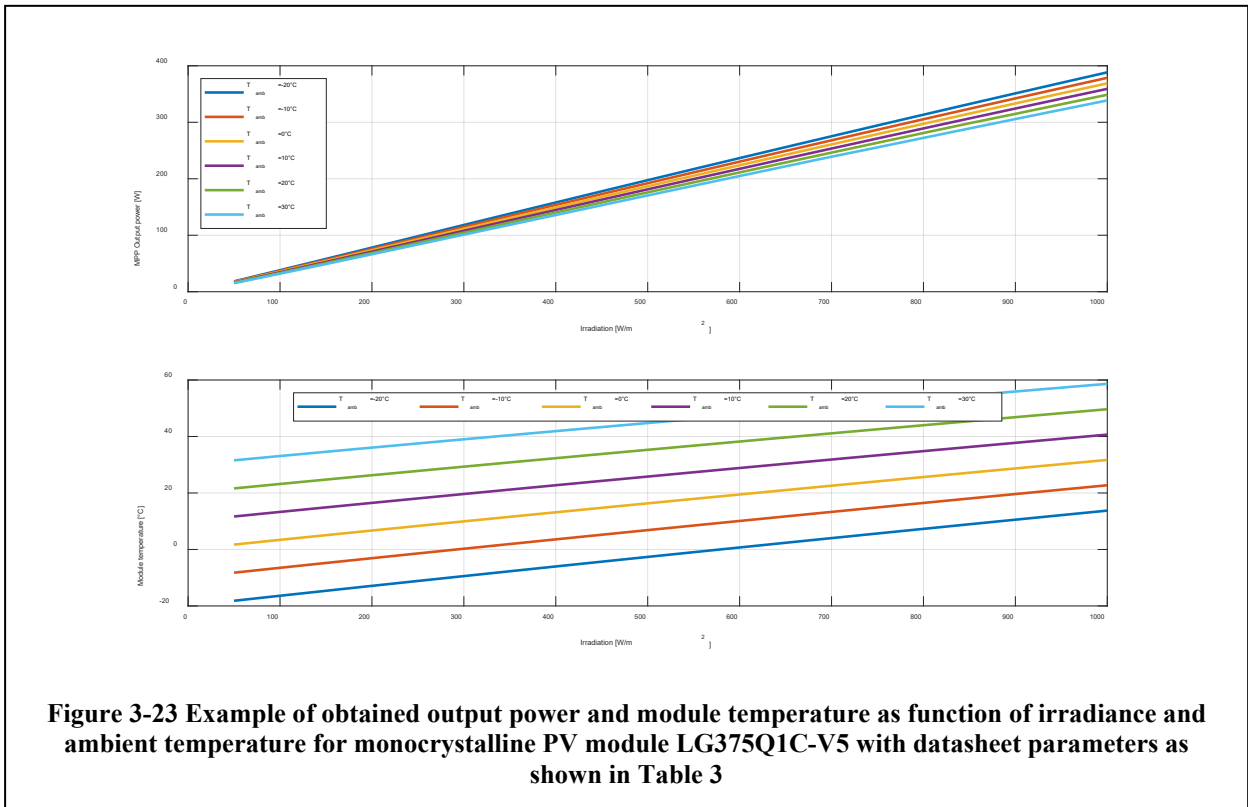
On the other hand, $h_{convPVfb}$ is calculated based on datasheet values for operating condition considering the Nominal Module Operating Temperature (NMOT), as following:

$$h_{convPVfb} = \frac{k_{hconvPV}}{v_{wNMOT}}$$

$$= \frac{G_{PVNMOT} \cdot (1 - \rho_{RPV}) - \frac{P_{MPPNMOT}}{A_{Mod}} - (h_{RadPVf} + h_{RadPVb}) \cdot (T_{ModNMOT}^4 - T_{ambNMOT}^4)}{(T_{ModNMOT} - T_{ambNMOT})}$$

Deliverable 2.2

Assessment of applicable renewable energy generation technologies on NRA land and assets



Where $G_{PV_{NMOT}}$, $P_{MPP_{NMOT}}$, $T_{Mod_{NMOT}}$, $T_{amb_{NMOT}}$, $v_{w_{NMOT}}$ are the values given for NMOT operating condition, which can be found at the PV module datasheet.

Figure 3-23 shows an example of obtained output power and module temperature as function of irradiance (G_{PV}) and ambient temperature for monocrystalline PV module LG375Q1C-V5 with datasheet parameters as shown in Table 3.

Finally, for a given PV module with defined voltage-current curve, the expected annual energy production ($AE_{P_{VM}}$) can be calculated by

$$AE_{P_{VM}} = \sum_{t_h=1}^{8760} P_{MPP}(G_{PV}(t_h), T_{amb}(t_h))$$

Where $G_{PV}(t_h)$ and $T_{amb}(t_h)$ are the time series for PV irradiance and ambient temperature that can be evaluated from available TYM data for the location of interest.

Deliverable 2.2

Assessment of applicable renewable energy generation technologies on NRA land and assets



3.4.2 TOTAL CAPITAL COST

The total capital cost for PV panels can be approximated by:

$$TCC_{PV} = N_{Mod} \cdot Cost_{Mod} + Cost_{PEPV} + Cost_{IPV}$$

Where N_{Mod} is the number of PV modules in the panel, $Cost_{PEPV}$ is the cost of the power electronics converter and $Cost_{IPV}$ is the cost of installing the PV system. $Cost_{PEPV}$ is modelled by

$$\frac{Cost_{PEPV}}{N_{Mod} \cdot P_{MPPSTC}} = Cost_{PEPV0} + k_{CPEPV0} \cdot (N_{Mod} \cdot P_{MPPSTC})^{k_{CPEPV1}}$$

According to the National Renewable Energy Laboratory (NREL), the racking system commonly costs about 0.10 USD per watt. Here, $Cost_{IPV}$ is assumed to be 0.3 EUR/W, which accounts for the cost to install the racks, labor cost for solar installation and other additional cost like permit fees, inspection fees and/or taxes. As a reference value, it has been reported in (IRENA 2021) an average total installed cost of PV utility-scale projects of 883 USD/kW.

3.4.3 EXPECTED LIFETIME AND WARRANTY PERIOD

The product warranty of the checked PV modules is between 5 years and 15 years, which varies depending on the manufacturer.

On the other hand, a performance guaranty of 25 years is typically given for crystalline silicon PV modules. This basically defines the expected lifetime of the module to be 25 years. The performance guaranty is normally associated to a linear output degradation provided by the manufacturer, which is the maximum output degradation per year that can be expected after the first year of usage. Collected data regarding maximum output degradation for the considered PV module technologies is presented in section 4.2

3.5 MODELLING OF OTHER COMPONENTS IN DEGS

3.5.1 DC/AC CONVERTER

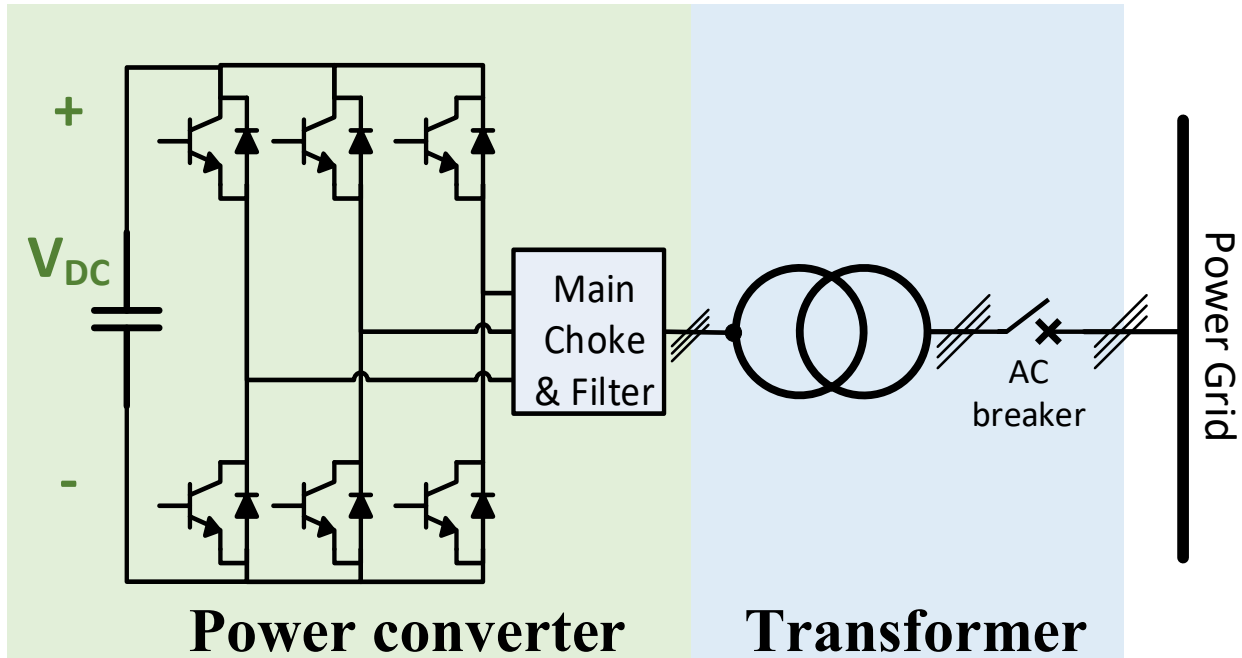


Figure 3-24 Considered DC/AC Converter topology

The Voltage Source Converter (VSC) with power transformer is the standard topology for the DC/AC conversion stage, so it has been considered within this analysis. The VSC losses are mainly determined by the power semiconductors and the filter inductors, as filter capacitors losses are typically negligible for this topology (Barrera-Cardenas 2015). Power semiconductor losses are calculated by the sum of conduction losses (P_{cond}) and switching losses (P_{sw}):

$$P_{Cond} = K_{cond0} \cdot P + K_{cond1} \cdot P^2$$

$$P_{sw} = K_{sw} \cdot f_{sw} \cdot V_{DC} \cdot P$$

where f_{sw} is the switching frequency of the VSC, and K_{cond0} , K_{cond1} and K_{sw} are proportionally parameters which depends on converter operation (inverter or rectifier), modulation strategy and semiconductor module on-state and dynamic characteristics. Additionally, the semiconductor module is selected

Deliverable 2.2

Assessment of applicable renewable energy generation technologies on NRA land and assets



Table 4 VSC Power Loss Model parameters

<i>Parameter</i>	<i>Value</i>	<i>Units</i>	<i>Parameter</i>	<i>Value</i>	<i>Units</i>
k_{RT}	1.4436	$\Omega \cdot A$	k_{RD}	0.8964	$\Omega \cdot A$
k_E	1.188	$\frac{\mu J}{V \cdot A}$	k_{OF}	1.8	--
M_{SN}	0.9	--	PF	1	--
δ_{iL}	0.1	--	α_L, β_L	1.1, 2	--
K_{VLO}	3.4353	dm^3	K_{VL1}	0.6865	--
K_{pw0}	9.412	kW	K_{pw1}	0.8536	--
K_{pc0}	8.242	kW	K_{pc1}	0.9993	--
$P_{TR.mn}$	0.005	--	f_1	50	Hz
$P_{TR.ref}$	0.02	--	$P_{N.ref}$	0.1	MW
Semiconductor Ref. Technology Infineon IGBT4 – 1.7kV			Inductor Ref. technology Siemens reactor series 4EUXX		

depending on VSC power rating and voltage class, making it hard to estimate the value for these loss parameters. In order to simplify the estimation of these parameters as function of the VSC power rating (P_N), the analysis presented in (Barrera-Cardenas 2015) is considered. Assuming a sinusoidal PWM modulation and a 1.7kV-class IGBT module technology, K_{cond0} , K_{cond1} and K_{sw} can be estimated by

$$K_{cond0} = \frac{6}{\pi \cdot V_{ac} \cdot PF}$$

$$K_{cond1} = \frac{6 \cdot \left(k_{a1T}^2 \cdot (k_{RT} - k_{RD}) + \frac{k_{RD}}{2} \right)}{\sqrt{6} \cdot k_{OF} \cdot V_{ac} \cdot PF \cdot P_N}$$

$$K_{sw} = \frac{2 \cdot \sqrt{6} \cdot K_E}{\pi \cdot V_{ac} \cdot PF}$$

where V_{ac} is the VSC line-to-line voltage, PF is the VSC power factor, k_{a1T} is the ratio of IGBT rms current to the VSC line current, k_{RT} and k_{RD} are the product of on-state resistances and nominal module current at 25°C for IGBT and diode, respectively, k_{OF} is the overrating factor for module selection and K_E is the total switching energy (Turn on, off and reverse recovery) per Ampere-Volt of the semiconductor module technology. The value of k_{a1T} depends on operation mode of VSC and it can be calculated as follows:

Deliverable 2.2

Assessment of applicable renewable energy generation technologies on NRA land and assets



$$k_{a1T.D}^2 = 1 - k_{a1T.C}^2 = \frac{3 \cdot \pi + 8 \cdot M_{sN} \cdot PF}{12 \cdot \pi} \quad (8)$$

where $k_{a1T.D}$ is for inverter mode (when BESS is discharging), $k_{a1T.C}$ is for rectifier mode (when BESS is charging), and M_{sN} is the modulation index at nominal operating point.

The filter inductor losses are composed of winding losses (P_{wL}) and core losses (P_{cL}). The winding losses can be calculated by using the equivalent winding resistance of the inductor (R_{wL}) and the core losses can be approximated by the empirical Steinmetz equation and assuming the peak flux density (B_L) to be proportional to the inductor current (I_L):

$$P_{wL} = R_{wL} \cdot I_L^2 = K_{wL} \cdot P^2$$

$$P_{cL} = K_{core} \cdot f_L^{\alpha_L} \cdot B_L^{\beta_L} \cdot Vol_{core} = K_{cL} \cdot P^{\beta_L}$$

where K_{core} , α_L and β_L are the usual Steinmetz coefficient, and Vol_{core} is the inductor core. The analysis presented in (Barrera-Cardenas 2015) is used to estimate K_{wL} and K_{cL} as function of the VSC power rating, where winding and core losses at nominal power are calculated by:

$$P_{wL}(P_N) = K_{pw} \cdot (K_{VL0} \cdot (K_{LN} \cdot P_N)^{K_{VL1}})^{K_{pw1}}$$

$$P_{cL}(P_N) = K_{pc} \cdot (K_{VL0} \cdot (K_{LN} \cdot P_N)^{K_{VL1}})^{K_{pc1}}$$

$$K_{LN} = \frac{\left(1 - 3\sqrt{2} \cdot \frac{M_{sN}}{8}\right)}{3\sqrt{2} \cdot PF \cdot \delta_{iL} \cdot f_{sw}}$$

$$K_{pw} = K_{pw0} \cdot \left(1 + \left(\frac{2}{3} + \left(\frac{2f_{sw}}{\pi f_1}\right)^2\right) \cdot \left(\frac{\delta_{iL}^2}{6}\right)\right)$$

Deliverable 2.2

Assessment of applicable renewable energy generation technologies on NRA land and assets



$$K_{pc} = K_{pc0} \cdot \left(\frac{\left(6 + \left(\delta_{iL} \cdot \frac{f_{sw}}{f_1} \right)^2 \right)^{\frac{\alpha_L}{2}}}{6 + \delta_{iL}^2} \right) \cdot \left(1 + \frac{\delta_{iL}}{2} \right)^2$$

where δ_{iL} is the ratio of peak-to-peak current ripple to maximum fundamental current, f_1 is the fundamental grid frequency and, K_{pwi} , K_{pci} and K_{VLi} ($i=0,1$) are proportionality regression coefficients found by taking data from reference inductor technology for nominal winding losses versus volume, nominal core losses versus volume and volume versus energy relationships, respectively. Then, K_{wL} and K_{cL} can be evaluated by:

$$K_{wL} = \frac{K_{pw} \cdot (K_{VL0} \cdot K_{LN}^{K_{VL1}})^{K_{pw1}}}{P_N^{(2-K_{VL1} \cdot K_{pw1})}}$$

$$K_{cL} = \frac{K_{pc} \cdot (K_{VL0} \cdot K_{LN}^{K_{VL1}})^{K_{pc1}}}{P_N^{(\beta_L - K_{VL1} \cdot K_{pc1})}}$$

3.5.2 POWER TRANSFORMER

The transformer losses can be estimated by:

$$P_{Loss.TR} = K_{TR0} \cdot P_N + K_{TR1} \cdot P^2$$

where K_{TR0} is the per unit transformer core losses and K_{TR1} is a proportionality constant related with the transformer winding losses. Normally for power transformers, the nominal transformer efficiency increases as transformer power rating increases, and by assuming that the core losses are equal to winding losses at nominal power, K_{TR0} and K_{TR1} can be estimated as follows:

Deliverable 2.2

Assessment of applicable renewable energy generation technologies on NRA land and assets



$$K_{TR0} = K_{TR1} \cdot P_N = \frac{P_{TR.mn}}{2} + \frac{(P_{TR.ref} - P_{TR.mn})P_{N.ref}}{2 \cdot P_N}$$

where $P_{TR.ref}$ is the reference transformer nominal loss in per unit, $P_{N.ref}$ is the reference transformer nominal power and $P_{TR.mn}$ is the minimum asymptotic transformer nominal loss in per unit.

3.6 WIND FARMS MODELLING AND EVALUATION

The evaluation of expected annual energy production of a wind farm allocated in each NRA land depends on the wind farm layout. Determining the optimal layout of a wind farm is a complex problem outside of the scope of this study. A simplified wind farm layout problem has been considered in this study. The main parameter definitions for the considered wind farm layout are presented in Figure 3-25.

Given an available area with equivalent length (L_{eqA}), equivalent width (W_{eqA}) and average orientation measured by the equivalent area azimuth angle (Φ_A) with south reference ($\Phi_A = 0^\circ$ when the equivalent area width in line with East-West direction), the wind farm layout is defined by the number of wind turbines that can be allocated considering an average prevalent wind direction in the site (Φ_{Wind}) measured from the south and assuming a rectangular distribution of the wind turbines with a separation between turbines parallel to the prevalent wind direction (D_{SOPW}) and a separation between turbines perpendicular to the prevalent wind direction (D_{S90PW}).

Figure 3-26 shows the geometric problem definition for determination of number of wind turbine rows parallel to prevalent wind direction. First, the delta azimuth angle ($\Delta\phi_{AW}$) between the prevalent wind direction and the equivalent area azimuth angle is calculated by

$$\Delta\phi_{AW} = \begin{cases} |\phi_{Wind} - \phi_A| & |\phi_{Wind} - \phi_A| \leq 90^\circ \\ |\phi_{Wind} - \phi_A| - 90^\circ & |\phi_{Wind} - \phi_A| > 90^\circ \end{cases}$$

The total number of wind turbines allocated in the equivalent area is calculated by

$$N_{WT} = \sum_{k=1}^{N_{WTRows}} N_{WTperRow(k)}$$

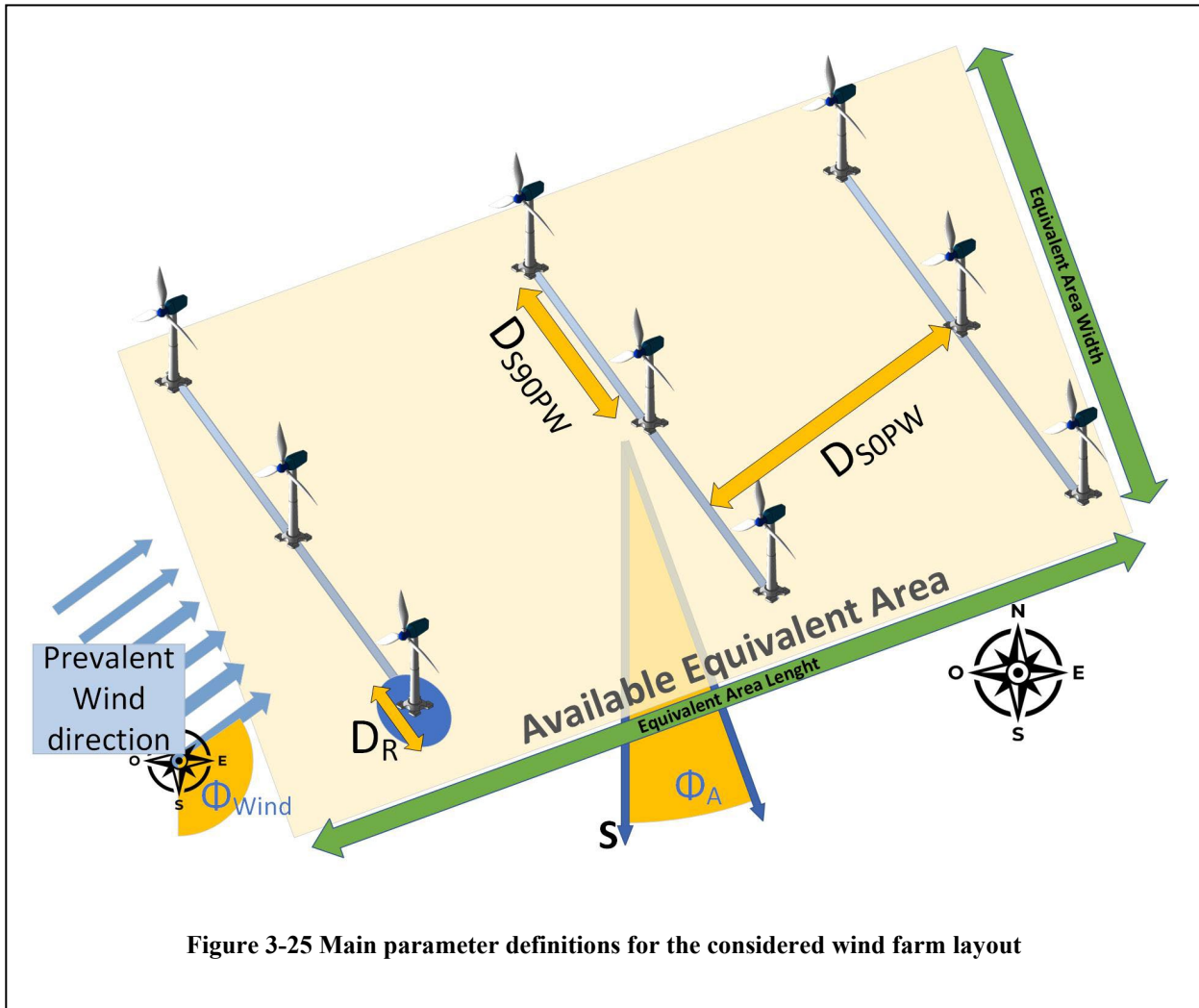


Figure 3-25 Main parameter definitions for the considered wind farm layout

where the number of wind turbine rows (N_{WTRows}) is calculated by

$$N_{WTRows} = \begin{cases} \left\lfloor \frac{W_{eqA}}{D_{S0PW}} \right\rfloor + 1 & \Delta\phi_{AW} = 0 \\ \left\lfloor \frac{L_{eqA}}{D_{S0PW}} \right\rfloor + 1 & \Delta\phi_{AW} = 90^\circ \\ N_{La} + N_{Wa} - 1 & 0 < \Delta\phi_{AW} < 90^\circ \end{cases}$$

$$N_{Wa} = \left\lfloor \frac{W_{eqA} \cdot \cos(\Delta\phi_{AW}) - D_R \cdot \cos(\Delta\phi_{AW}) \cdot \sin(\Delta\phi_{AW})}{D_{S0PW}} \right\rfloor + 1$$

$$\Delta W_{eqA} = \Delta L_{eqA} = W_{eqA} - \frac{W_{eqA} \cdot \cos(\Delta\phi_{AW}) - D_{S0PW}}{\cos(\Delta\phi_{AW})}$$

Deliverable 2.2

Assessment of applicable renewable energy generation technologies on NRA land and assets



$$N_{La^*} = \text{floor} \left\{ \frac{L_{eqA}}{\Delta W_{eqA}} \right\} + 1$$

$$N_{La} = \begin{cases} N_{La^*} & \frac{L_{eqA} - N_{La^*} \cdot \Delta W_{eqA}}{\cos(\Delta\phi_{AW})} \leq D_R \\ N_{La^*} - 1 & \frac{L_{eqA} - N_{La^*} \cdot \Delta W_{eqA}}{\cos(\Delta\phi_{AW})} > D_R \end{cases}$$

And the number of wind turbines per row are calculated by

$$N_{WTperRow(k)} = \begin{cases} \text{floor} \left\{ \frac{L_{eqA}}{D_{S90PW}} \right\} + 1 & \Delta\phi_{AW} = 0 \\ \text{floor} \left\{ \frac{W_{eqA}}{D_{S90PW}} \right\} + 1 & \Delta\phi_{AW} = 90^\circ \end{cases}$$

And for $0 < \Delta\phi_{AW} < 90^\circ$:

$$N_{WTperRow(k)} = \begin{cases} \text{floor} \left\{ \frac{W_{eqA} \cdot \cos(\Delta\phi_{AW}) - (N_{Wa} - k) \cdot D_{S0PW}}{D_{S90PW} \cdot \cos(\Delta\phi_{AW}) \cdot \sin(\Delta\phi_{AW})} \right\} + 1 & k \leq N_{Wa} \\ \text{floor} \left\{ \frac{W_{eqA}}{D_{S90PW} \cdot \sin(\Delta\phi_{AW})} \right\} + 1 & \frac{W_{eqA} / \tan(\Delta\phi_{AW})}{\Delta W_{eqA}} + (k - N_{Wa}) \leq \frac{L_{eqA}}{\Delta W_{eqA}} \\ \text{floor} \left\{ \frac{L_{eqA} - (k - N_{Wa}) \cdot \Delta W_{eqA}}{D_{S90PW} \cdot \cos(\Delta\phi_{AW})} \right\} + 1 & \frac{W_{eqA} / \tan(\Delta\phi_{AW})}{\Delta W_{eqA}} + (k - N_{Wa}) > \frac{L_{eqA}}{\Delta W_{eqA}} \end{cases}$$

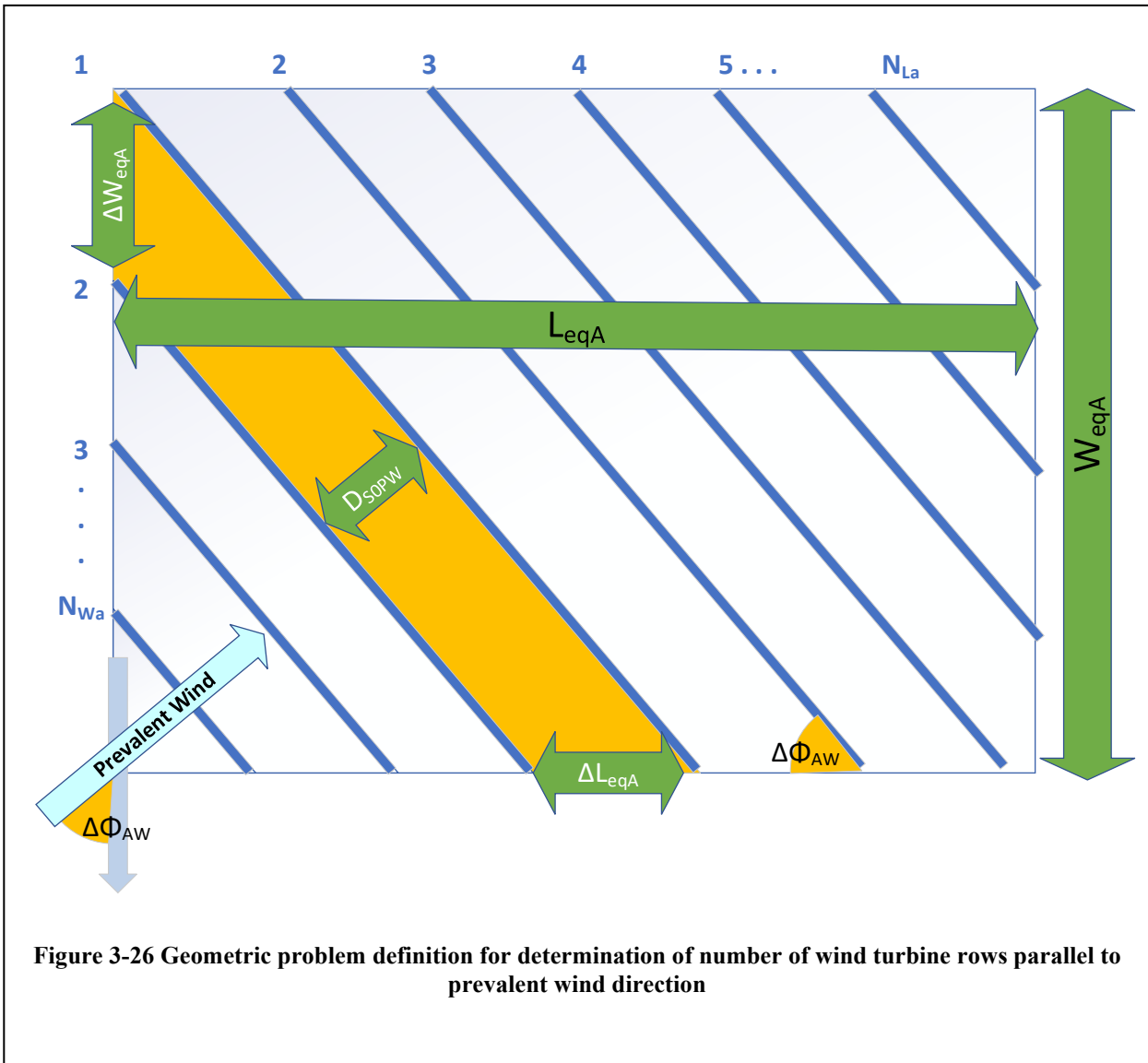
The expected total wind farm annual energy production ($AEP_{WindFarm}$) can be estimated by:

$$AEP_{WindFarm} = \sum_{k=1}^{N_{WTRows}} AEP_{WTFACT} \cdot N_{WTperRow(k)} \cdot k_{WTDerated}(k)$$

With the wind turbine derated factor ($k_{WTDerated}(k)$), accounting for the power ratio of downstream wind turbines respect to upstream wind turbine (POR_{DUWT}), calculated by

$$k_{WTDerated}(k) = \begin{cases} 1 & k = 1 \\ 1 + (POR_{DUWT}^{k-1} - 1) \cdot \frac{1}{N_{WTperRow(k)}} \cdot \frac{N_{WTperRow(k)} - N_{WTperRow(k-1)}}{POR_{DUWT}^{k-1}} & 1 < k \leq N_{Wa} \\ POR_{DUWT}^{k-1} & k > N_{Wa} \end{cases}$$

Deliverable 2.2



and the expected contribution of front wind turbines to the total annual energy production (AEP_{WTFCT}) approximated by

$$AEP_{WTFCT} = 8760 \cdot k_{WTA} \cdot \sum_{i=1}^{N_{vw}} P_{WT}(v_{wi}) \cdot f_W(v_{wi}) \cdot \eta_{WTFCT}(P_{WF.nom}, v_{wi})$$

Where η_{WTFCT} is the equivalent efficiency of the wind farm grid connection including power converter and power transformer.

3.7 SOLAR PV FARMS MODELLING AND EVALUATION

In a similar fashion as the wind farm case, the evaluation of the expected annual energy production of a solar PV farm allocated in each NRA land depends on the solar farm layout, which basically is defined by the number of PV modules with defined tilt and azimuth orientation that can be placed in the given area. To determine the optimal layout of a solar farm is a complex problem outside of the scope of this study. A simplified solar farm layout problem has been considered in this study. The main parameter definitions for the considered solar PV farm layout is presented in Figure 3-27.

Given an available area with equivalent length (L_{eqA}), equivalent width (W_{eqA}) and average orientation measured by the equivalent area azimuth angle (Φ_A) with south reference ($\Phi_A = 0^\circ$ when the equivalent area width aligns with East-West direction), the solar farm layout is defined by the number of PV modules that can be allocated considering a module tilt (β_{Mod}) and azimuth orientation (ψ_{Mod}) measured from the south and assuming a rectangular distribution of the PV modules with a separation between PV

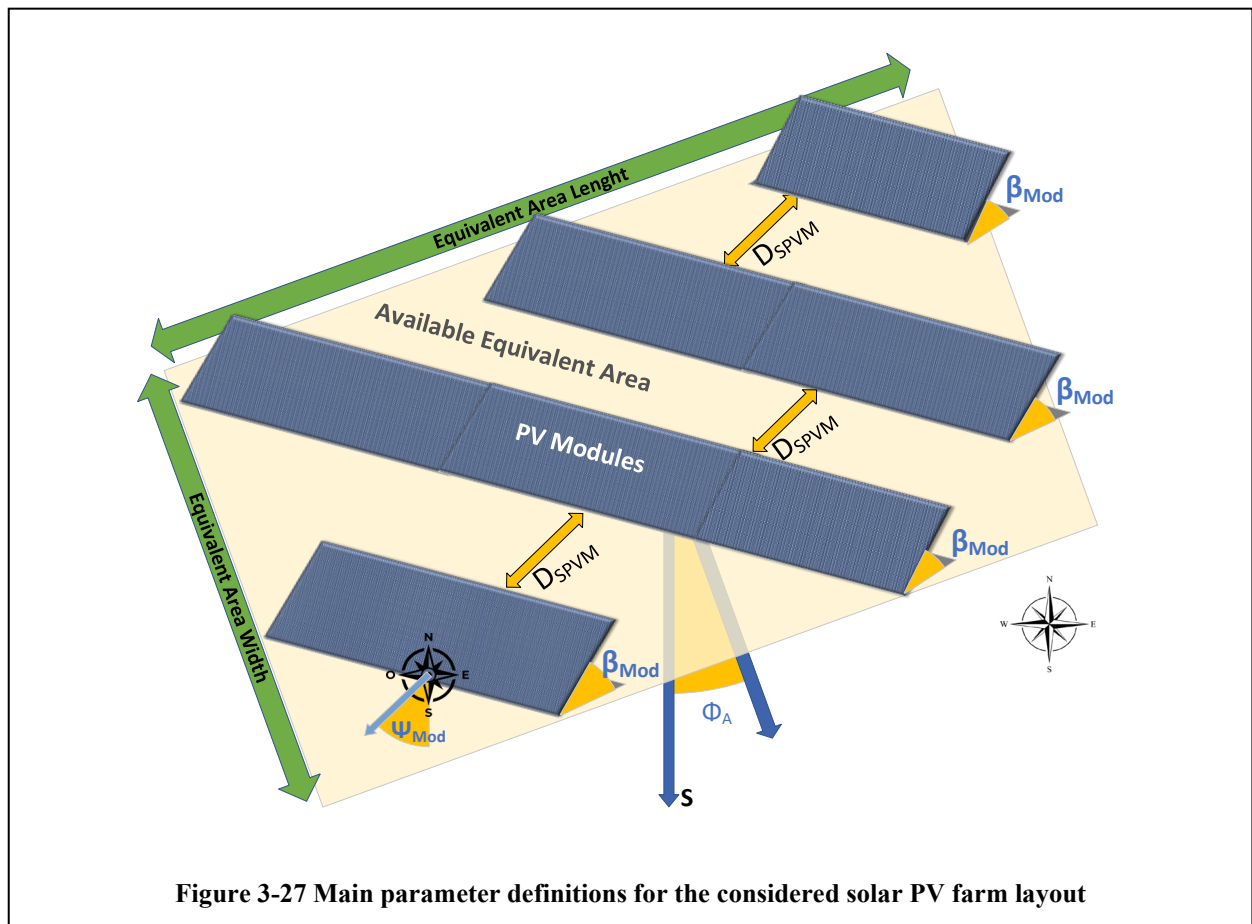
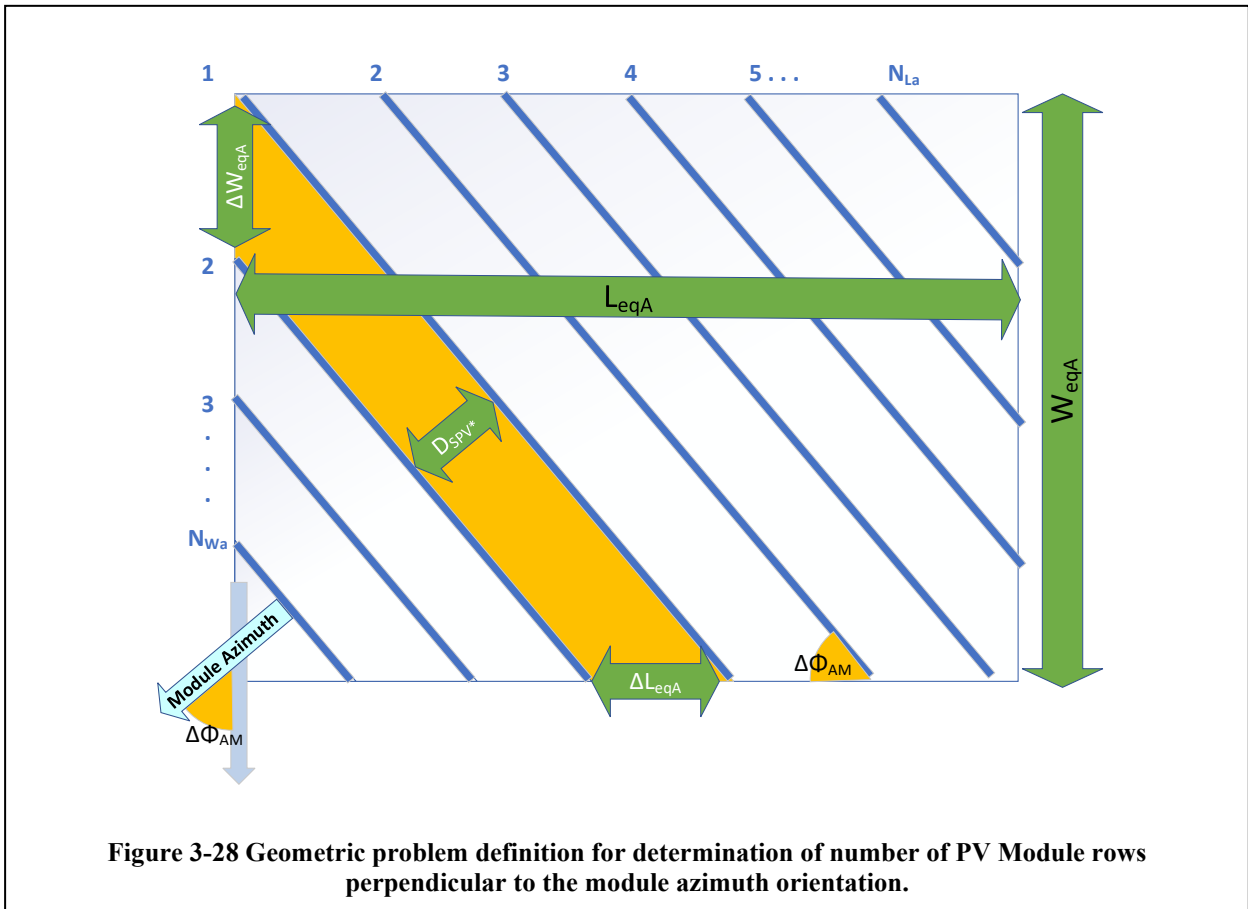


Figure 3-27 Main parameter definitions for the considered solar PV farm layout

Deliverable 2.2



modules parallel to the module azimuth orientation (D_{SPVM}) but not separation between PV modules in the same row perpendicular to the module azimuth orientation.

Figure 3-28 shows the geometric problem definition for determination of number of PV Module rows perpendicular to the module azimuth orientation. It can be noted that this is a similar geometric problem as for wind farm case, which is represented in Figure 3-26, so the problem solution introduced in section 3.6 has been adapted to this case. First, the delta azimuth angle ($\Delta\phi_{AM}$) between the module azimuth and the equivalent area azimuth angle is calculated by

$$\Delta\phi_{AM} = \begin{cases} |\psi_{Mod} - \phi_A| & |\psi_{Mod} - \phi_A| \leq 90^\circ \\ ||\psi_{Mod} - \phi_A| - 90^\circ| & |\psi_{Mod} - \phi_A| > 90^\circ \end{cases}$$

The maximum number of PV modules that can be allocated in the equivalent area is calculated by

$$N_{PVM} = \sum_{k=1}^{N_{PVRows}} N_{ModperRow(k)}$$

Deliverable 2.2

Assessment of applicable renewable energy generation technologies on
NRA land and assets



Where the number of PV rows (N_{PVRows}) is calculated by

$$N_{PVRows} = \begin{cases} \left\lfloor \frac{W_{eqA}}{D_{SPV*}} \right\rfloor + 1 & \Delta\phi_{AM} = 0 \\ \left\lfloor \frac{L_{eqA}}{D_{SPV*}} \right\rfloor + 1 & \Delta\phi_{AM} = 90^\circ \\ N_{La} + N_{Wa} - 1 & 0 < \Delta\phi_{AM} < 90^\circ \end{cases}$$

$$D_{SPV*} = D_{SPV} + W_{Mod} \cdot \cos(\beta_{Mod})$$

$$N_{Wa} = \left\lfloor \frac{W_{eqA} \cdot \cos(\Delta\phi_{AM}) - L_{Mod} \cdot \cos(\Delta\phi_{AM}) \cdot \sin(\Delta\phi_{AM})}{D_{SPV*}} \right\rfloor + 1$$

$$\Delta W_{eqA} = \Delta L_{eqA} = W_{eqA} - \frac{W_{eqA} \cdot \cos(\Delta\phi_{AM}) - D_{SPV*}}{\cos(\Delta\phi_{AM})}$$

$$N_{La*} = \left\lfloor \frac{L_{eqA}}{\Delta W_{eqA}} \right\rfloor + 1$$

$$N_{La} = \begin{cases} N_{La*} & \frac{L_{eqA} - N_{La*} \cdot \Delta W_{eqA}}{\cos(\Delta\phi_{AM})} \leq L_{Mod} \\ N_{La*} - 1 & \frac{L_{eqA} - N_{La*} \cdot \Delta W_{eqA}}{\cos(\Delta\phi_{AM})} > L_{Mod} \end{cases}$$

And the number of PV modules per row are calculated by

$$N_{ModperRow(k)} = \begin{cases} \left\lfloor \frac{L_{eqA}}{L_{Mod}} \right\rfloor & \Delta\phi_{AM} = 0 \\ \left\lfloor \frac{W_{eqA}}{L_{Mod}} \right\rfloor & \Delta\phi_{AM} = 90^\circ \end{cases}$$

And for $0 < \Delta\phi_{AM} < 90^\circ$:

$$N_{ModperRow(k)} = \begin{cases} \left\lfloor \frac{W_{eqA} \cdot \cos(\Delta\phi_{AM}) - (N_{Wa} - k) \cdot D_{SPV*}}{L_{Mod} \cdot \cos(\Delta\phi_{AM}) \cdot \sin(\Delta\phi_{AM})} \right\rfloor & k \leq N_{Wa} \\ \left\lfloor \frac{W_{eqA}}{L_{Mod} \cdot \sin(\Delta\phi_{AM})} \right\rfloor & \frac{W_{eqA} / \tan(\Delta\phi_{AM})}{\Delta W_{eqA}} + (k - N_{Wa}) \leq \frac{L_{eqA}}{\Delta W_{eqA}} \\ \left\lfloor \frac{L_{eqA} - (k - N_{Wa}) \cdot \Delta W_{eqA}}{L_{Mod} \cdot \cos(\Delta\phi_{AM})} \right\rfloor & \frac{W_{eqA} / \tan(\Delta\phi_{AM})}{\Delta W_{eqA}} + (k - N_{Wa}) > \frac{L_{eqA}}{\Delta W_{eqA}} \end{cases}$$

Deliverable 2.2

Assessment of applicable renewable energy generation technologies on NRA land and assets



Once the maximum N_{PVM} for the given area is estimated, then the number of strings in the solar farm ($N_{stringPV}$) can be evaluated. The maximum number of strings ($N_{stringPV.MX}$) is constrained by the maximum open circuit voltage of individual PV modules (V_{OCmx}) and the maximum DC voltage of the PV farm connection (V_{DCmx}), which normally is limited to 1000V for the silicon PV modules considered here.

$$N_{stringPV.MX} = floor \left\{ \frac{V_{DCmx}}{V_{OCmx}} \right\}$$

As the PV modules has a negative thermal coefficient for the pen circuit voltage, the V_{OCmx} can be estimated considering the lowest expected ambient temperature in the location of interest. On the other hand, the minimum number of strings ($N_{stringPV.MN}$) is constrained by the minimum operating voltage of individual PV modules (V_{MPPmn}) and the minimum DC voltage of the PV farm connection (V_{DCmn}), which normally is limited by the PV inverter operation limits:

$$N_{stringPV.MN} = floor \left\{ \frac{V_{DCmn}}{V_{MPPmn}} \right\}$$

The number of strings in the solar farm is selected to fulfil:

$$N_{stringPV.MN} \leq N_{stringPV} \leq N_{stringPV.MX}$$

Then, the number of PV modules per string ($N_{ModString}$) and the string voltage limits can be evaluated:

$$N_{ModString} = floor \left\{ \frac{N_{PVM}}{N_{stringPV}} \right\}$$

$$V_{stringMax} = N_{ModString} \cdot V_{OCmx}$$

$$V_{stringMin} = N_{ModString} \cdot V_{MPPmn}$$

The expected total solar PV farm annual energy production ($AEP_{SolarFarm}$) can be estimated by:

Deliverable 2.2

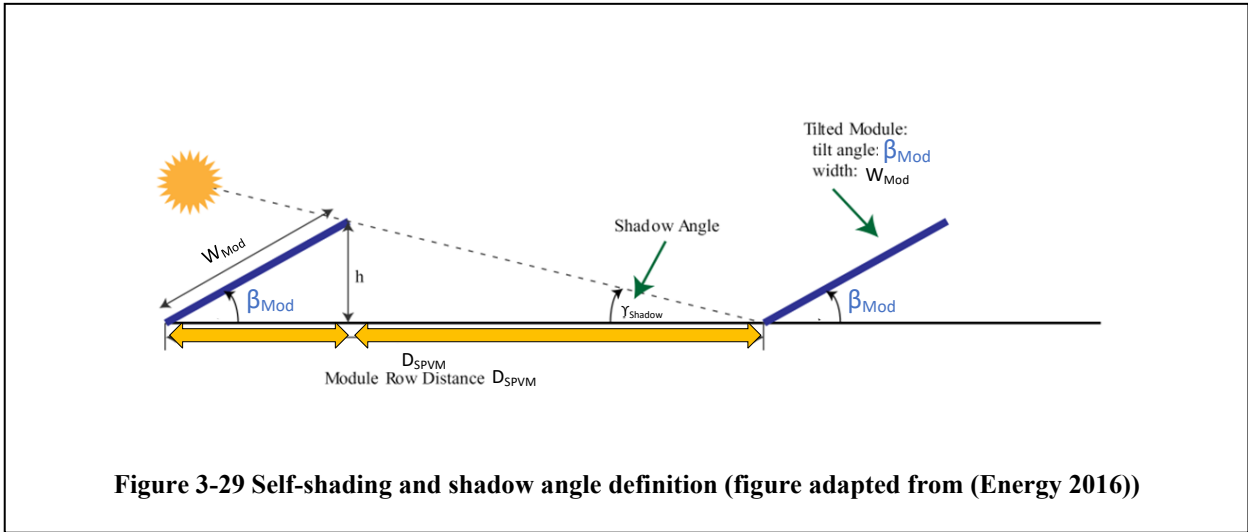


Figure 3-29 Self-shading and shadow angle definition (figure adapted from (Energy 2016))

$$AEP_{SolarFarm} = \sum_{k=1}^{NPVRows} N_{ModperRow(k)} \cdot k_{PVShadow}(k) \cdot \left(\sum_{t_h=1}^{8760} P_{MPP}(G_{PV}(t_h), T_{amb}(t_h)) \cdot \eta_{PESF}(P_{SF.nom}, N_{PVM} \cdot P_{MPP} \cdot k_{PVShadow}(k)) \right)$$

Where P_{MPP} is the output power of a single PV module, which can be evaluated as described in section 3.4, η_{PESF} is the power electronics converter efficiency of the solar farm interconnection, which depends on the nominal solar farm power and the output power, and $k_{PVShadow}$ is the PV row self-shading factor, which models the effect whereby PV rows cause shading of subsequent rows. The self-shading factor is modelled based on the Self-shading and shadow angle definition show in Figure 3-29.

$$k_{PVShadow}(k) = 1 - k_{ShadowOnPVmodW}(k) \cdot k_{ShadowOnPVrowL}(k)$$

$$k_{ShadowOnPVrowL}(k)$$

$$= \begin{cases} \min\left\{\frac{L_0}{L_1}, 1\right\} & k > 1 \text{ and } (\psi_{Sun} - \psi_{Mod}) < \Delta\psi_1 \\ 0 & k = 1 \text{ or } (\psi_{Sun} - \psi_{Mod}) > \Delta\psi_2 \\ \frac{L_0 - \left(D_0 \cdot \tan(|\psi_{Sun} - \psi_{Mod}|) - \frac{L_1 - L_0}{2}\right)}{L_1} & \text{otherwise} \end{cases}$$

$$L_0 = N_{ModperRow(k-1)} \cdot L_{Mod}$$

$$L_1 = N_{ModperRow(k)} \cdot L_{Mod}$$

Deliverable 2.2

Assessment of applicable renewable energy generation technologies on
NRA land and assets



$$\Delta\psi_1 = \text{atan}\left(\frac{|L_1 - L_0|}{2 \cdot D_0}\right)$$

$$\Delta\psi_2 = \text{atan}\left(\frac{|L_1 + L_0|}{2 \cdot D_0}\right)$$

$$D_0 = D_{SPV*} - W_{Mod} \cdot \cos(\beta_{Mod})$$

$$\psi_{Sun} = \text{acos}\left(\frac{\sin(\delta_{sun}) \cdot \cos(\varphi_{Lat}) - \cos(\delta_{sun}) \cdot \sin(\varphi_{Lat}) \cdot \cos(HRA)}{\cos(\delta_{sun})}\right)$$

$$k_{ShadowOnPVmodW}(k) = \begin{cases} \frac{L_{Shadow} - D_0}{D_0} & D_0 < L_{Shadow} < D_{SPV*} \\ 1 & L_{Shadow} > D_{SPV*} \\ 0 & L_{Shadow} < D_0 \end{cases}$$

$$L_{Shadow} = W_{Mod} \cdot \frac{\cos(\beta_{Mod})}{\tan(\delta_{sun})}$$

4 RET TRENDS AND PERFORMANCE COMPARISON

4.1 WIND TURBINES META-PARAMETRIZATION

Correlation between the main wind turbine parameters and its size (dimensions) has been established based on analyzed reference database for large scale HAWT (GARCIA 2013) and created database from collected information for small scale wind turbines.

Figure 4-1 shows the definition of main sizing parameters for the considered wind turbine technologies.

Based on the observed and analyzed data, the following trends/relationships are proposed:

The nominal power, $P_{WT.nom}$, and the turbine diameter (D_R) are related by:

$$P_{WT.nom} = k_{PD0} \cdot D_R^{k_{PD1}}$$

The swept area (A_{swept}) can be estimated as function of turbine diameter by

$$A_{swept} = k_{AD0} \cdot D_R^{k_{AD1}}$$

The nominal wind speed is approximated by:

$$v_{w.nom} = k_{WND0} \cdot D_R^{k_{WND1}}$$

The cut-in and cut-out wind speed are estimated by

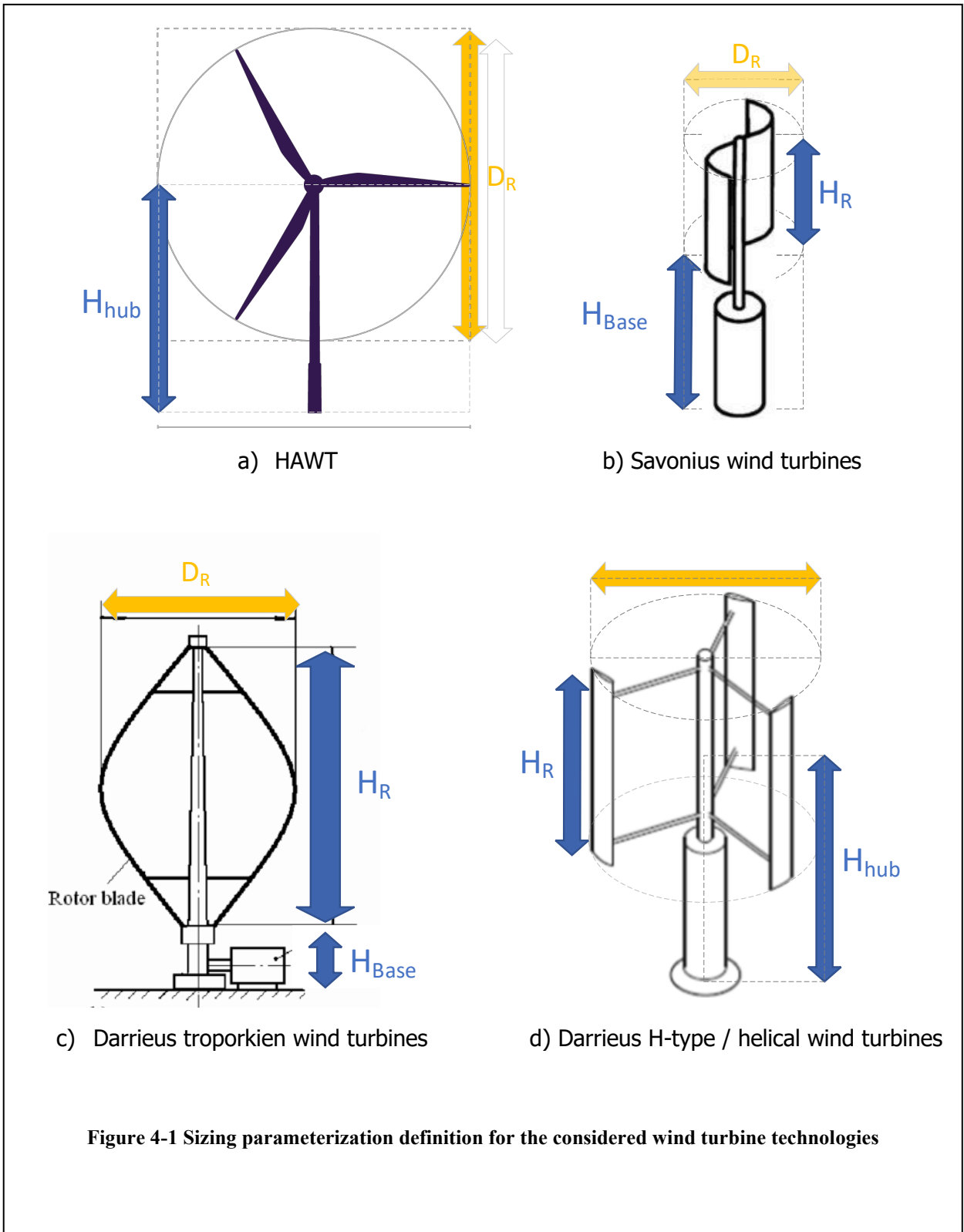
$$v_{w.in} = k_{WID0} \cdot D_R^{k_{WID1}}$$

$$v_{w.out} = k_{WOD0} \cdot D_R^{k_{WOD1}}$$

For small scale wind turbines, the peak power ($P_{WT.peak}$) and the wind speed when peak power is reached ($v_{w.peak}$) are estimated by

$$\frac{P_{WT.peak}}{P_{WT.nom}} = \max \left\{ 1, k_{ppPn0} \cdot P_{WT.nom}^{k_{ppPn1}} \right\}$$

$$\frac{v_{w.peak}}{v_{w.nom}} = \max \left\{ 1, k_{WpWn0} \cdot D_R^{k_{WpWn1}} \right\}$$



Deliverable 2.2

Assessment of applicable renewable energy generation technologies on NRA land and assets



For Savonius and Darrieus-troposkien vertical axis technologies, the minimum base height is related to the rotor diameter by

$$H_{base} = k_{HbD0} \cdot D_R^{k_{HbD1}}$$

For vertical axis technologies, the blade vertical length (H_R) is calculated by

$$H_R = k_{HR} \cdot \frac{A_{swept}}{D_R}$$

For large scale wind turbines, the turbine hub height (H_{hub}) can be related to rotor diameter as follows:

$$H_{hub} = k_{HhD0} \cdot D_R^{k_{HhD1}}$$

For small scale wind turbines, the tower high (H_{Tower}) and H_{hub} are calculated by

$$H_{hub} = H_{Tower} + H_{base} + \frac{1}{2} H_R$$

$$H_{Tower} = \begin{cases} k_{HTD0} \cdot D_R^{k_{HTD1}} & \left(k_{HTD0} \cdot D_R^{k_{HTD1}} + H_{base} + \frac{1}{2} H_R \right) > H_{hubMin} \\ \max \left\{ H_{hubMin} - H_{base} - \frac{1}{2} H_R, 0 \right\} & \left(k_{HTD0} \cdot D_R^{k_{HTD1}} + H_{base} + \frac{1}{2} H_R \right) \leq H_{hubMin} \end{cases}$$

For small scale wind turbines, the output power before cut-out wind speed ($P_{WT.out}$) is calculated by

$$\frac{P_{WT.out}}{P_{WT.nom}} = k_{PoPn0} + (1 - k_{PoPn0}) \cdot \left(1 - \frac{1}{1 + e^{\frac{k_{PoPn1} - P_{WT.out}}{k_{PoPn2}}}} \right)$$

For small scale wind turbines, the wind turbine weight ($Weight_{WT}$) and the rotor diameter are related by

$$Weight_{WT} = Weight_{WT0} + k_{WeightD0} \cdot D_R^{k_{WeightD1}}$$

The wind turbine cost ($Cost_{WT}$) can be estimated by

$$\frac{Cost_{WT}}{P_{WT.nom}} = Cost_{P_{WT0}} + k_{CostWT0} \cdot (P_{WT.nom})^{k_{CostWT1}}$$

For large scale wind turbines, the turbine cost parameters have been estimated based on data reported in (International Renewable Energy Agency 2016), while for small scale wind turbines the parameters have been calculated based on collected information.

Deliverable 2.2

Assessment of applicable renewable energy generation technologies on NRA land and assets



For small scale wind turbines, the cost of the power electronics converter ($Cost_{PEWT}$) and the cost of the tower and foundation ($Cost_{TWT}$) can be modelled as follows:

$$\frac{Cost_{PEWT}}{P_{WT.nom}} = Cost_{PEWT0} + k_{CPEWT0} \cdot (P_{WT.nom})^{k_{CPEWT1}}$$

$$Cost_{TWT} = k_{CTWT0} \cdot (Weight_{WT} \cdot A_{swept})^{k_{CTWT1}} \cdot (H_{Tower})^{k_{CTWT2}}$$

The parameters for the cost model of the power electronics converter have been fitted based on a combination of collected data and reported data in (Gabriel Domingues-Olavarria 2017) while the parameters for tower and foundation cost model have been fitted using collected data for different types of towers.

Table 5 summarizes the calculated meta-parameters for the considered small scale wind turbine technologies.

Figure 4-2 and Figure 4-3 show the parameter trends for the considered small scale wind turbine technologies and the estimations based on the proposed models.

Figure 4-4 shows the collected data for tower and foundation cost as well as the fitted models for three types of wind turbine towers: monotype, hydraulic and roof top towers.

Deliverable 2.2

Assessment of applicable renewable energy generation technologies on NRA land and assets



Table 5 Small Scale Wind Turbine Meta-parameters

		HAWT	Darrieus	Savonius	Hybrid (Sav+Dar)
P_{eWN} [kW]	k_{PD0}	0.1931	0.3368	0.4786	0.1263
	k_{PD1}	1.9572	1.9739	1.6022	2.5075
A_{swept} [m ²]	k_{AD0}	$\pi/4 \approx 0.7854$	1.3972	2.0160	0.9504
	k_{AD1}	2	1.8306	1.5257	2.1490
$v_{w.nom}$ [m/s]	k_{WND0}	10.9693	11.1864	12.1060	10.5139
	k_{WND1}	-0.0223	0.0310	0.0442	0.0804
$v_{w.in}$ [m]	k_{WID0}	2.8346	2.8723	3.0913	2.9829
	k_{WID1}	-0.0046	0.0363	-0.2565	-0.1112
$v_{w.out}$ [m/s]	k_{WOD0}	46.9414	34.4153	38.2369	36.2740
	k_{WOD1}	-0.1133	-0.1858	-0.0285	-0.1072
$P_{WT.peak}$	k_{PPpN0}	1.6542	1.6006	3.5941	2.3986
$P_{WT.nom}$	k_{PPpN1}	-0.0884	-0.1195	-0.1383	-0.1289
$v_{w.peak}$	k_{WpWn0}	1.2999	1.2721	2.0649	2.0245
$v_{w.nom}$	k_{WpWn1}	-0.0244	-0.0489	-0.1556	-0.1994
H_{hub} [m]	k_{HhD0}	--	--	--	--
	k_{HhD1}	--	--	--	--
H_R	k_{HR}	--	1	1	1
H_{base} [m]	k_{HbD0}	--	--	0.8535	--
	k_{HbD1}	--	--	0.6152	--
H_{Tower} [m]	k_{HTD0}	2.6308	2.5038	--	2.5038
	k_{HTD1}	0.9873	0.6981	--	0.6981
$\frac{P_{WT.out}}{P_{WT.nom}}$	k_{PoPn0}	0	0.6	4.4	1.5
	k_{PoPn1}	2	5	6	0.8
	k_{PoPn2}	1	2	8	2.5
$Weight_{WT}$ [kg]	$Weight_{WT0}$	0	0	8	0
	$k_{WeightD0}$	4.7162	30.1595	114.7895	23.2011
	$k_{WeightD1}$	2.3117	2.0156	1.9339	2.5599
$Cost_{WT}$ [EUR/kW]	$Cost_{P_{WT0}}$	100	500	800	650
	$k_{CostWT0}$	1904	2805	10745	5489
	$k_{CostWT1}$	-0.2338	-0.2122	-0.3845	-0.2983

Deliverable 2.2

Assessment of applicable renewable energy generation technologies on NRA land and assets

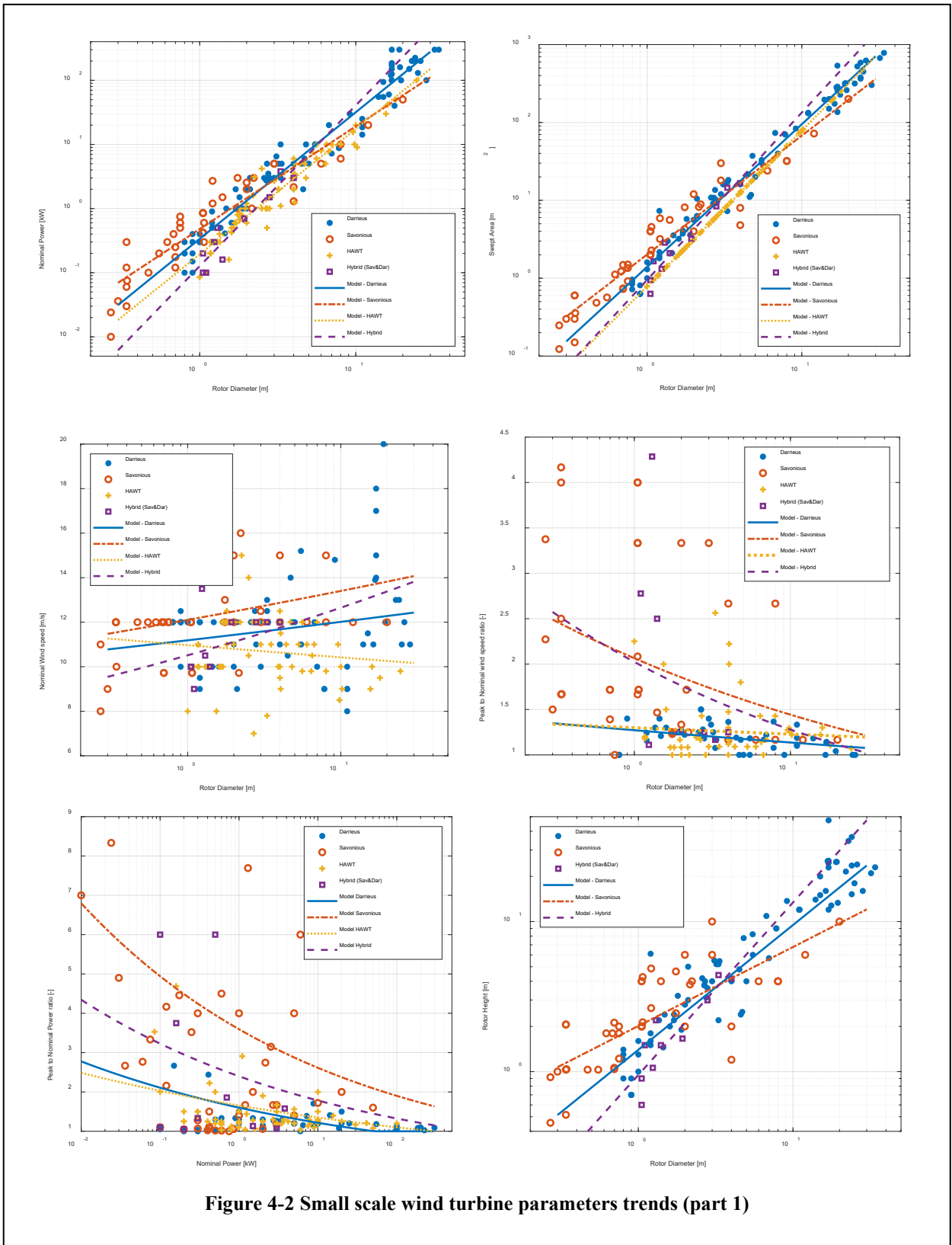


Figure 4-2 Small scale wind turbine parameters trends (part 1)

Deliverable 2.2

Assessment of applicable renewable energy generation technologies on NRA land and assets

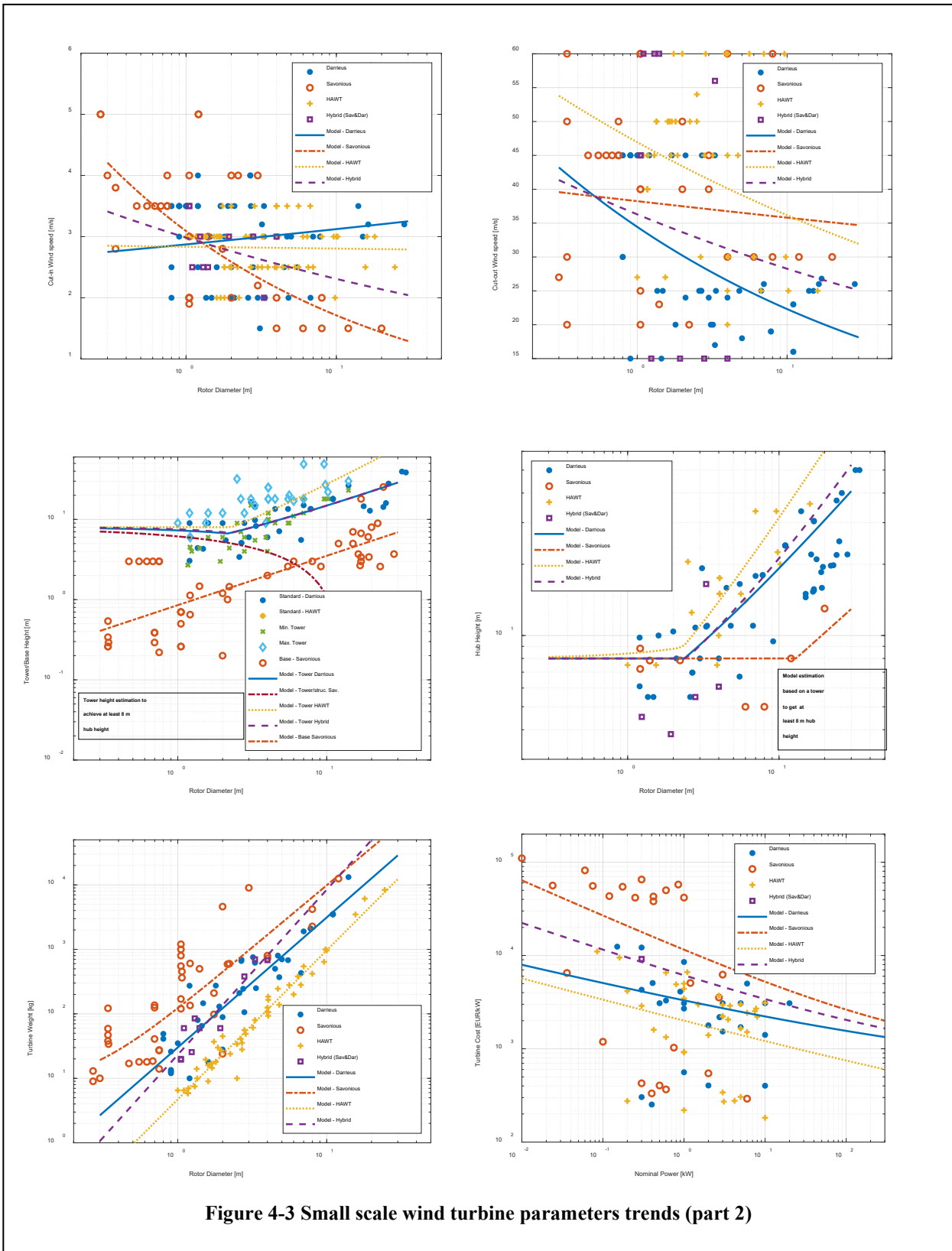


Figure 4-3 Small scale wind turbine parameters trends (part 2)

Deliverable 2.2

Assessment of applicable renewable energy generation technologies on NRA land and assets

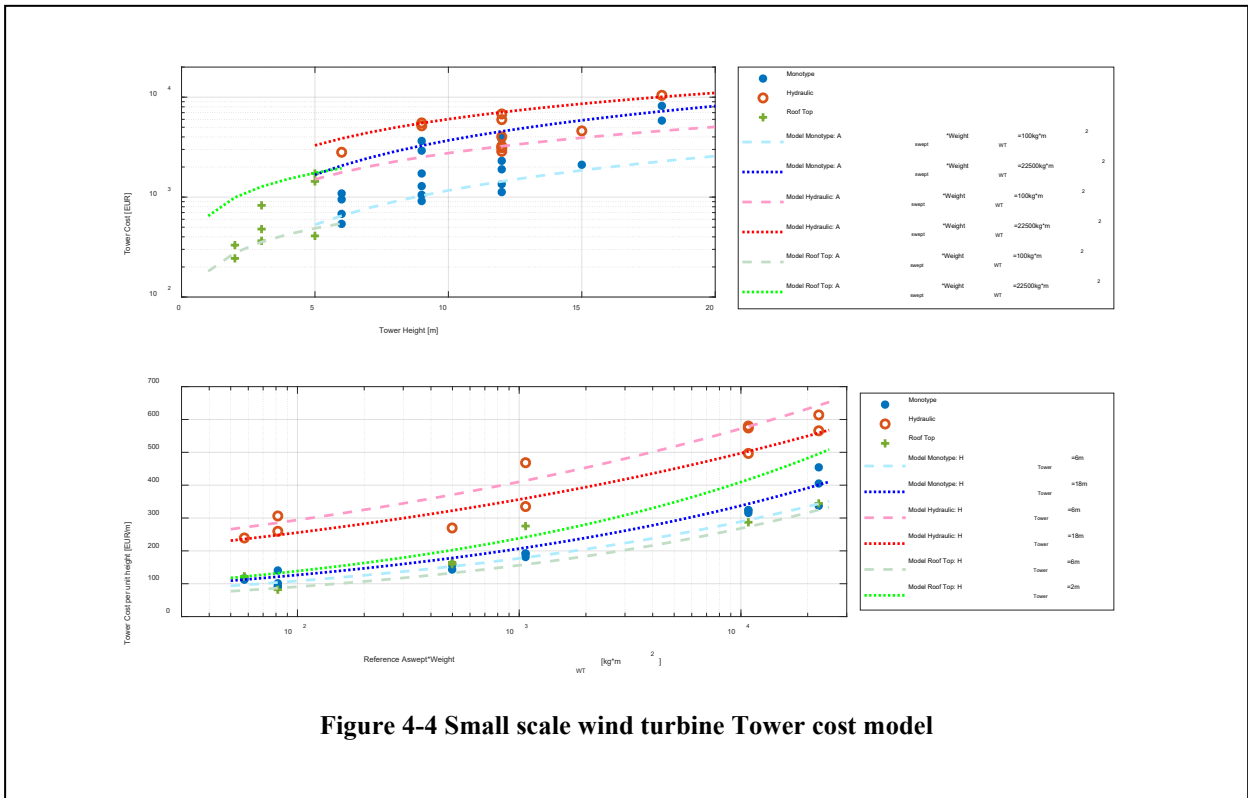


Figure 4-5 shows the calculated power curve parameters for the considered small scale wind turbine technologies and the estimations based on the proposed models.

Figure 4-6 and Figure 4-7 show an example of calculated power curves and respective power coefficients for different virtual small scale wind turbines (based on different nominal power) for the four considered technologies.

Deliverable 2.2

Assessment of applicable renewable energy generation technologies on NRA land and assets

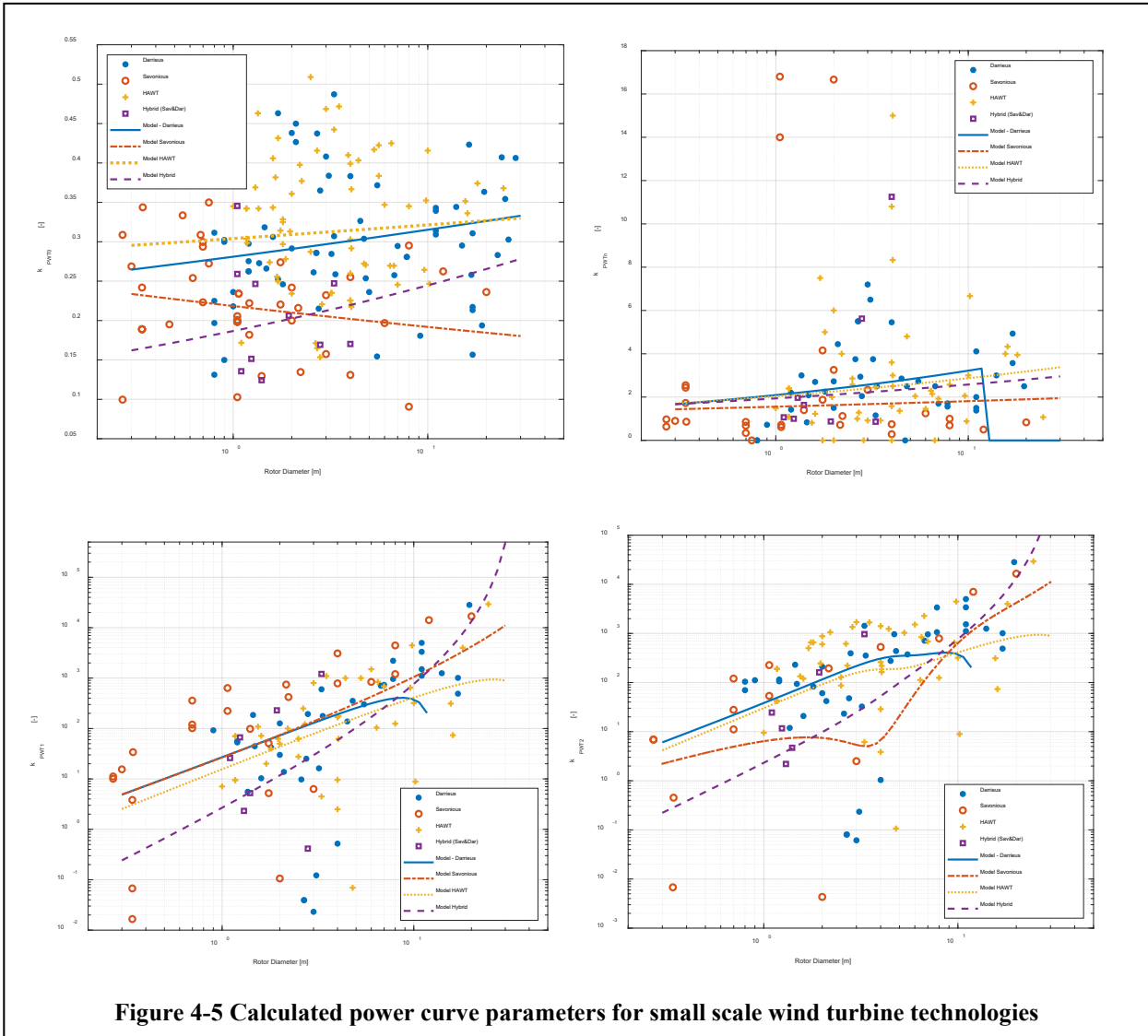


Figure 4-5 Calculated power curve parameters for small scale wind turbine technologies

Deliverable 2.2

Assessment of applicable renewable energy generation technologies on NRA land and assets

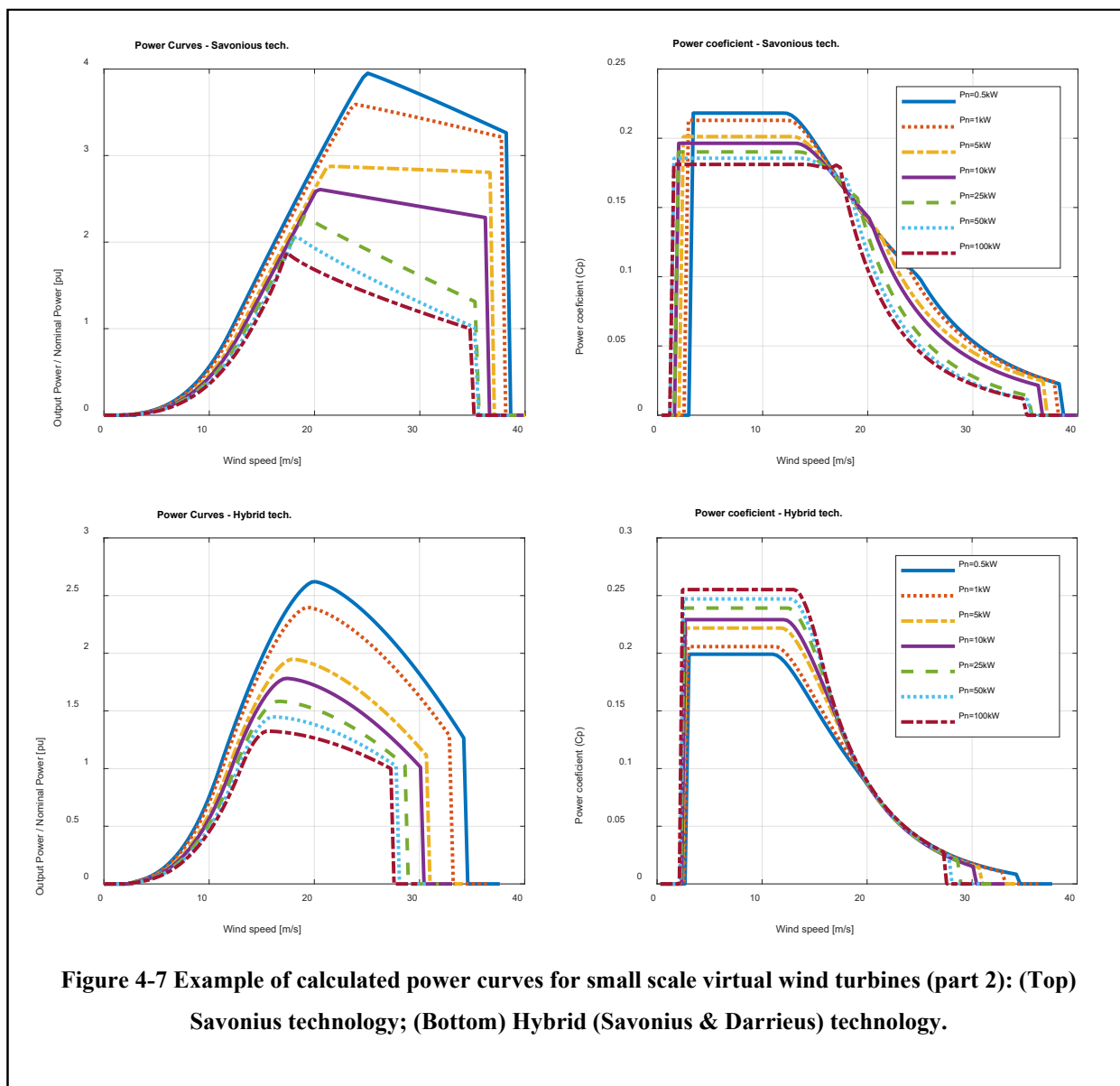


Figure 4-7 Example of calculated power curves for small scale virtual wind turbines (part 2): (Top) Savonius technology; (Bottom) Hybrid (Savonius & Darrieus) technology.

Deliverable 2.2

Assessment of applicable renewable energy generation technologies on NRA land and assets

**Table 6 Large Scale Wind Turbine Meta-parameters**

		HAWT	Darrieus Troposkien	Darrieus H-Rotor	Darrieus Equivalent
P_{eWN} [kW]	k_{PD0}	0.0802	0.2557	0.1469	0.3441
	k_{PD1}	2.292	2.2129	2.2864	2.0883
A_{swept} [m ²]	k_{AD0}	$\pi/4 \approx 0.7854$	1.0331	0.9388	0.9773
	k_{AD1}	2	1.9493	1.9789	1.9674
$v_{w.nom}$ [m/s]	k_{WND0}	9.3327	13.5042	11.5895	15.1879
	k_{WND1}	0.0435	0.0340	0.0487	-0.0135
H_{hub} [m]	k_{HhD0}	3.413	1.9715	2.8611	1.2845
	k_{HhD1}	0.6958	0.7827	0.7647	0.9521
H_R	k_{HR}	--	3/2	1	1.25
$v_{w.in}$ [m/s]	k_{WID0}	5	5	5	5
	k_{WID1}	0	0	0	0
$v_{w.out}$ [m/s]	k_{WOD0}	25	25	25	25
	k_{WOD1}	0	0	0	0
$Cost_{WT}$ [EUR/kW]	$Cost_{P_{WT0}}$	560	560	560	560
	$k_{Cost_{WT0}}$	4732	4732	4732	4732
	$k_{Cost_{WT1}}$	-0.4065	-0.4065	-0.4065	-0.4065

Table 6 summarizes the calculated meta-parameters for the considered large scale wind turbine technologies.

Figure 4-8 shows the parameter trends for the considered large scale wind turbine technologies and the estimations based on the proposed/considered models.

Deliverable 2.2

Assessment of applicable renewable energy generation technologies on
NRA land and assets



Figure 4-9 shows an example of calculated power curves and respective power coefficients for different virtual large scale wind turbines (based on different nominal power).

Deliverable 2.2

Assessment of applicable renewable energy generation technologies on NRA land and assets

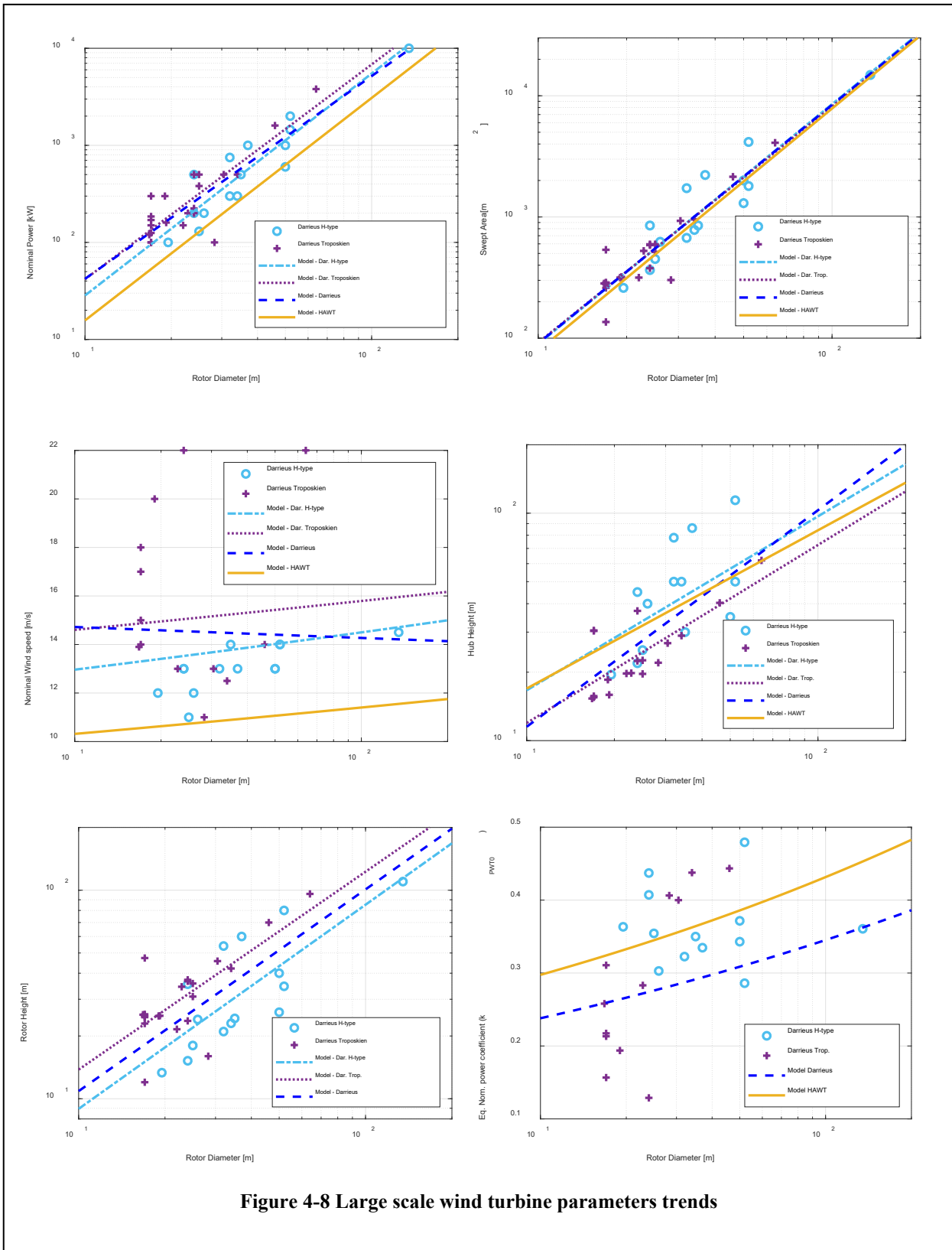


Figure 4-8 Large scale wind turbine parameters trends

Deliverable 2.2

Assessment of applicable renewable energy generation technologies on NRA land and assets

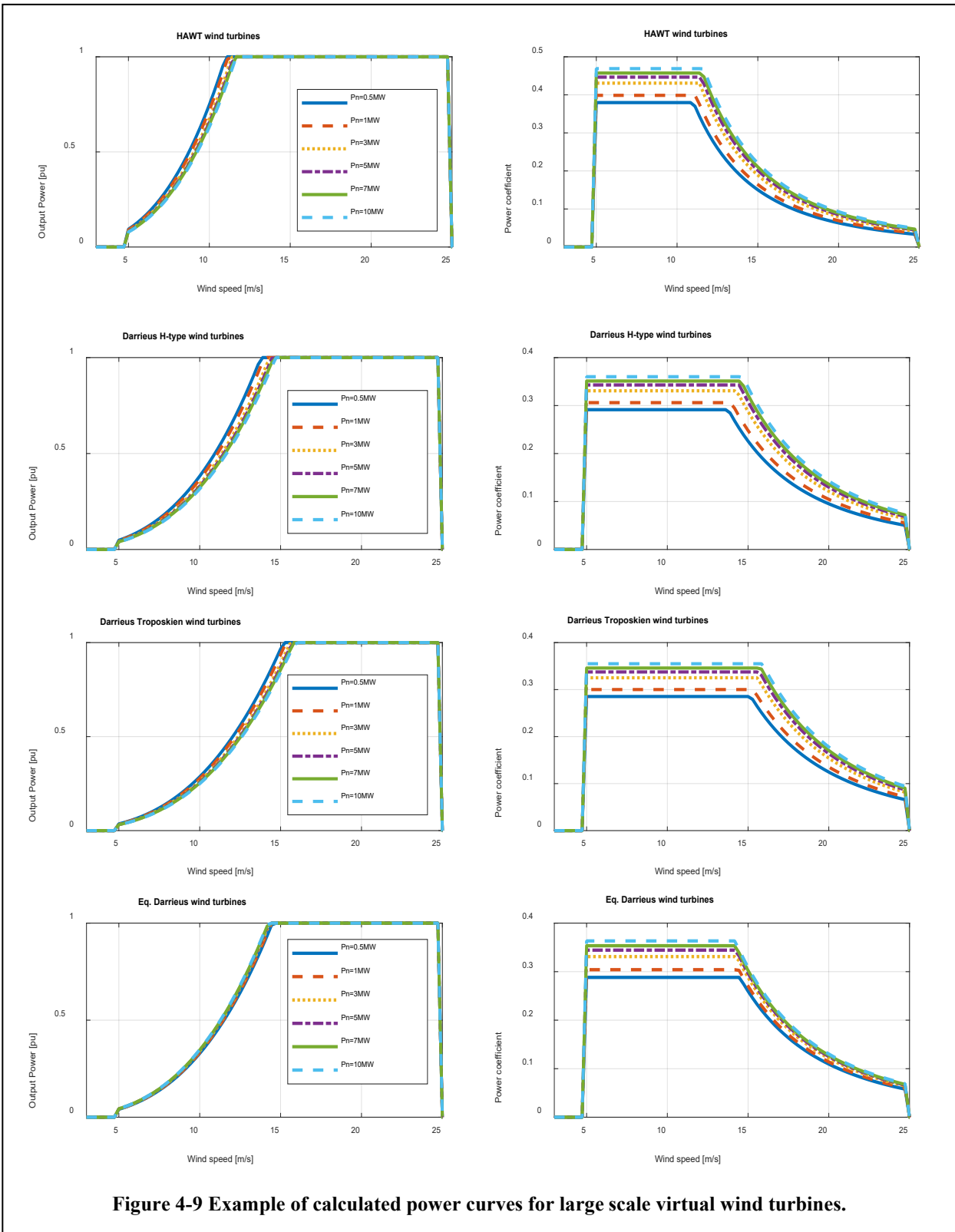


Figure 4-9 Example of calculated power curves for large scale virtual wind turbines.

Deliverable 2.2

Assessment of applicable renewable energy generation technologies on NRA land and assets

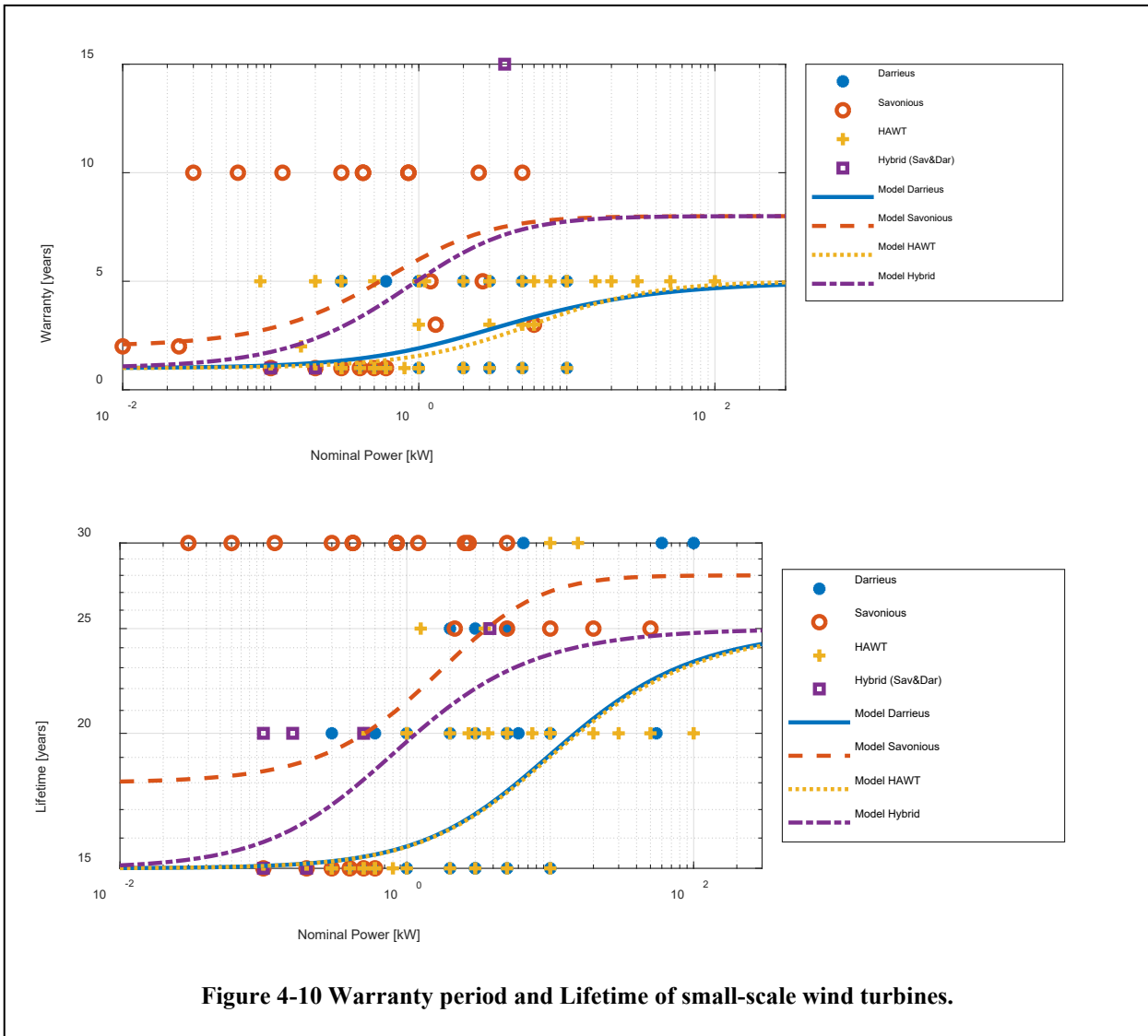


Figure 4-10 Warranty period and Lifetime of small-scale wind turbines.

Regarding the expected lifetime and warranty period for wind turbines, based on the collected data for small wind turbines, it is observed that bigger wind turbines have longer warranty period and lifetime. The following models are proposed to estimate the different trends in turbine warranty period and lifetime for the considered wind turbine technologies:

$$WR Y_{WT} = WR Y_{MX} - (WR Y_{MX} - WR Y_{MN}) \cdot \left(\frac{P_{NrefWR Y}}{P_{WT.nom} + P_{NrefWR Y}} \right)^{k_{nWR Y}}$$

$$k_{nWA} = \frac{\log \left(\frac{WR Y_{MX} - WR Y_{MN}}{WR Y_{MX} - WR Y_{REF}} \right)}{\log(2)}$$

Deliverable 2.2

$$LFT_{WT} = LFT_{MX} - (LFT_{MX} - LFT_{MN}) \cdot \left(\frac{P_{NrefLFT}}{P_{WT.nom} + P_{NrefLFT}} \right)^{k_{nLFT}}$$
$$k_{nLFT} = \frac{\log\left(\frac{LFT_{MX} - LFT_{MN}}{LFT_{MX} - LFT_{REF}}\right)}{\log(2)}$$

Figure 4-10 shows the collected data regarding warranty period and lifetime for small scale wind turbines as well as estimations based on proposed models.

For large scale wind turbines, a typical warranty period of 5 years can be considered. Regarding the lifetime, most of the manufacturers specified a minimum lifetime of 20 years, which can be extended up to at least 25 years depending on environmental factors and the correct maintenance procedures being followed.

4.2 PV MODULE META-PARAMETRIZATION

The meta-parametrization of PV modules is presented in this sub-section. First, the correlation between the main PV module parameters and its nominal power (P_{MPPSTC}) has been analyzed based on the created database from collected data for silicon crystalline PV modules. It has been observed that the module parameters have at least a two-dimensional correlation, and the number of series connected cells per module (n_{sMod}) has been selected as additional input (besides the nominal power) for the meta-parametrization process, meaning that a PV module can be characterized by its nominal power and the number of series connected solar cells.

The PV module area (A_{Mod}) can be estimated by

$$A_{Mod} = k_{APN0} \cdot P_{MPPSTC}^{k_{AP}} \cdot n_{sMod}^{k_{AN}}$$

The PV module dimensions, length (L_{Mod}) and width (W_{Mod}), are determined as follows:

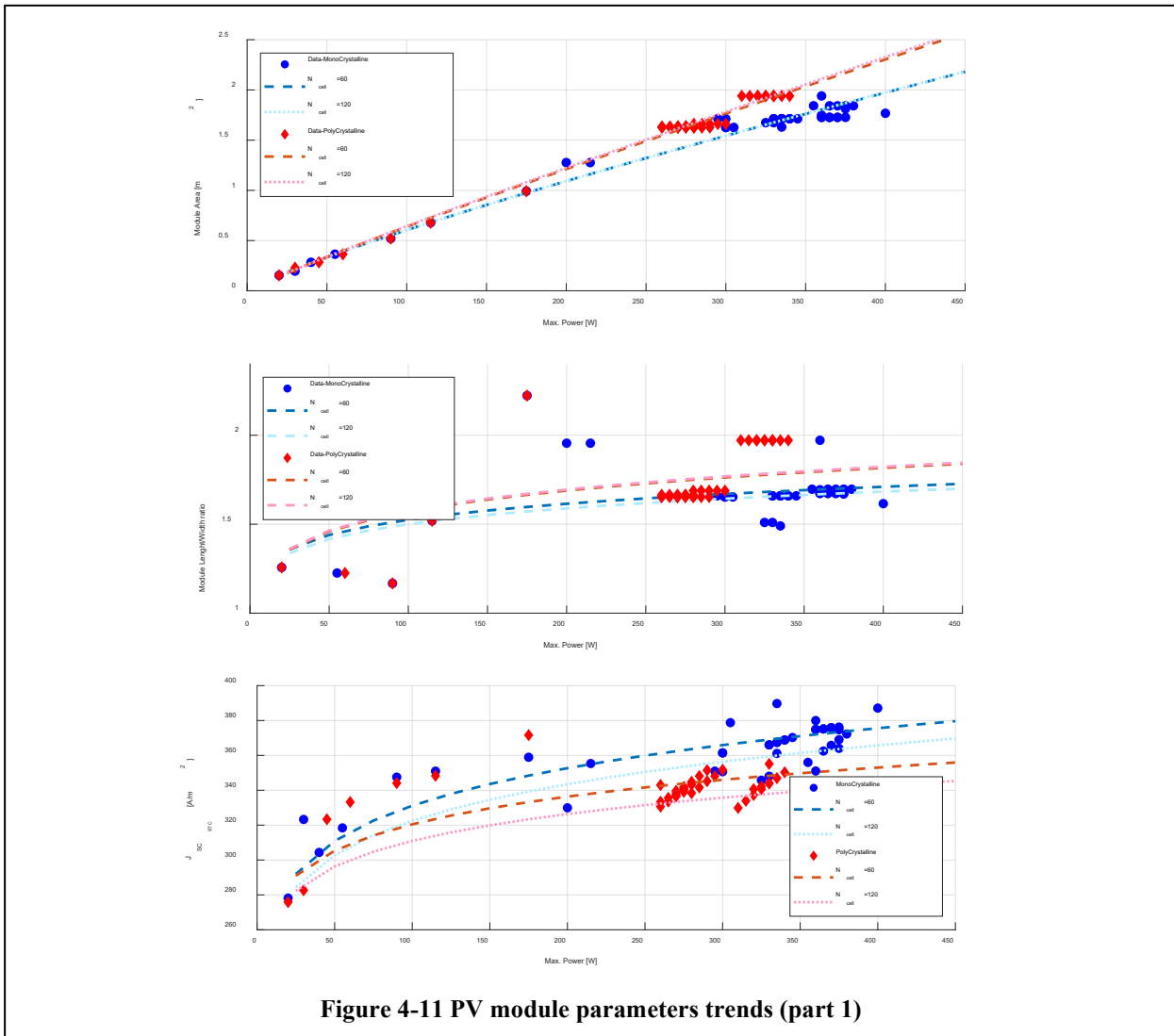
$$LW_{ratio} = \frac{L_{Mod}}{W_{Mod}} = k_{LWPN0} \cdot P_{MPPSTC}^{k_{LWP}} \cdot n_{sMod}^{k_{LWN}}$$

$$L_{Mod} = \sqrt{A_{Mod} \cdot LW_{ratio}}$$

$$W_{Mod} = \frac{A_{Mod}}{L_{Mod}}$$

Deliverable 2.2

Assessment of applicable renewable energy generation technologies on NRA land and assets



The electrical parameters at STC are evaluated based on the equivalent cell current density and voltage values as follows:

$$J_{SCSTC} = \frac{I_{SCSTC} \cdot n_{sMod}}{A_{Mod}} = k_{JSCPNO} \cdot P_{MPPSTC}^{k_{JSCP}} \cdot n_{sMod}^{k_{JSCN}}$$

$$\frac{V_{OCSTC}}{n_{sMod}} = k_{VOCPNO} \cdot P_{MPPSTC}^{k_{VOCP}} \cdot n_{sMod}^{k_{VOCN}}$$

$$J_{MPPSTC} = \frac{I_{MPPSTC} \cdot n_{sMod}}{A_{Mod}} = k_{JMPPNO} \cdot P_{MPPSTC}^{k_{JMPP}} \cdot n_{sMod}^{k_{JMPPN}}$$

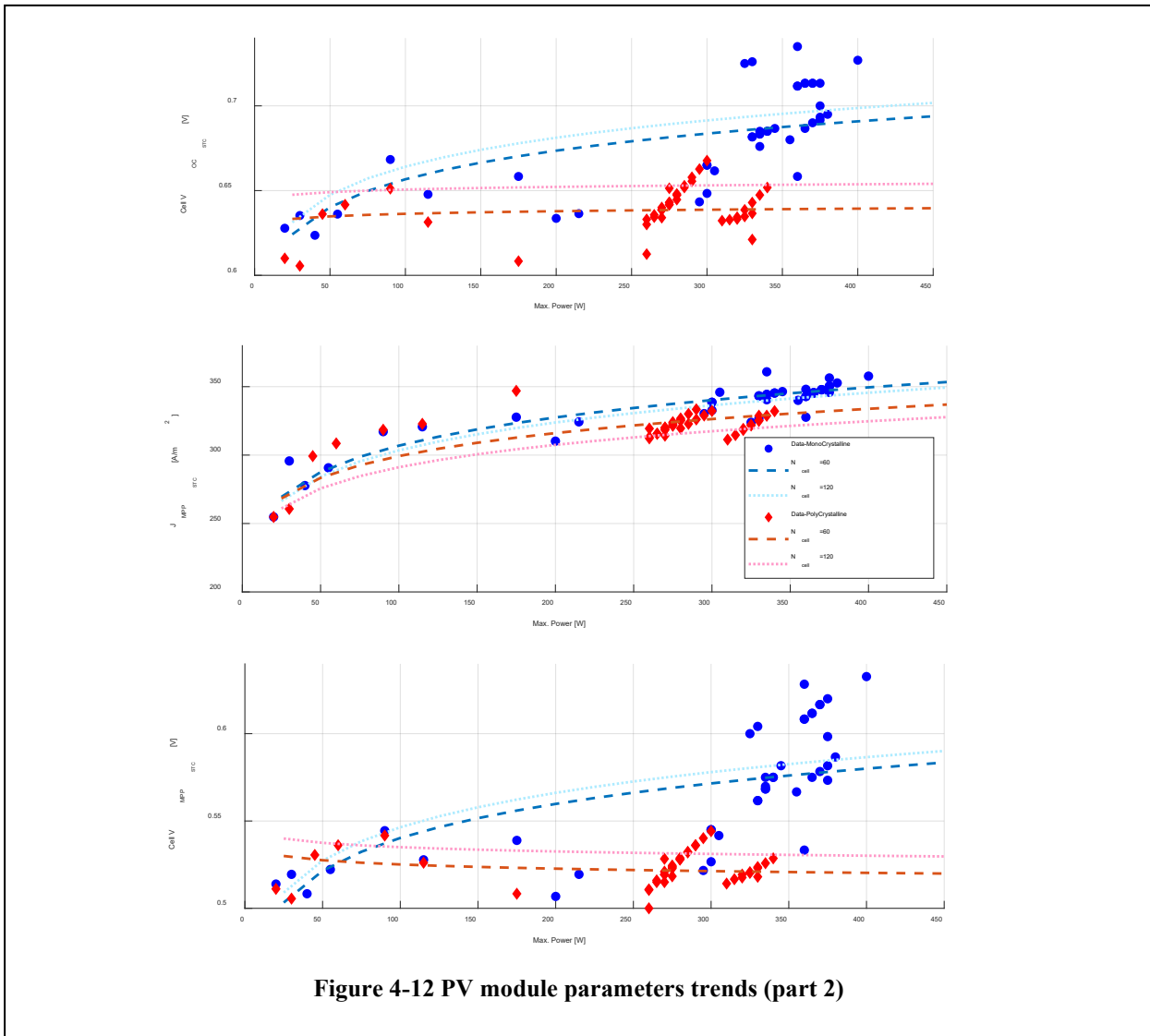


Figure 4-12 PV module parameters trends (part 2)

$$\frac{V_{MPPSTC}}{n_{sMod}} = k_{VMPPN0} \cdot P_{MPPSTC}^{k_{VMPP}} \cdot n_{sMod}^{k_{VMPPN}}$$

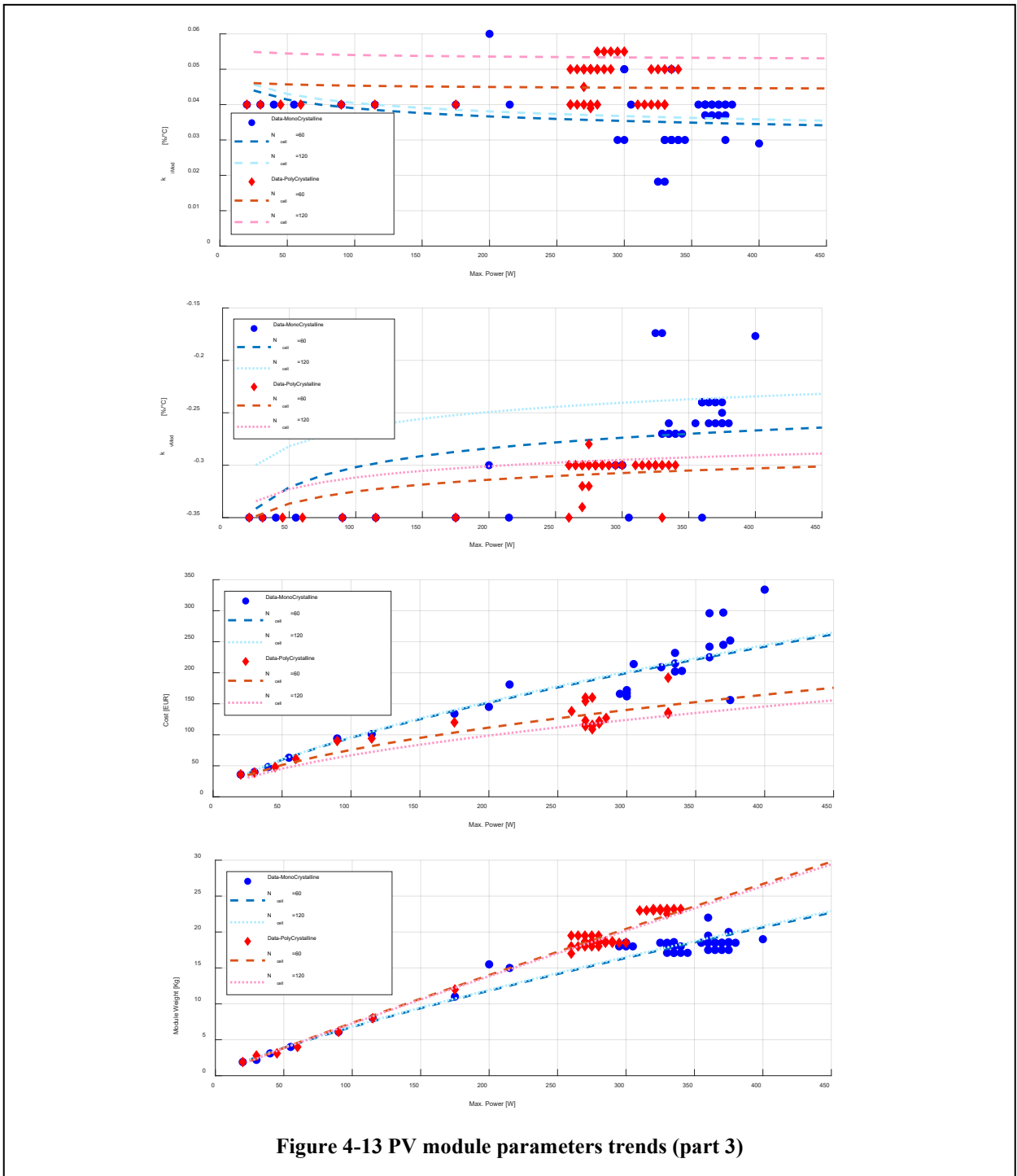
The thermal coefficients for short-circuit current and open-circuit voltage, k_{iMod} and k_{vMod} , are estimated by

$$k_{iMod} = k_{ITPN0} \cdot P_{MPPSTC}^{k_{ITP}} \cdot n_{sMod}^{k_{ITN}}$$

$$k_{vMod} = k_{VTPN0} \cdot P_{MPPSTC}^{k_{VTP}} \cdot n_{sMod}^{k_{VTN}}$$

Deliverable 2.2

Assessment of applicable renewable energy generation technologies on NRA land and assets



The PV module cost ($Cost_{Mod}$) is approximated by

$$Cost_{Mod} = k_{CostPN0} \cdot P_{MPPSTC}^{k_{CostP}} \cdot n_{sMod}^{k_{CostN}}$$

Deliverable 2.2

Assessment of applicable renewable energy generation technologies on NRA land and assets



Table 7 Silicon PV Module Crystalline Meta-parameters

Parameter	Meta-Parameter	PV Si-Crystalline Technology		Parameter	Meta-Parameter	PV Si-Crystalline Technology		
		Mono	Poly			Mono	Poly	
$P_{STC.Max}$ [W]		700	500	η_{STC} [%]	$k_{0\eta}$	14.38	11.21	
γ_a [%]	$k_{0\gamma L}$	0.670	0.670		$k_{1\eta}$	0.12	0.147	
	$k_{1\gamma L}$	1.2e-3	6.8e-4		$k_{p\eta}$	0.64	0.64	
	$k_{0\gamma U}$	0.560	0.650		$\Delta\eta_{STC}$	2	1.8	
	$k_{1\gamma U}$	8.1e8	26e10		$\eta_{STC.Min}$	12	8	
	$k_{p\gamma U}$	3.860	5.178		$\eta_{STC.Max}$	24.5	20.5	
	$\gamma_{a.Min}$	0.225	0.475		L_{Mod} [m]	k_{0L}	0.419	0.680
	$\gamma_{a.Max}$	0.715	0.795			k_{pL}	0.571	0.617
$Cost_{Mod}$ [€]	k_{0C}	1.840	0.563	k_{eL}		0.645	0.905	
	k_{pC}	0.543	0.341	M_{Mod} [kg]	k_{0M}	2.527	1.879	
	k_{eC}	0.338	0.858		k_{pM}	1.021	0.987	
	k_{dC}	0.395	1.497		k_{eM}	1.326	1.149	
$k_{PT1,STC}$ [%/°C]	k_{PT10}	-0.495	-0.544	$k_{PT0,STC}$ [p.u.]	k_{PT00}	0.911	0.674	
	k_{0PT1}	3.1e-4	6.8e-3		k_{0PT0}	0.222	0.290	
	k_{pPT1}	0.141	-0.004		k_{pPT0}	0.2196	0.041	
	k_{ePT1}	1.796	0.925		k_{ePT0}	-0.695	-0.02	
	k_{dPT1}	-0.177	-1.116		k_{dPT0}	0.0732	0.063	
k_{GT1} [%/°C]	k_{GT10}	-1.5e-2	-1.6e-2	k_{GT0} [m ² /W]	k_{GT00}	9.3e-4	9.1e-4	
	k_{0GT1}	2.3e-5	2.8e-3		k_{0GT0}	7.3e-6	2.3e-5	
	k_{pGT1}	-0.091	-0.227		k_{pGT0}	-0.080	-0.058	
	k_{eGT1}	2.04	0.384		k_{eGT0}	0.891	0.439	
	k_{dGT1}	0.10	-1.074		k_{dGT0}	-0.027	-0.202	
$V_{OC,STC}$ [V/m ²]	k_{VA0}	8.081	17.95	k_{vMod} [%/°C]	k_{kv0}	-0.368	-0.399	
	k_{0VA}	919.4	8.48e3		k_{0kv}	1.5e-5	4.6e-6	
	P_{VA0}	5	-5.55		k_{pkv}	0.388	-0.06	
	k_{pVA}	-0.695	-1.324		k_{ekv}	2.034	3.023	
k_{MP20C} [p.u.]	0.841	0.814		k_{dkv}	-0.46	-2.483		

The PV module weight ($Weighth_{Mod}$) can be evaluated by

$$Weighth_{Mod} = k_{WPN0} \cdot P_{MPP_{STC}}^{k_{WP}} \cdot n_{sMod}^{k_{WN}}$$

Figure 4-11, Figure 4-12 and Figure 4-13 show the parameter trends for the considered PV module technologies and the estimations based on the proposed/considered meta-parameters.

Deliverable 2.2

Table 7 summarizes the calculated meta-parameters from the created database of collected data for silicon crystalline PV modules.

Figure 4-14 shows the collected data related to linear output degradation for the analysed PV modules.

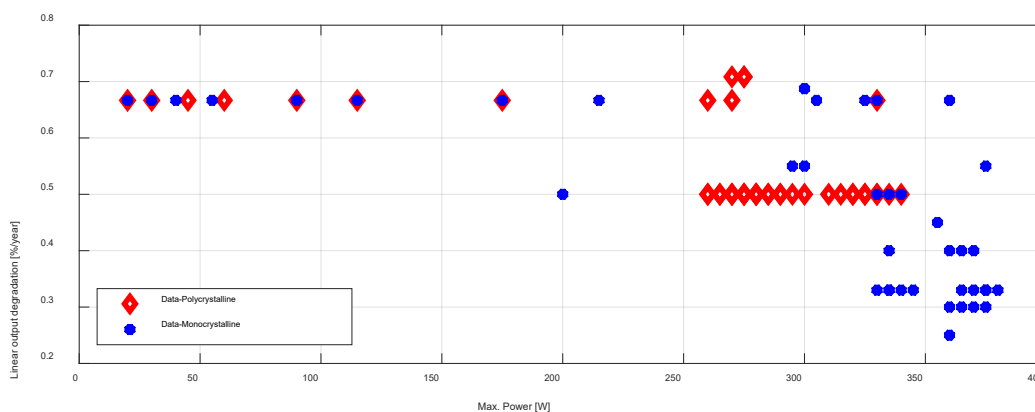


Figure 4-14 Guaranty - Linear Output Degradation for analyzed PV modules

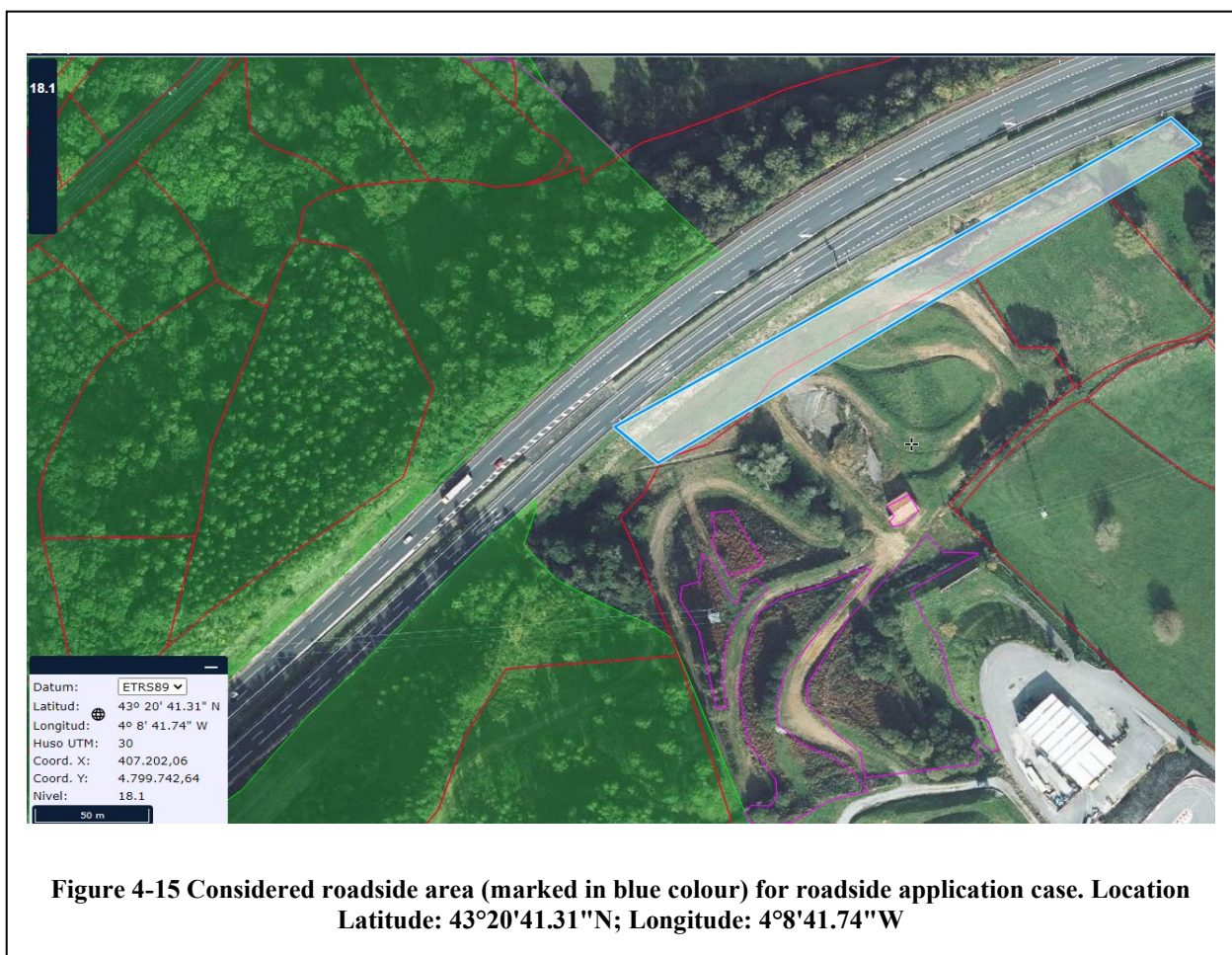
Deliverable 2.2

Assessment of applicable renewable energy generation technologies on NRA land and assets

4.3 CASE STUDY: ROADSIDE LOCATION

For this case study, the comparison of different RETs to maximize the annual energy production is done for a specific location. Figure 4-15 shows the considered roadside area for this case. The considered area is located at latitude: 43°20'41.31"N and longitude: 4°8'41.74"W. For example, the target area is located near the main road. The wind speed statistics for this location is shown in Figure 3-8. The solar radiation data is plotted in Figure 3-12.

Table 8 summarizes the terrain main characteristics needed for the RET evaluation. The comparison is done from the technology point of view but not from the discrete generation device point of view, so a meta-parameterized approach as introduced in (Barrera-Cardenas 2015) is considered and the obtained meta-parameters for each technology are used.



Deliverable 2.2**Table 8 Terrain characteristics for roadside case study**

Latitude	φ_{Lat}	43.342°	Longitude	λ_{Lon}	-4.145°
Equivalent Length	L_{eqA}	284.9 m	Equivalent Width	W_{eqA}	19.81 m
Total Available Area	A_{eq}	5643.869 m ²	Terrain Orientation (Azimuth)	Φ_A	30.47°
Surface roughness length	z_0	0.03	Zero plane displacement	z_d	4 m
Average air density	ρ_{air}	1.225 kg/m ³	UTC zone	ΔT_{UTC}	2
Mean wind speed at reference high	\bar{V}_{wREF}	6.4 m/s	Reference high for wind speed measurement	z_{REF}	50 m
Weibull shape factor	k_{wREF}	1.8	Prevalent wind orientation	ϕ_{Wind}	135°

4.3.1 SMALL SCALE WIND

First, small scale wind energy technologies have been evaluated. Based on the meta-parameters of each wind turbine technology obtained in section 4.1, different virtual wind turbines (with different nominal power) from each technology has been evaluated and wind farm design based on methodology presented in section 3.6 has been carried out for each wind turbine. In this way, a design space for each wind turbine technology has been evaluated in terms of annual energy production and total installed cost.

It has been considered a separation distance parallel to the prevailing wind direction of 9 rotor diameters for HAWT technology, 3 rotor diameters for Darrieus and hybrid type turbines and 2 rotor diameters for Savonius turbines. On the other hand, a separation distance perpendicular to the prevailing wind direction of 3 rotor diameters for HAWT technology, 2 rotor diameters for Darrieus and hybrid type turbines and 1 rotor diameters for Savonius turbines, have been considered in this study.

Deliverable 2.2

Assessment of applicable renewable energy generation technologies on NRA land and assets

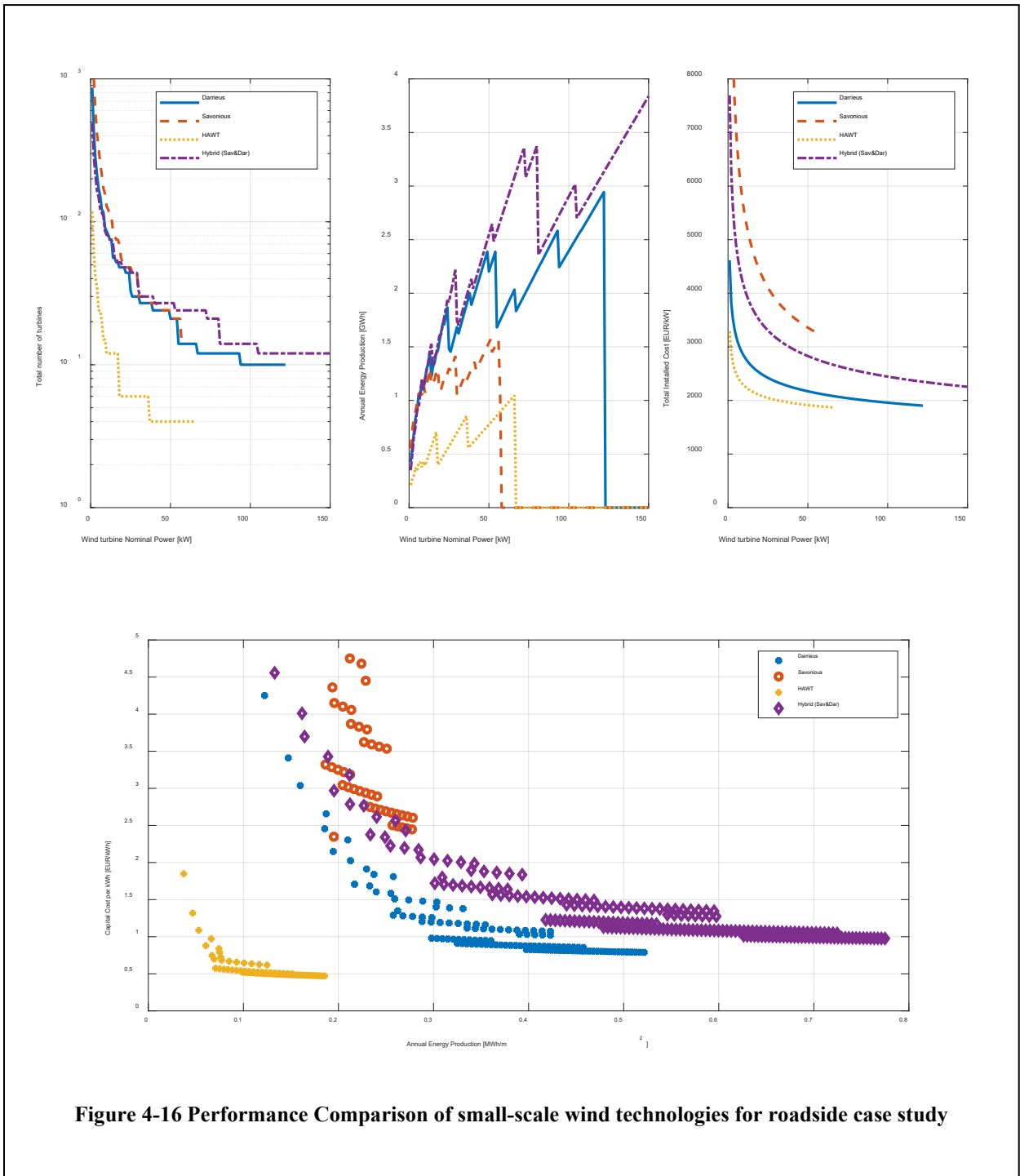


Figure 4-16 Performance Comparison of small-scale wind technologies for roadside case study

Figure 4-16 shows the results of small-scale wind turbine technology for the specific location of this case study. In top of Figure 4-16 the number of wind turbines that can be installed in the terrain, the expected annual energy production and the total installed cost against the wind turbine nominal power is plotted for each turbine technology. It can be noted that the number of turbines decreases as the wind turbine

Deliverable 2.2

Assessment of applicable renewable energy generation technologies on NRA land and assets



nominal power increases, as it can be expected because the turbine size increases with the nominal power, and therefore at some point the size of the turbine exceeds the available width of the terrain which limits the use of medium/large wind turbines in this case. A lower number of wind turbines based on HAWT technology can be installed compared to VAWT technologies because of the higher required separation distances for HAWT.

Regarding the expected annual energy production (AEP), it increases with the size of the turbine in all cases, showing that it is preferred to install a few big turbines than many too small turbines. However, it can be observed that the increment on AEP is not uniform, showing local maximums for the range of the considered wind turbines. The wind turbine technologies with the highest AEP are Darrieus and hybrid, while the lowest values for AEP are obtained with HAWT technology. This fact is linked with the limitation on the number of turbines that be installed for HAWT.

On the other hand, the total installed cost for the wind farm decreases as bigger turbines are used in all cases, as it can be noted from Figure 4-16. HAWT shows the lowest total installed cost and Savonius technology shows the highest cost. The expected total installed cost for small scale wind in this case range between 2000 and 4000 EUR/kW, which agrees with the reported in literature (IRENA 2021)

Finally, the AEP per unit area and capital cost per produced annual energy is plotted in bottom of Figure 4-16. It can be noted that a clear trade-off between these two performance indices is obtained for all technologies. It can be observed that a capital cost of 0.5 EUR per annual kWh produced with about 0.18 MWh per m² annual production can be achieved when HAWT is considered, while for Darrieus technology an annual energy production of 0.51 MWh per m² with capital cost of 0.8 EUR per kWh annually produced can be obtained, and the highest AEP of around 0.78 MWh per m² is obtained for Darrieus-Savonius hybrid technology with an associated capital cost of 1 EUR per kWh. The use of Savonius technology by itself does not show any advantage in this case.

4.3.2 SOLAR PV FARMS

The design of solar PV farms to be installed in the roadside terrain in this case study, has been done considering the monocrystalline and polycrystalline PV technologies. Similar approach as for small scale wind has been used, so the comparison has been done based on the monocrystalline and polycrystalline meta-parameters obtained in section 4.2, then different PV modules, based on different power ratings for each technology are evaluated and the solar PV farm evaluation approach, introduced in section 3.7, has been applied to each virtual PV module. As the evaluation of the solar PV farm does not only depends on the selected module, but also on the module orientation, tilt angle and distribution of the modules in the terrain, then additional degrees of freedom in the design have been considered for the sake of completeness.

First, for each type of module (mono- or poly-crystalline with a given rated power), different separation distances between PV modules have been explored. Also, as previously commented in section 3.2.2, an optimal module orientation and tilt angle that maximize the total annual average PV irradiance can be obtained, however these values does not guaranty the maximum annual energy production and therefore different values has been explored in the design. For this example, the optimal values are $\beta_{Mod.OPT} = 36^\circ$ and $\psi_{Mod.OPT} = -44^\circ$, and a design space including values for tilt angle between $\beta_{Mod.OPT} \pm 10^\circ$ and module orientation values between $\psi_{Mod.OPT} \pm 10^\circ$ have been considered.

Figure 4-17 shows the results of Si Crystalline technology for the specific location of this case study. The design space for monocrystalline and polycrystalline technologies are plotted along with the solutions that maximize the AEP for each PV module nominal power. As can be expected, the total number of PV modules that can be installed in the terrain decreases as the module nominal power increases, which is linked to the size/area of the module. A higher number of monocrystalline modules with given nominal power can be installed compared with polycrystalline modules with same nominal power. Also, it can be noted that higher AEP can be achieved when modules with higher nominal power are used. Monocrystalline technology will leave the highest expected AEP in all cases.

Deliverable 2.2

Assessment of applicable renewable energy generation technologies on NRA land and assets

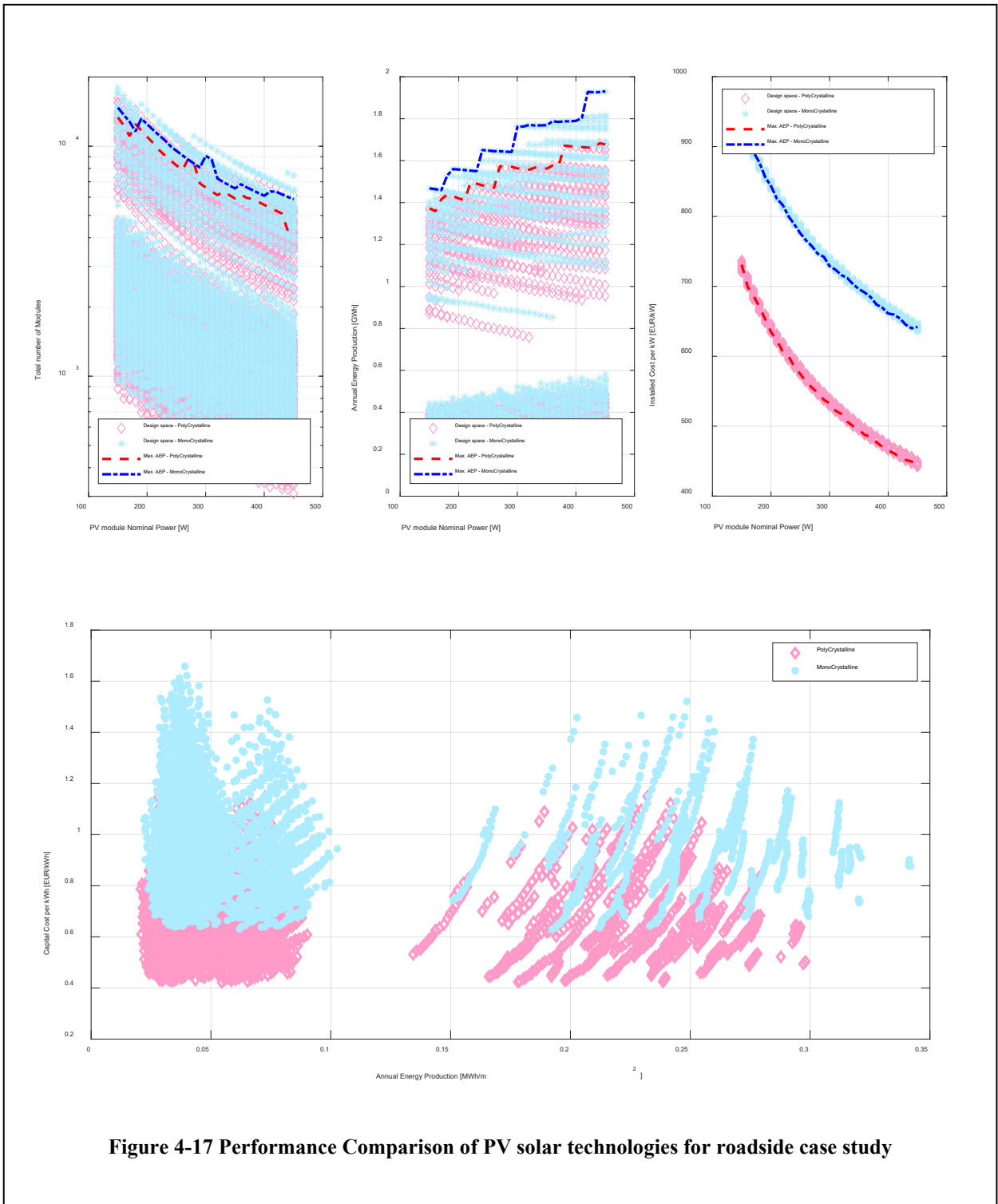


Figure 4-17 Performance Comparison of PV solar technologies for roadside case study

Deliverable 2.2

Assessment of applicable renewable energy generation technologies on NRA land and assets



Regarding the capital cost, it can be noted that the installed cost per kW decreases as the module nominal power increases. The lowest installed costs can be obtained with polycrystalline technology for all cases, which clearly introduces a trade-off between AEP and cost when both technologies are considered.

Finally, the AEP per unit area and capital cost per produced annual energy is plotted in bottom of Figure 4-17. It can be noted that a clear trade-off between these two performance indices is obtained for both technologies. It can be observed that a capital cost of 0.5 EUR per annual kWh produced with about 0.3 MWh per m² annual production can be achieved when polycrystalline PV technology is considered, while for monocrystalline PV technology, an annual energy production of 0.32 MWh per m² with capital cost of 0.75 EUR per kWh annually produced can be obtained.

5 CONCLUSION

This report reviewed the performance of different RETs and introduced a methodology for the assessment of applicable renewable energy generation technologies on NRA land and assets. It has been shown that the proposed methodology allows for the design and evaluation of renewable generation energy systems based on small- and large-scale wind turbines and solar PV modules.

A database of small-scale wind turbines and solar PV modules has been created within the framework of this study. The collected information has been used for analyzing the different trends and correlation between the different device's parameters needed for the performance evaluation of RETs. It has been shown that the technology trends can be quantified using meta-parametrization concept.

On the other hand, a methodology for the modelling and design of renewable energy generation systems based on solar and wind technologies has been proposed and adapted for evaluation of DEGS in NRA land and assets.

The main RET trends have been obtained and at the same time a comparison of different RETs has been made. The found meta-parameters have been used together with the proposed design approach for wind- and solar-farms, so a general comparison including different degrees of freedom can be performed and therefore the selection of the most appropriate RET can be achieved in future steps. It should be mentioned that the optimal selection of a RET depends not only on the RET performance itself but also on the terrain properties and available renewable energy sources in the location of interest.

For small scale wind turbines, it has been found that wind turbines based on Darrieus-rotor architecture, or a hybrid Savonius-Darrieus rotor architecture can bring some advantages in terms of allocation of wind turbines in terrains near the main roads.

Regarding PV modules, monocrystalline modules show better performance in terms of power density and efficiency but with a higher cost compared with polycrystalline modules.

A comparison of the different RETs considered in this report has been made for a specific application case with defined location and renewable energy characterization of a roadside terrain near the main road. The trade-off between annual energy production per unit area and capital cost per produced annual energy has been obtained for wind and solar technologies. For wind technologies, it has been shown that

Deliverable 2.2

Assessment of applicable renewable energy generation technologies on NRA land and assets



Darrieus wind turbines will allow for an annual energy production of 0.51 MWh per m² with capital cost of 0.8 EUR per kWh annually produced in the considered roadside location and available terrain. For solar PV technologies, it has been found that a capital cost of 0.5 EUR per annual kWh produced with about 0.3 MWh per m² annual production can be achieved when polycrystalline PV technology is considered, which shows the best trade-off for solar PV technologies.

The proposed method for annual energy production and capital cost estimation can be used in combination with other tools including regulatory framework, environmental impact, and business analysis to provide a clearer picture when selection of RET for a specific location needs to be done.

6 LIST OF REFERENCES

- Alahakoon, Sanath, and Mats Leksell. 2015. "Emerging Energy Storage Solutions for Transportation – A Review: An Insight into Road, Rail, Sea and Air Transportation Applications." *2015 International Conference on Electrical Systems for Aircraft, Railway, Ship Propulsion and Road Vehicles (ESARS)*. Aachen, Germany.
- Barrera-Cardenas, Rene A. 2015. *Meta-parametrised meta-modelling approach for optimal design of power electronics conversion systems: Application to offshore wind energy*. Trondheim, Norway: PhD Thesis, NTNU.
- Borunda, Monica & Rodriguez, Katya & Garduno, Raul & De la Cruz, Javier & Antunez-Estrada, Javier & Jaramillo. 2020. "Long-Term Estimation of Wind Power by Probabilistic Forecast Using Genetic Programming." *Energies* 13 (8): 1-24. doi:10.3390/en13081885.
- CENER; ERA-Net Plus NEWA. 2019. *Mapa Iberico de alta resolution*. Accessed 01 15, 2022. <https://www.mapaeolicoiberico.com/>.
- Cooper, P. I. 1969. "The absorption of radiation in solar stills." *Solar Energy* 333-346.
- Dezso Sera, Remus Teodorescu, Pedro Rodriguez. 2007. "PV panel model based on datasheet values." *2007 IEEE International Symposium on Industrial Electronics*. Vigo, Spain: IEEE. 2392-2396. doi:10.1109/ISIE.2007.4374981.
- Djohra Saheb, Mustapha Koussa and Seddik Hadji. 2014. "Technical and economical study of a Stand-alone Wind Energy System for Remote Rural Area Electrification in Algeria." *Renewable Energy and Power Quality Journal (RE&PQJ)* 638-643.
- Elbarbary, Z.M.S. and Alranini, M.A. 2021. "Review of maximum power point tracking algorithms of PV system." *Frontiers in Engineering and Built Environment* 68-80. doi:<https://doi.org/10.1108/FEBE-03-2021-0019>.
- Energy, Green Rhino. 2016. *Impact of Shading*. Accessed 06 2022. <http://www.greenrhinoenergy.com/solar/performance/shading.php>.
- European Commission - EU Science Hub. 2020. *PVGIS tool version 5.2*. March. Accessed May 2022. https://re.jrc.ec.europa.eu/pvg_tools/en/.
- Gabriel Domingues-Olavarría, Pontus Fyhr, Avo Reinap, Mats Andersson, and Mats Alakula. 2017. "From Chip to Converter: A Complete Cost Model for Power Electronics Converters." *IEEE TRANSACTIONS ON POWER ELECTRONICS* 8681-8692.
- GARCIA, JUAN PABLO SANCHEZ DE LARA. 2013. *Wind turbine database: Modelling and analysis with focus on upscaling*. Master's thesis in the Master programme Applied Mechanics, Goteborg: CHALMERS UNIVERSITY OF TECHNOLOGY.
- Hammami, Manel, Simone Torretti, Francesco Grimaccia, and Gabriele Grandi. 2017. "Thermal and Performance Analysis of a Photovoltaic Module with an Integrated Energy Storage System." *Applied Sciences (MDPI)* 7 (1107). doi:10.3390/app7111107.
- Holmes, JD. 2015. *Wind Loading of Structures*. Boca Raton, Florida: CRC Press.
- International Renewable Energy Agency. 2016. *Wind Power*. Technology Brief, IEA-ETSAP and IRENA. www.irena.org.
- IRENA. 2021. *Renewable Power Generation Cost in 2020*. Abu Dhabi: International Renewable Energy Agency.
- J. F. Manwell, J. G. McGowan, A. L. Rogers. 2009. *Wind energy explained: Theory, Design and Application*. 2nd. Amherst, USA: John Wiley & Sons.

Deliverable 2.2

Assessment of applicable renewable energy generation technologies on NRA land and assets



- Jake Badger, Neil Davis, Ray Drummond, Andrea Hahmann, Duncan Heathfield, Niels Gylling Mortensen and Marko Onninen. 2021. *Global Wind Atlas*. 04. Accessed 02 2022. <https://globalwindatlas.info/>.
- Justus, C. G, W. R Hargraves, A Mikail, and D. Graber. 1978. "Methods for estimating wind speed frequency distributions." *Journal of Applied Meteorology* 350-353.
- Kharade, Vishwajeet and Kunal K. Jagtap. 2019. "A Review Study on Vertical axis Wind Turbines(lift and drag type) for Optimizing the Aerodynamic and Structural Performance." *IOSR Journal of Engineering (IOSR JEN)* 61-65.
- Kumar, P.M., Sivalingam, K., Narasimalu, S., Lim, T.-C., Ramakrishna, S. and Wei, H. 2019. "A Review on the Evolution of Darrieus Vertical Axis Wind Turbine: Small Wind Turbines." *Journal of Power and Energy Engineering* 7: 27-44. doi:10.4236/jpee.2019.74002.
- Lukic, Srdjan M., Jian Cao, Ramesh C. Bansal, Fernando Rodriguez, and Ali Emadi. 2008. "Energy Storage Systems for Automotive Applications." *IEEE Transactions on Industrial Electronics* 55 (6): 2258 - 2267.
- Mehrpooya, Payam. 2014. "IMPROVEMENT OF VERTICAL-AXIS WIND TURBINE PERFORMANCE VIA TURBINE COUPLING." *Thesis for Master of science in Mechanical and Aerospace Engineering*. Chicago: Illinois Institute of Technology, July. doi:10.13140/RG.2.2.13616.76808.
- Milne, R. M. 1921. "Note on the Equation of Time." *The mathematical Gazette* 372-375.
- National Renewable Energy Laboratory. 2021. *National Solar Radiation Database (NSRDB) Ver 3.2.1*. Dec. Accessed May 2022. <https://nsrdb.nrel.gov/>.
- NREL - EnergyPlus. 2021. *EnergyPlus weather data*. Accessed 2022. <https://www.google.com/maps/d/viewer?msa=0&dg=feature&mid=1BhMLmWuS8BVuqdkGCYsAsilqFy4&ll=42.30004341517257%2C25.28416418536264&z=4>.
- Okil, M., M. S. Salem, Tarek M. Abdolkader, and A. Shaker. 2021. "From Crystalline to Low-cost Silicon-based Solar Cells: a Review." *Silicon*. doi:<https://doi.org/10.1007/s12633-021-01032-4>.
- S.G.Bowden, C.B.Honsberg and. 2019. *Photovoltaics Education Website*. Accessed May 2022. <https://www.pveducation.org/>.
- Sarlioglu, Bulent, Casey T. Morris, Di Han, and Silong Li. 2017. "Driving Toward Accessibility: A Review of Technological Improvements for Electric Machines, Power Electronics, and Batteries for Electric and Hybrid Vehicles." *IEEE Industry Applications Magazine* 23 (1): 14-25.
- Sedagha, Ahmad, Mohamed Gaith, Khalil Khanafer, and Ehab Bani-Hani. 2016. "Rated Wind Speed Reality or Myth for Optimization in Design of Wind Turbines." *Eleventh International Conference on Ecological Vehicles and Renewable Energies (EVER)*. IEEE. 1-4.
- Skjong, E., R. Volden, E. Rødskar, M. Molinas, T. A. Johansen, and J. Cunningham. 2016. "Past, Present, and Future Challenges of the Marine Vessel's Electrical Power System." *IEEE Transactions on Transportation Electrification* 2 (4): 522-537.
- Tony Burton, David Sharpe, Nick Jenkins, Ervin Bossanyi. 2001. *Wind Energy Handbook*. John Wiley and Sons Ltd.
- Tummala, Abhishiktha, Ratna Kishore Velamati, Dipankur Kumar Sinha, V. Indrajaya, and V. HariKrishna. 2016. "A Review on small scale wind turbines." *Renewable and Sustainable Energy Reviews* 1351-1371.
- University of Cantabria. 2021. *Deliverable 2.1: Report of main renewable energy technologies (RETs) for the road infrastructure*. ENROAD.

Deliverable 2.2

Assessment of applicable renewable energy generation technologies on NRA land and assets



-
- Wass, Ryan. 2018. "Design of Wind Turbine Tower Height and Blade Length: an Optimization Approach." *Mechanical Engineering Undergraduate Honors Theses*. Fayetteville: University of Arkansas, 09.
2021. *Wikipedia*. 26 08. Accessed 02 01, 2022. https://en.wikipedia.org/wiki/Log_wind_profile.
- World Bank Group . 2021. *Global Solar Atlas (GSA 2.6)*. July. Accessed May 2022. <https://globalsolaratlas.info/map>.

ANNEX 1:

Study of energy storage technologies (BESS)

Supporting the implementation by NRAs of renewable energy technologies in the road infrastructure



Annex to Deliverable 2.2

Study of energy storage technologies (BESS)

Deliverable no.:	2.2
Work Package no.:	2
Status	Submitted
Version:	01
Author:	ARUP
Date:	27/04/2023
Dissemination level:	Confidential

Disclaimer: ENROAD has received funding from the CEDR Transnational Road Research Program – Call 2019. This document reflects only the author’s views. The Conference of European Directors of Roads (CEDR) is not responsible for any use that may be made of the information contained therein.

List of AUTHORS		
Sofie Kirk	ARUP	sofie.kirk@arup.com
Javier Anton	ARUP	javier.anton@arup.com

List of REVIEWERS		
Ramón Rodríguez	ARUP	ramon.rodriquez@arup.com

TABLE OF CONTENTS

1	INTRODUCTORY REMARKS	5
1.1	<i>Purpose of the report</i>	5
1.2	<i>Methodology</i>	5
2	STUDY OF AVAILABLE BATTERY ENERGY STORAGE SYSTEMS TECHNOLOGIES FOR RENEWABLE GENERATION	6
2.1	<i>Key applications for battery storage in grid</i>	7
2.2	<i>Battery technologies for renewables integration</i>	8
2.2.1	<i>Lithium-Ion</i>	8
2.2.2	<i>Flow Battery</i>	10
2.2.3	<i>Lead Acid</i>	12
2.2.4	<i>Sodium sulphur</i>	14
2.2.5	<i>Nickel based</i>	15
2.2.6	<i>Flywheels</i>	16
2.3	<i>Battery lifetime & Degradation</i>	18
3	EUROPEAN MARKET	19
3.1	<i>Market overview</i>	19
3.1.1	<i>Regulations and incentives</i>	19
3.1.2	<i>Manufacturers</i>	20
4	TYPICAL BATTERY COSTS	21
	LIST OF REFERENCES	24

LIST OF TABLES

Table 1.- The need for storage. (Arup, 2019)	7
Table 2: Summary of Li-ion technologies (Cubes, 2022)	9
Table 3.- decision-making findings. Lithium-ion. (Arup, 2019) (BloombergNEF, 2023)	10
Table 4.- Decision-making findings. Flow Battery. (Arup, 2019) (BloombergNEF, 2023)	12
Table 5.- Decision-making findings. Lead Acid. (Arup, 2019) (BloombergNEF, 2023)	13
Table 6.- Decision-making findings. Sodium Sulphur. (Arup, 2019) (BloombergNEF, 2023)	15
Table 7.- Decision-making findings. Nickel Based. (Arup, 2019) (BloombergNEF, 2023)	16
Table 8: Expected lifespan of different battery technologies.	18

LIST OF FIGURES

Figure 1.- Application and technology overview. (Arup, 2019).....	6
Figure 2.- Global share of commissioned and planned renewables integration energy storage projects by energy storage technology since 2013 (BloombergNEF, 2023).....	8
Figure 3: Lithium-ion battery make-up (Source: Arup Five Minute Guide).....	9
Figure 4: Diagram of flow battery (Arup, 2019).....	11
Figure 5: Diagram of lead-acid technology (Arup, 2019).....	13
Figure 6: Diagram of a sodium sulphur battery (Arup, 2019).....	14
Figure 7: Diagram of sodium nickel chloride battery technology (Arup, 2019).....	15
Figure 8: Diagram of flywheel technology (Arup, 2019).....	17
Figure 9: Overview of battery storage capacities for varying applications in Europe (BloombergNEF, 2023).....	19
Figure 10: Gigafactories within Europe (EnergiGune, 2021).....	20
Figure 11: Capital costs for battery packs for different battery technologies (Arup, 2019) (Lazard, 2018).	21
Figure 12: Average global cost of battery pack since 2010.....	22
Figure 13.- Global average capital costs for varying lithium-ion chemistries battery packs (BloombergNEF).....	22
Figure 14.- Total CAPEX for lithium-ion installations for projects within Europe (excludes grid connection and transformer cost).....	23

1 INTRODUCTORY REMARKS

1.1 PURPOSE OF THE REPORT

This report aims to identify the Battery Energy Storage Systems (BESS), potentially applicable to NRA's in the area of renewable energy production. This study will focus on the market and technologies available for renewables integration in the grid. This application is considered to be the most suitable for the purpose of integrating renewables on the road infrastructure.

By setting out and summarising the work done to identify the applicable BESS technologies, the report can act as a reference resource for the project team to help the NRA's answer the following questions:

- Based on the research undertaken by the ENROAD team, what are the relevant technologies available in the market suitable for the integration of renewables?
- What are the opportunities and challenges arising from each specific technology applications? What are the decision-making parameters to select a BESS technology depending on the application?
- How developed is the European market and which technologies are being implemented? How are BESS being applied in the European energy market?
- What are the estimated main costs to consider when implementing BESS?

1.2 METHODOLOGY

The methodology adopted was to carry out research and analysis at a global level and then to do the same exercise at European level of existing and foreseen BESS technologies and applications for renewables on the road infrastructure.

Arup has based the report on public available data and its own benchmarks, when available.

The analysis intends to identify potential use of BESS. How and what technologies could be used in the business models to be proposed for the NRAs in their aims.

The results of the desktop based research was complemented by the outcomes of the stakeholder integration workshops held together with the NRAs and the stakeholder selected and invited by them.

2 STUDY OF AVAILABLE BATTERY ENERGY STORAGE SYSTEMS TECHNOLOGIES FOR RENEWABLE GENERATION

This section of the report aims to give an overall view of the key applications for battery storage and the various technologies available for utility scale renewables integration in the grid.

There is a wide range of battery and cell technologies available on the market for energy storage purposes. As such, depending on the application, the most appropriate technology will vary. Each type of battery technology has its own advantages and disadvantages. For example, energy density, response time and shelf life are some of the key characteristics which are used in the selection of a battery technology in a particular application. Figure 1 details the suitability of varying battery technologies across applications in fast response systems, distribution scale systems and large capacity grid scale systems.

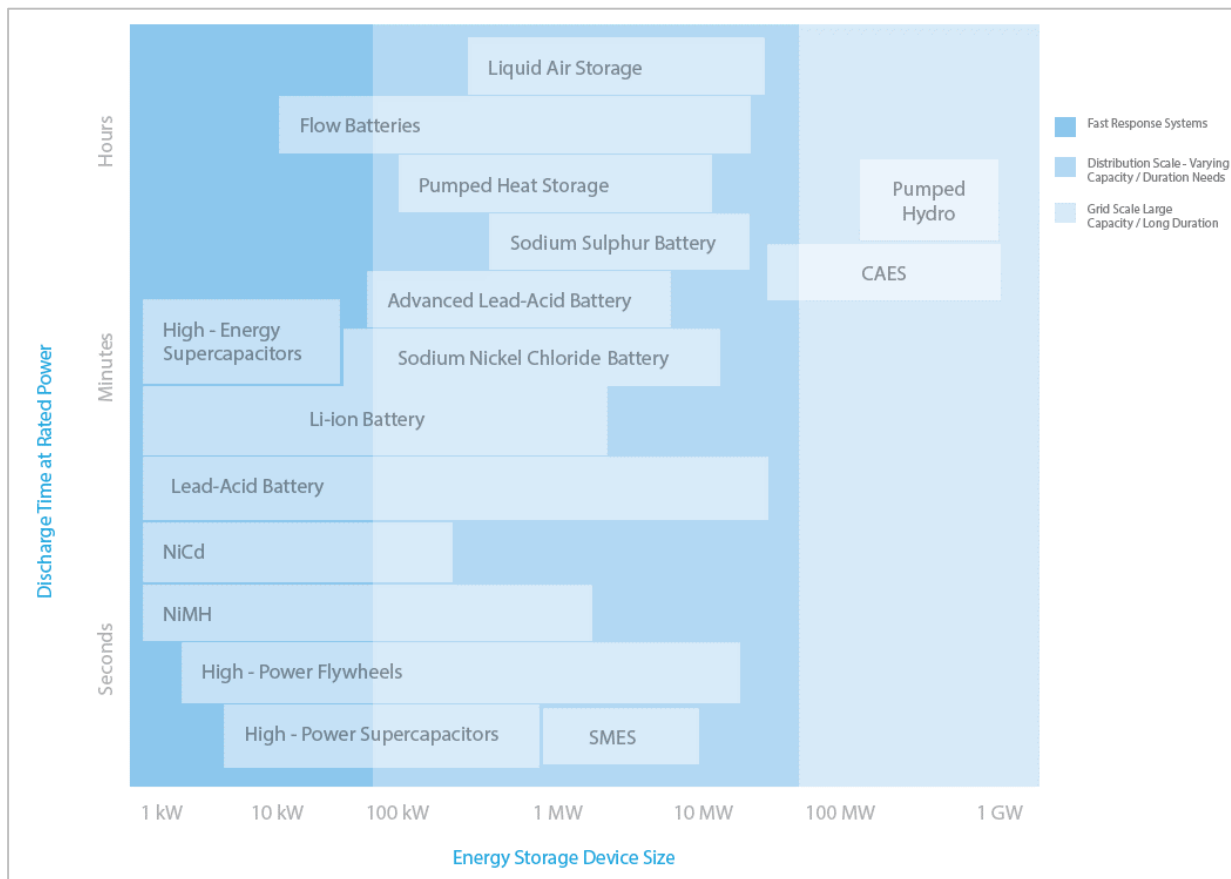


Figure 1.- Application and technology overview. (Arup, 2019)

Technologies appropriate for grid scale applications are those which have been considered as part of this study due to the requirement of integration of renewables technologies on the road infrastructure. Other applications for stationary batteries include, for example, distributed batteries. These are batteries situated close to the end user of electricity, e.g., in a house or office building.

2.1 KEY APPLICATIONS FOR BATTERY STORAGE IN GRID

Grid scale batteries may be implemented into the energy system to serve a range of functions.

- Grid services to provide system stability e.g. frequency response and reserves, voltage control and reactive power, constraint management and inertia.
- Capacity markets e.g., the integration of batteries with renewable technologies to provide long term security in supply of renewables.
- Wholesale energy arbitrage e.g., storing or purchasing electricity from grid when prices are low and reselling back to grid when prices are higher.

Table details different storage needs within the sector of stationary battery applications. As part of this study, a review of technologies used within renewables integration applications will be considered.

Table 1.- The need for storage. (Arup, 2019)

Storage need	Revenue stream	Revenue stream	Revenue stream
The ability to match generation and demand. Shift generated energy from off peak times to when it is needed. Grid level and small scale domestic applications.	Price arbitrage, reduction in demand charges	Minutes - Hours	kW - MW
Peaking plants are needed in order to meet changes in supply and demand conditions. Storage could provide this capacity in certain circumstances and reduce the need for fossil fuel peaking.	Electric supply capacity – power capacity contract and price arbitrage	Hours	MW
Increase the efficiency of thermal generation by ensuring a constant output. Storage can provide these load following services.	Load following – power capacity contract	Minutes - Hours	MW
Storage can be used to reconcile momentary differences between supply and demand. Storage can both adsorb and provide energy providing a twofold service.	Balancing services – power capacity contract	Seconds - Minutes	MW
Storage can provide reserve capacity that can be called upon in the event of the usual electricity supply resources becoming unexpectedly unavailable.	Electric supply reserve	Hours	MW
To maintain voltage and frequency at the required levels following a large disturbance requires a fast response. Storage can provide this service.	Regulation response and voltage support – Avoided penalties from system operator	Milliseconds - Seconds	kW - MW
Energy storage used for transmission support improves T&D system performance by compensating for electrical anomalies almost instantly.	Transmission network support – Avoided penalties from system operator	Milliseconds - Seconds	kW - MW
Transmission systems are becoming congested during periods of peak and off-peak demand. Storage can be used to mitigate this issue instead of investment in new transmission assets.	Asset upgrade deferral – Avoided cost of infrastructure investments	Hours	kW - MW
Storage to provide energy in the event of a system failure until the system is restored, or alternative energy sources are available.	Electric service reliability – Reducing production / operating losses	Hours	kW - MW

2.2 BATTERY TECHNOLOGIES FOR RENEWABLES INTEGRATION

A review of global existing and planned installations with applications in renewable energy integration was taken to determine technologies for detailed review. Figure 2 shows the percentage share for different battery storage technologies in applications for renewable energy integration projects globally for the previous 10 year (since 2013).

Based on the figure 2 and table 1 Arup selected the technologies for review. The technologies that will be reviewed in depth as part of this study are lithium-ion, flow batteries, lead-acid, sodium sulphur, flywheels and nickel-based batteries.

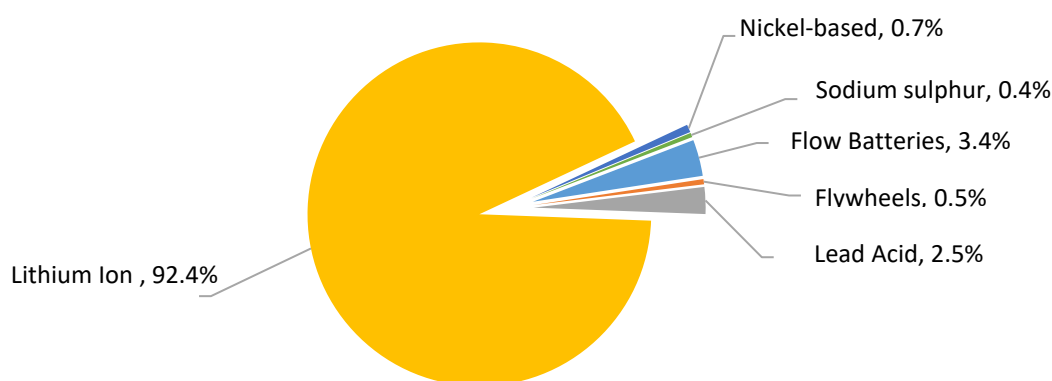


Figure 2.- Global share of commissioned and planned renewables integration energy storage projects by energy storage technology since 2013 (**BloombergNEF, 2023**)

2.2.1 LITHIUM-ION

Lithium-ion batteries are a type of rechargeable battery in which lithium ions move from the negative electrode to the positive electrode during discharge and back when charging. Due to their high energy density, they are commonly used in consumer electronic products such as smart phones. They are also commonly used in electric vehicles, a deployment which is expected to drive down cost and improve performance. The technology can be scaled up to utility scale size and used in grid applications such as frequency response. Research and development is on-going in various other chemistries of the battery type with a view to improving performance and reducing the cost. Lithium-ion battery technologies comprise a range of chemical make-ups, for example, lithium iron phosphate (LFP), lithium manganese oxide (LMO), lithium nickel cobalt manganese oxide (NCM) and lithium titanate (LTO). The main two lithium-ion sub-chemistries used within the stationary storage market and LFP and NMC.

Table 2: Summary of Li-ion technologies (Cubes, 2022)

Chemistry	Abbreviation	Typical Use
Lithium Cobalt Oxide	LCO	Mobile consumer devices, laptops, smartphones
Lithium Iron Phosphate	LFP	Stored energy for mission critical environments, EVs
Lithium Nickle Cobalt Aluminium Oxide	NCA	EVs
Lithium Manganese Oxide	LMO	Medical devices, power tools, consumer devices
Lithium Nickel Manganese Cobalt Oxide	NMC	EV powertrains, power tools, electrical grid storage

Lithium-ion batteries are the most widely used technology for grid energy storage purposes in the European and global market, having the ability to supply megawatts of power for hours at a time. At the time of writing, 610 out of 723 battery storage projects listed in Europe on BloombergNEF databases use lithium-ion technologies as the primary energy storage technology in their systems (BloombergNEF, 2023). Markets for integration in the grid include frequency regulation, price arbitrage and renewables integration.

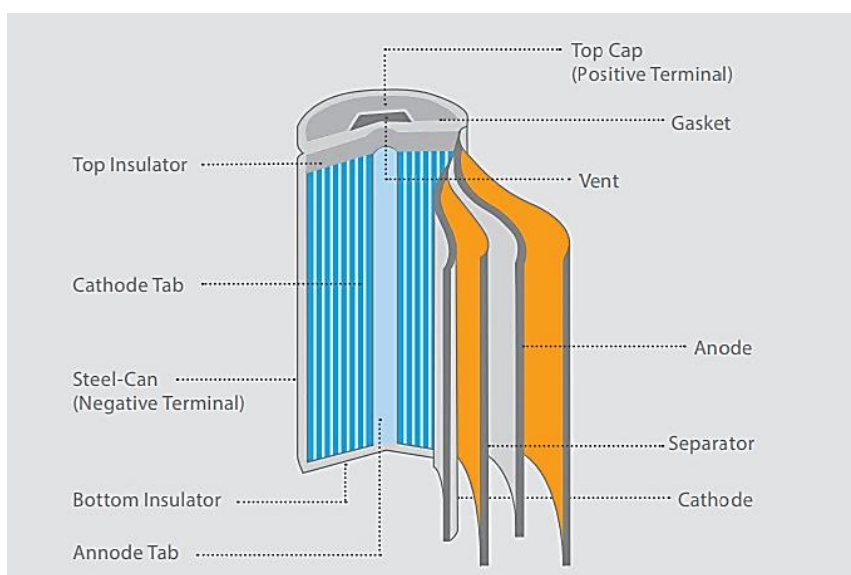


Figure 3: Lithium-ion battery make-up (Source: Arup Five Minute Guide)

Renewables integration projects

At the time of writing, Arup has identified 80 commissioned energy storage projects in Europe serving the purpose of renewable systems integration. Some examples are:

- GIGA Buffalo Solar Wind Energy Storage Project** (BloombergNEF, 2023)
 A 24MW/48MWh storage project located in the Netherlands, developed by GIGA Storage BV. This project was commissioned in 2022 and is co-located with both wind and solar assets.
- Enerparc Buettel Energy Storage Project** (BloombergNEF, 2023)
 A 12MW/8MWh energy storage system located in Germany, commissioned in April 2023. This project supports a 35MW distributed generation solar PV installation.

- **GRIDSERVE Clayhill Farm Energy Storage Project** (BloombergNEF, 2023)
This project is a 6MW/6MWh energy storage installation in Bedfordshire, UK, commissioned in 2016. The energy storage facilitates a 10MW PV plant.
- **Akuo Energy Mortella Corsica Solar Energy Storage Project** (BloombergNEF, 2023)
A 7MW/7MWh battery installation, supporting a 7MW PV plant in Corsica. This project was commissioned in 2015.

Additionally, Arup has identified 65 projects for battery storage in the pipeline, either recently announced or with financing already secured. Upon review of these projects, the trends in upscaling of capacity can be seen within the market.

- **Quinbrook Fortress Energy Storage Project** (BloombergNEF, 2023)
Announced in 2020, this battery storage project will provide 150MW/300MWh of storage to a 350MW PV plant in Kent, England.
- **Enlight Renewable Gecama Solar Energy Storage Project** (BloombergNEF, 2023)
A 100MW/200MWh storage project in Spain, announced in January 2023. This project will provide energy storage to a 250 MW solar PV farm.
- **Hive Energy Bluesky300 Hybrid Solar Energy Storage Project** (BloombergNEF, 2023)
A 100MW energy storage project will be connected to a 100MW PV plant located in Greece. This project was announced in September 2022.

Key findings

Table 3.- decision-making findings. Lithium-ion. (Arup, 2019) (BloombergNEF, 2023)

Lithium ion	
Round-trip Efficiency	88-90%
Total identified capacity and output in Europe in renewable energy integration (includes announced, under development and commissioned projects)	512 MW / 742 MWh
Advantages	<ul style="list-style-type: none"> • Very high energy density • Ability to tolerate large number of discharges cycles • High efficiency • Most mature energy storage technology for renewable energy integration purposes
Disadvantages	<ul style="list-style-type: none"> • High costs • Negative effects of overcharging and over discharging

2.2.2 FLOW BATTERY

Flow batteries are a rechargeable battery using two liquid electrolytes, one positively charged and one negative, as the energy carriers. The electrolytes are separated using an ion-selective membrane, which under charging and discharging conditions allows selected ions to pass and complete chemical reactions. The electrolyte is stored in separate tanks and is pumped into the battery when required. The storage capacity of flow batteries can be increased by simply utilising larger storage tanks for the electrolyte. Several chemistries are possible for the battery.

Like Li-ion batteries, flow batteries can comprise of a range of chemistries, the most common ones being vanadium redox and zinc bromine. Vanadium redox is the most commercially mature technology available for flow batteries.

The modularity and scalability of flow batteries mean that they are suitable for many grid applications such as load balancing, standby power and the integration of renewable energy sources.

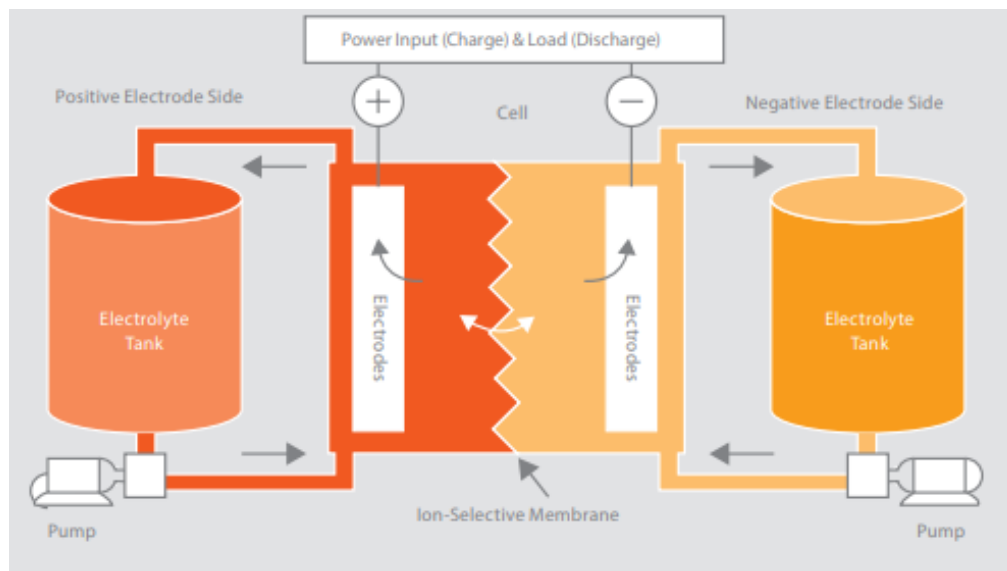


Figure 4: Diagram of flow battery (Arup, 2019)

Renewables integration projects

The number of flow battery installations identified for renewables integration in Europe is limited. A total of 6 projects have been identified in state of commissioned within Europe, with each installation having relatively low capacities when compared to those which are installed using lithium-ion technologies (BloombergNEF, 2023).

- REDT Cornwall Energy Storage project** (BloombergNEF, 2023)
 A vanadium redox flow battery installation in the UK with a storage capacity of 1.08MWh. The battery was commissioned in 2017 and supports a 350kWp solar PV installation.
- Robert Bosch & BWP Braderup-Tinningstedt Braderup Flow Battery Energy Storage Project** (BloombergNEF, 2023)
 A 0.325MW/1MWh vanadium redox flow battery installed in Germany. This project was commissioned in 2014 and is located alongside a 18MW wind farm.
- EGPE Son Orlandis Solar Energy Storage Project** (BloombergNEF, 2023)
 This project is a 1.1MW/5.5MWh vanadium redox battery installation in the Balearic Islands, Spain. Construction for this project began in December 2021. It will support energy storage needs for a 3.34MW solar farm.

Although the identified market for flow batteries in Europe is currently limited, there are a range of installations elsewhere which confirm the technical viability of the technology for renewable systems integration within the grid.

- Liaoning Datang International Wanfangdian Zhenhai Wind Energy Storage Project** (BloombergNEF, 2023)
 A 10MW/40MWh vanadium redox Energy storage installation, commissioned in 2020 in China. This project serves a 100MW windfarm.
- Hokkaido Electric Minamihayakita Substation Energy Storage Project** (BloombergNEF, 2023)
 A 15MW/60MWh vanadium redox storage system installed in Japan in 2015. This project stores energy and smooths output from a utility scale solar and wind farm.

Key findings

Table 4.- Decision-making findings. Flow Battery. (Arup, 2019) (BloombergNEF, 2023)

Flow battery	
Round-trip Efficiency	74-77%
Total identified capacity and output in Europe in renewable energy integration (includes announced, under development and commissioned projects)	3MW / 12MWh
Advantages	<ul style="list-style-type: none"> • Less sensitive to high depths of discharge • Ability to tolerate large number of discharge cycles • Virtual unlimited capacity
Disadvantages	<ul style="list-style-type: none"> • Low energy density • Limited project examples in Europe

2.2.3 LEAD ACID

Lead acid battery technology is the most established battery technology. There are several variants of the technology available. Flooded lead-acid batteries immerse the electrodes in liquid electrolytes and release gases upon charging. An example of this is a standard 12V car battery. Sealed lead acid batteries come in two forms - absorbed glass mat batteries create energy by immobilising electrolytes with a microfiber glass mat, while gel cell batteries have the electrolyte mixed with silica dust to form an immobilised gel. Sealed batteries do not require the regular addition of water to the cells and vent less gas than flooded lead-acid batteries. However, they have a longer re-charge time and shorter useful life. Advanced lead acid batteries have been developed and are particularly suited to energy storage applications.

Lead acid batteries are predominantly used for starting vehicle engines as well as for backup power supplies and for grid energy storage. The technology is mature for use as ancillary service such as an Uninterruptible Power Supply (UPS), with demonstrated applications for bulk energy storage. Lead acid has been demonstrated as storing between 0.1 and 10 MW over a period of hours, but there are examples of projects which have capacities up to 50MW. The technology can be used in applications in grid-scale storage and distributed storage.

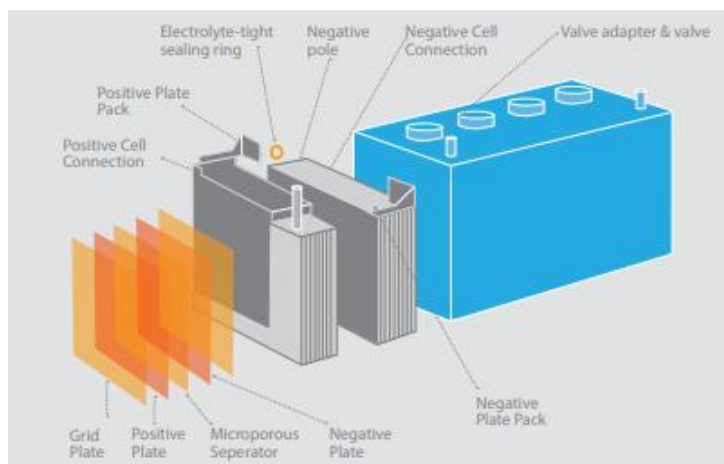


Figure 5: Diagram of lead-acid technology (Arup, 2019)

Renewables integration projects

Arup has identified 3 projects in Europe (in Germany) which utilise lead-acid technology for renewables integration applications, the most recent being commissioned in 2019. An example project includes:

- Belectric Germany Energy Storage Project** (BloombergNEF, 2023)
 A 1.6MW/2MWh lead acid battery installation in Germany. This project was commissioned in 2014 and supports a 67.8MW solar PV plant.

Outside of Europe exists wider selection of lead-acid installations supporting renewables, for example:

- Kazenomatsubara Shizen Energy Noshiro Energy Storage Project** (BloombergNEF, 2023). A 9.64MW/24.1MWh installation in Japan, commissioned in 2016. This energy storage project supports a 39.1MW wind farm.
- Three Gorges Group Changdu Basu Yiqing Solar Energy Storage Project Phase I** (BloombergNEF, 2023). A 5MW/20MWh lead acid battery installation connected to a 20MW PV plant in Tibet, China, commissioned in 2022.

Key findings

Table 5.- Decision-making findings. Lead Acid. (Arup, 2019) (BloombergNEF, 2023)

Lead acid	
Round-trip Efficiency	82%
Total identified capacity and output in Europe in renewable energy integration (includes announced, under development and commissioned projects)	2 MW / 2MWh (last installation in 2014, note no planned installations in pipeline)
Advantages	<ul style="list-style-type: none"> End of life recycling infrastructure in place Relatively efficient Low self-discharge
Disadvantage	<ul style="list-style-type: none"> Low energy density Susceptible to high depths of discharge

2.2.4 SODIUM SULPHUR

A sodium sulphur battery is a molten state battery constructed from sodium (Na) and sulphur (S). The battery casing is the positive electrode while the molten core is the negative electrode. The battery operates at high temperatures of between 300-350°C, while lower temperature versions are under development. In charging, the sodium ions are transported through the ion selective conductor to the anode reservoir. Discharge is the reverse of this process. Because sodium ions move easily across the ion selective conductor, but electrons cannot, there is no self-discharge. When not in use the batteries are typically left under charge so that they will remain molten and be ready for use when needed. If shut down and allowed to solidify, a reheating process is initiated before the batteries can be used again.

NaS batteries can be used for many grid applications such as: power quality applications, grid stabilisation and the integration of renewable energy sources.

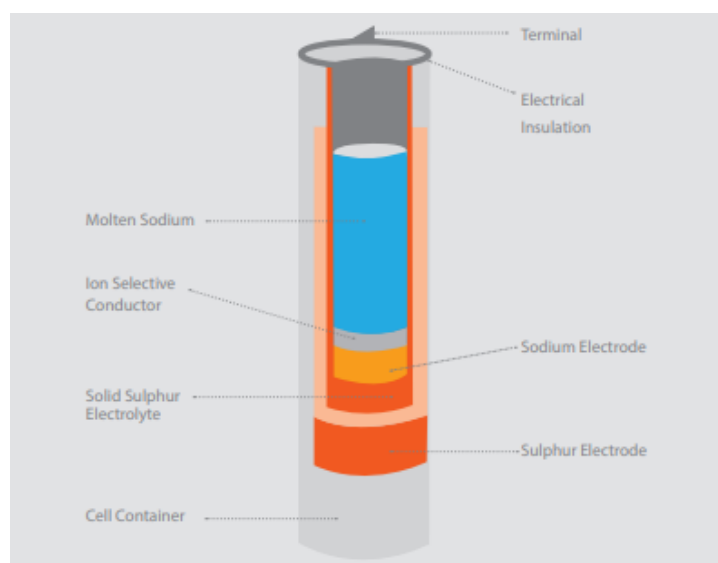


Figure 6: Diagram of a sodium sulphur battery (Arup, 2019)

Renewables integration projects

This type of installation is not popular in Europe, with a total of 10 identified project examples in grid applications. With the specific application of renewables integration, there is one identified project example within Europe.

- **Enercon Emden Energy Storage Project** (BloombergNEF, 2023)
A 0.8MW/5.8MWh sodium sulphur battery project commissioned in 2009 in Germany to support a wind farm.

Outside of Europe, additional examples of installations exist but the technology uptake is still low with just 13 identified commissioned installations in renewables integration globally, many of which are located in Japan. Examples include:

- **Kyushu Electric Buzen Energy Storage Project** (BloombergNEF, 2023)
A 50MW/300MWh NaS Energy storage project in Japan, commissioned in 2016.

Key Findings

Table 6.- Decision-making findings. Sodium Sulphur. (Arup, 2019) (BloombergNEF, 2023)

Sodium Sulphur	
Round-trip Efficiency	80%-82%
Total identified capacity and output in Europe in renewable energy integration (includes announced, under development and commissioned projects)	3 MW / 18 MWh (last installation in 2012, note no planned installations in pipeline)
Advantages	<ul style="list-style-type: none"> • High energy density • Long life cycle • Quick response
Disadvantages	<ul style="list-style-type: none"> • Heating required in process • Safety issues with molten sodium

2.2.5 NICKEL BASED

Nickel-based batteries are a type of rechargeable battery technology that use nickel-based compounds as their positive electrode or cathode. There are two main types of nickel-based batteries. There are a variety of different chemistries which make up this technology group, for example, nickel-cadmium (Ni-Cd), nickel-metal hydride (Ni-MH) and nickel-sodium chloride. Nickel sodium chloride is used within stationary storage applications, a chemistry consists of a nickel chloride cathode, a beta alumina separator and a liquid sodium anode. The operating temperature of the cell is between 270 C and 350°C. In charging, the sodium ions are transported through the beta alumina to the anode reservoir. Discharge is the reverse of this process. Because sodium ions move easily across the beta alumina but electrons cannot, there are no side reactions, and therefore no self-discharge.

When not in use the batteries are typically left under charge so that they will remain molten and be ready for use when needed. If shut down and allowed to solidify, a reheating process is initiated before the batteries can be used again.

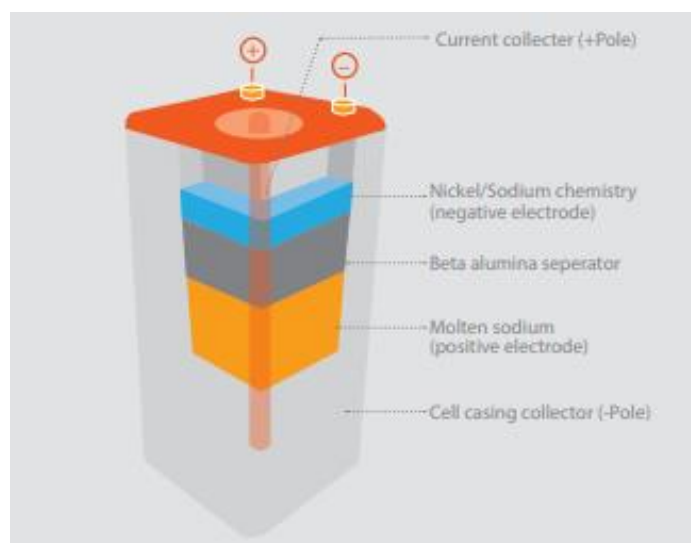


Figure 7: Diagram of sodium nickel chloride battery technology (Arup, 2019)

Renewables integration projects

Uptake of nickel based battery installations has not been popular within Europe – the most recent installation was commissioned in 2015 and supports a 10MW PV plant.

- **Enel Green Power Catania Energy Storage Project** (BloombergNEF, 2023)
This 1MW/2MWh sodium nickle chloride installation was commissioned in 2015 and supports a 10MW PV plant.

Outside of Europe, major examples of the use of nickle based technologies for renewables integration is also limited. Existing commissioned installations of energy storage plants which use solely nickel based technology are of smaller scale, with capacities in the range of 0.1 – 2MW.

Key Findings

Table 7.- Decision-making findings. Nickel Based. (Arup, 2019) (BloombergNEF, 2023)

Nickel based	
Round-trip Efficiency	85%
Total identified capacity and output in Europe in renewable energy integration (includes announced, under development and commissioned projects)	3 MW / 1 MWh (last installation in 2015)
Advantages	<ul style="list-style-type: none"> • High energy density • Fully recyclable • Long life (20 years)
Disadvantages	<ul style="list-style-type: none"> • Heat may be required • Unsuitable for short cycling

2.2.6 FLYWHEELS

Flywheel energy storage makes use of the mechanical inertia contained within a rotating flywheel in order to store energy. Flywheels store electrical energy by using the electrical energy to spin a flywheel (usually by means of a reversible motor/generator). In order to retrieve the stored energy, the process is reversed with the motor that accelerated the flywheel acting as a brake extracting energy from the rotating flywheel. In order to reduce friction losses it is common to place the flywheels inside a vacuum with the actual flywheel magnetically levitated instead of using conventional bearings.

Flywheels as energy storage devices are more suited to improving power quality by smoothing fluctuations in generation, as opposed to having long output durations. This is because of the ability of flywheels to rapidly charge and discharge. Controlling grid frequency is an important feature and the need for this service will increase as the penetration of intermittent generating units increase.

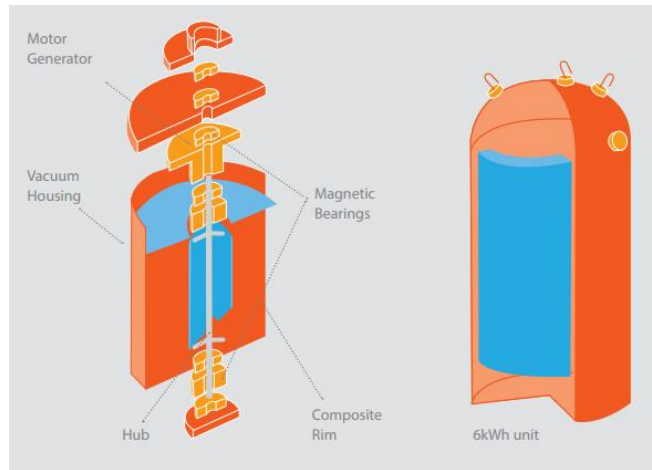


Figure 8: Diagram of flywheel technology (Arup, 2019)

Renewable integration projects

Examples of flywheel installations within Europe for renewables integration is limited. This is partly due to the technology being more suited to improving grid stability and smoothing instead of power storage. An example project includes:

- S4 Energy and ABB Heerhugowaard Wind Energy Storage Project**
 (BloombergNEF, 2023)
 Commissioned in 2022, this project combines lithium ion and flywheel technologies to support a wind farm. The projects features a 10MWh battery systems with a 3MW flywheel.

Key findings

Table 8: Decision-making findings. Flywheels. (Arup, 2019) (BloombergNEF, 2023)

Nickle based	
Round-trip Efficiency	82% - 85%
Total identified capacity and output in Europe in renewable energy integration (includes announced, under development and commissioned projects)	4 MW / 3 MWh
Advantages	<ul style="list-style-type: none"> • Rapid response time • Low maintenance • Effectively maintains power quality
Disadvantages	<ul style="list-style-type: none"> • Requirement for precision engineered components. • Must be housed in robust containers

2.3 BATTERY LIFETIME & DEGRADATION

The reported market benchmarks may be limited depending on the technology and commercial operation date they might not be representative of the current market figures. Moreover, without application, details on capacity and number of cycles for an installation, it is difficult to accurately determine degradation. Various batteries technologies do differ however in their expected lifespan depending on the mentioned factors.

Battery lifetime refers to the length of time a battery can be used before it no longer provides adequate performance. This is often measured in terms of cycles, or the number of times a battery can be charged and discharged before its performance degrades significantly. Battery degradation is the gradual loss of battery capacity and performance over time due to a number of factors, including usage patterns, temperature, and charging and discharging rates.

Between 60% and 80% remaining capacity is often considered end of the useful life as internal resistance and thus losses increase in older cells.

For stationary batteries, such as those used in renewable energy storage systems, the financial considerations of battery lifetime and degradation are important. Without application, details on capacity and number of cycles for an installation, it is difficult to accurately determine degradation. Various batteries technologies do differ however in their expected lifespan, as detailed in Table 9.

Table 9: Expected lifespan of different battery technologies.

Battery Chemistry	Expected lifespan
Lithium Ion	10 – 15 years (Cubes, 2022)
Flow Batteries	30 years (Power, 2020)
Lead Acid	5 – 7 years (Cubes, 2022)
Nickel Based (sodium nickel chloride)	15 years (ScienceDirect, 2021)
Sodium Sulphur	15 years (Insulators, 2023)

3 EUROPEAN MARKET

3.1 MARKET OVERVIEW

Although China is the global leader in the BESS sector, investments in Europe are increasing significantly, with lithium-ion battery production within the continent anticipated to increase rapidly. Utility-scale installations in Europe are expected to scale 11-fold in the coming years, increasing from 3GW/4GWh in 2021 to 33GW/95GWh by 2030 (Nsitem, 2023).

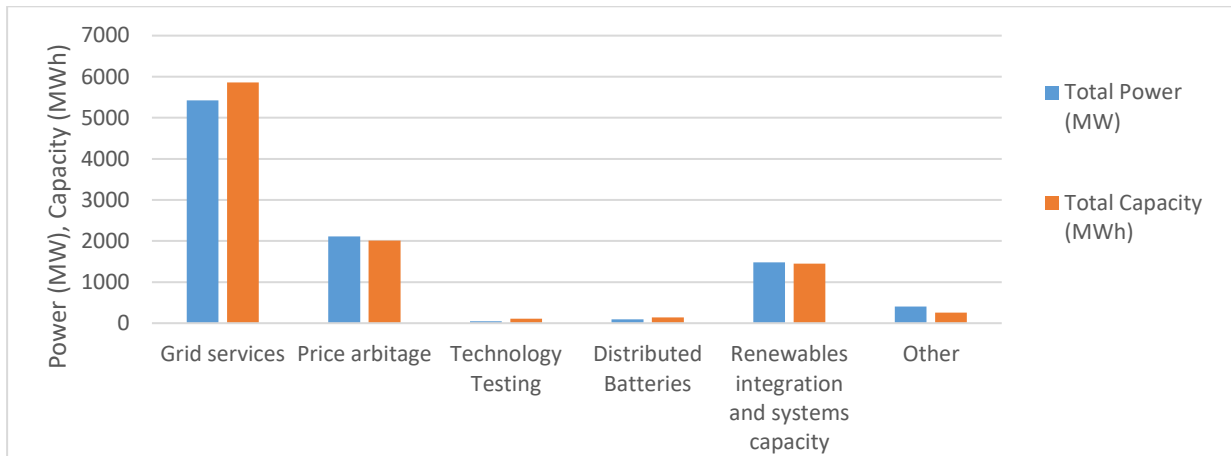


Figure 9: Overview of battery storage capacities for varying applications in Europe (BloombergNEF, 2023)

In terms of existing installed capacity within Europe, the market is still very much focused on grid services and price arbitrage applications more so than renewables integration application, as highlighted by the graph of installed/planned powers and capacities in Europe for varying energy storage applications in Figure 9.

The integration of energy storage technologies for renewable energy applications may be implemented through renewable energy and storage tenders or through storage tenders within the capacity market. Many energy storage projects are being secured via long-term contacts when capacity markets exist such as UK, Italy, Ireland and France. In Portugal and Germany, storage projects are being secured through tender processes.

3.1.1 REGULATIONS AND INCENTIVES

Europe has set out some of the world’s most ambitious decarbonisation targets. The war between Russia and Ukraine has accelerated this decarbonisation, after the European Commission set out a ‘RePowerEU’ plan to cut Europe energy dependency on Russian gas well before 2030. The proposed plan will double the share of variable renewables in power generation, passing 60% by 2030. It is true, however, that whilst having ambitious climate actions plans to combat reductions in emissions, many European countries lack energy storage specific targets in their policies. Italy and Spain are the only European countries which have specific energy storage targets in their NECPs, while the UK, Greece and France have independently set energy storage targets.

Despite lack of energy storage specific targets in many countries across the EU, it will be necessary for energy storage to play a role to enable Europe to achieve its decarbonisation targets and to cut reliance on Russian gas. Grid scale batteries will play a vital role in balancing and integrating renewable energy generation into the European grid. They will also aid in the distribution of electricity during peak times (to prevent network reinforcements). Batteries are also essential to meet the growing EV demand and to reduce transportation related emissions to meet set emission targets.

A number of EU countries including Belgium, Finland, France, Germany, Italy, Poland and Sweden announced funding of up to €3.2 billion for battery projects until 2031. However, this focus is mostly on EV batteries rather than battery cells.

3.1.2 MANUFACTURERS

China is the frontrunner in battery manufacturing with 82% of the world’s cell manufacturing. As of the end of 2022, 84% of the 132GWh battery manufacturing capacity within Europe was owned by companies headquartered in Asia. Batteries produced in Europe are more expensive than those produced in China – the cost of battery production in China in 2022 was \$127/kWh compared to \$169/kWh in Europe. This means that many of the battery technologies installed within Europe are manufactured outside of Europe. Key battery manufacturers globally include CATL (China), LG (South Korea), BYD (China) and Tesla (USA). Many of these companies also have factories situated within Europe, such as the Tesla Gigafactory in Berlin and an LG factory situated within Poland.

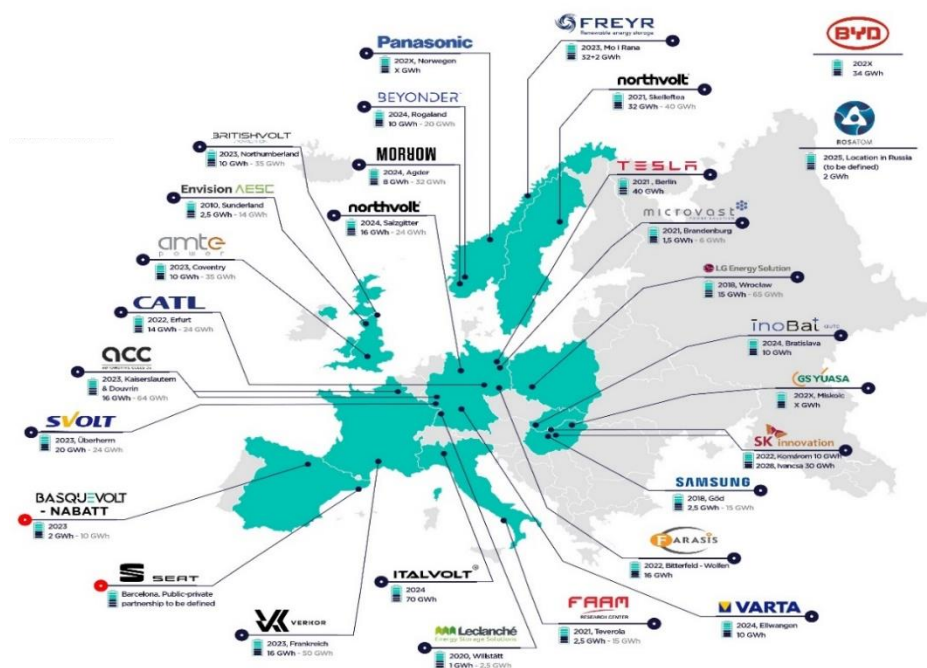


Figure 10: Gigafactories within Europe (EnergiGune, 2021)

In terms of battery production within Europe, the generation capacity is expected to grow in the coming year, thus reducing the cost of production alongside. Key European manufacturers include Northvolt (Sweden), Italtot (Italy), Morrow (Norway), PowerCo (Germany/Spain) and ElevenEs (Serbia) (Leach, 2023).

4 TYPICAL BATTERY COSTS

Arup has conducted this section of the report based on available public data and Arup’s most recent benchmarks. The reported market benchmarks are limited and may not be representative of current market figures. Real installations are dependent on the technology and commercial operation date, among other factors.

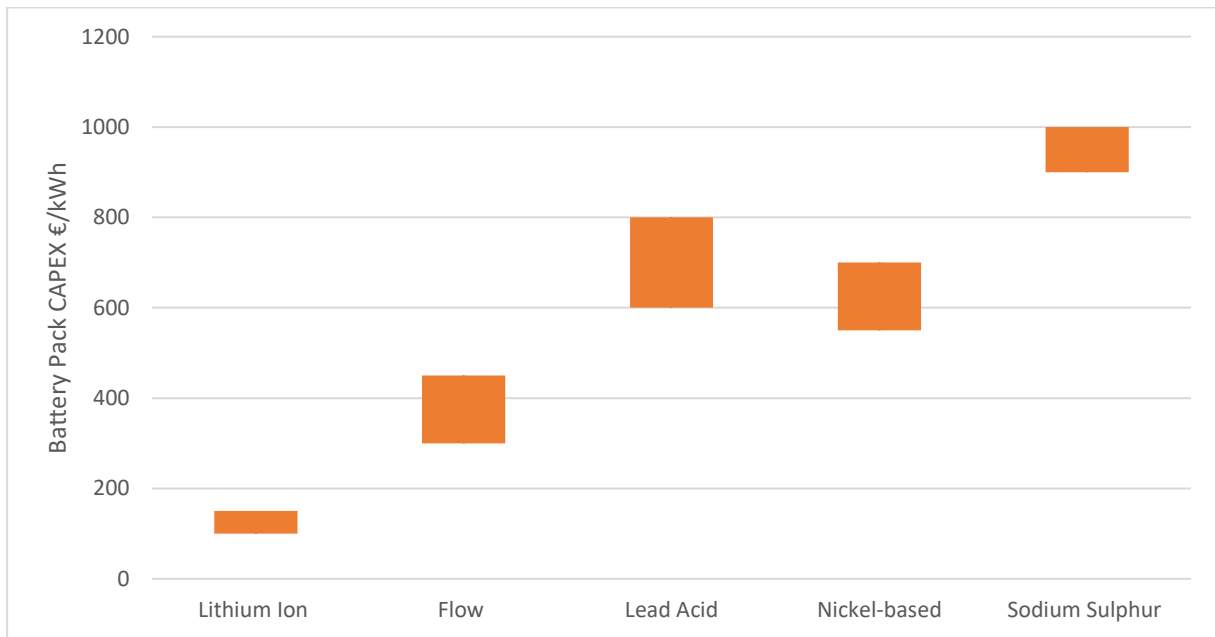


Figure 11: Capital costs for battery packs for different battery technologies (Arup, 2019) (Lazard, 2018).

The graph in Figure 11 shows costs ranges for battery packs for varying battery technologies. Note that costs to create benchmarks for batteries other than lithium ion is limited, mainly due to the lack of installations for comparison. Historical data has been used in these cases. Finance assessors such as Bloomberg focus their costing analysis on lithium ion due to the dominance of this technology within the market. With market maturity the cost of lithium-ion batteries has decreased significantly, particularly in China. The same cannot be said for other battery technologies as their lack of commercialisation means that costs are not expected to decrease to the same levels to that of lithium ion.

Not included is the capital cost of flywheel, as this technology has a relatively high capital cost when considering unit cost per unit of energy stored. This is mainly due to flywheels being relatively unsuitable for large energy storage purposes, and instead uses for smaller, instantaneous power applications in the grid.

The cost of lithium-ion batteries has decreased steadily and significantly since 2010, with a average global cost of €1188/kWh in 2010 to €129/kWh in 2021, as detailed in Figure 12. An increase was seen however in 2022, where the price increased to €137/kWh. This was mainly due to supply chain impacts after the pandemic, as well as the existence of an undersupplied market with high demand.

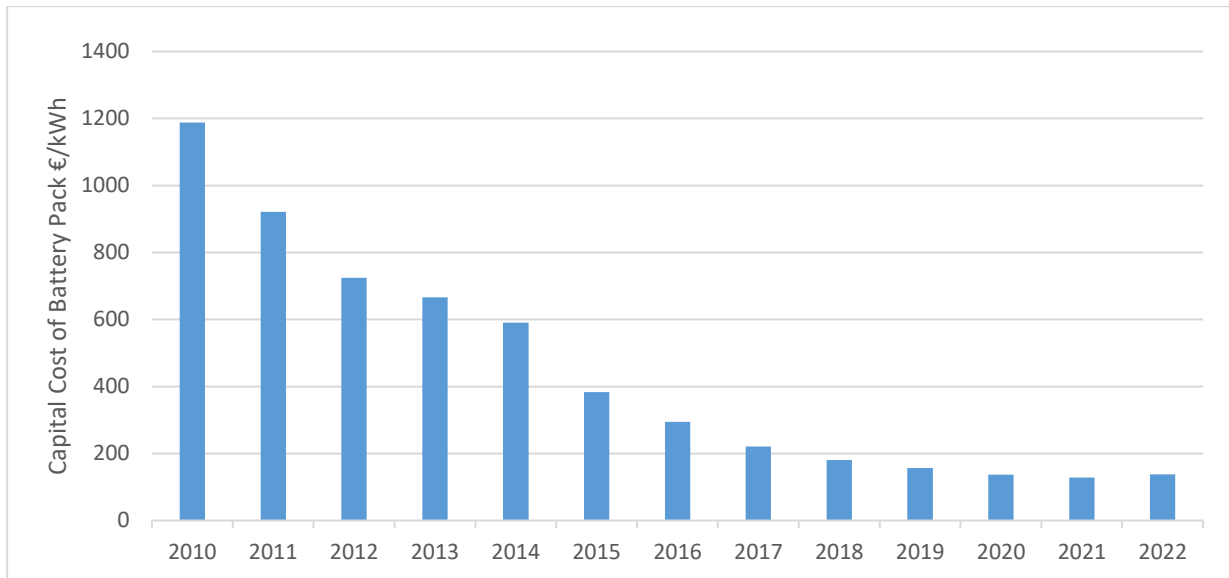


Figure 12: Average global cost of battery pack since 2010

The cost for lithium-ion batteries can be further split into their sub-chemistries, as detailed in Figure 13. As previously mentioned, NMC and LFP are the sub-chemistries most commonly used in stationary energy storage applications. In 2023, capital costs associated with NMC has an approximate cost of €140/kWh, while that for LFP is €100/kWh. It is important to note that the prices of batteries fluctuates and is extremely sensitive to the price of raw materials such as lithium and cobalt.

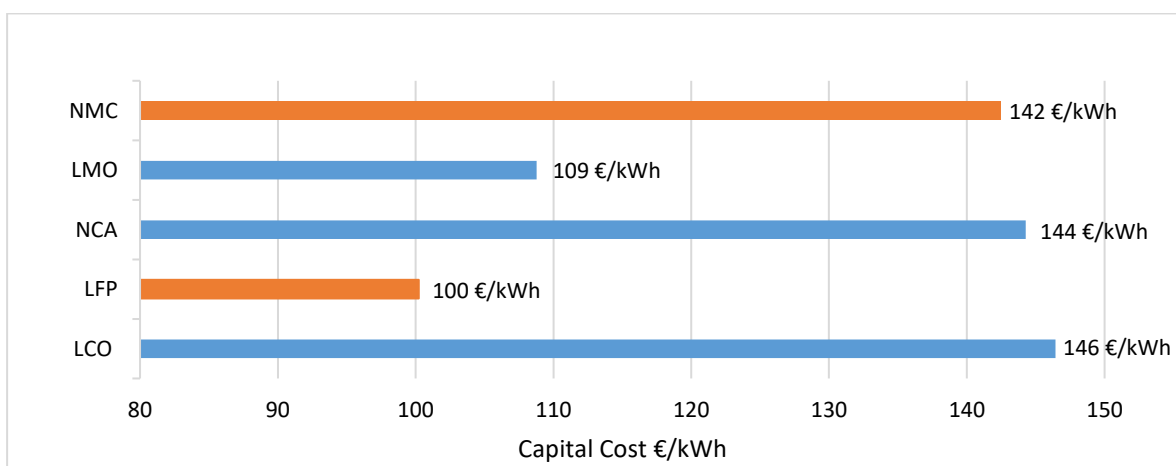


Figure 13.- Global average capital costs for varying lithium-ion chemistries battery packs (BloombergNEF)

It is important to consider other costs than the battery that would account for the total cost of such an installation. The costs of the battery accounts for a significant proportion of the battery installation cost, but other aspects in an energy storage projects such as but not limited to, Balance of Plant costs, construction costs... The overall cost of the installation per unit installed capacity therefore increases. A range of total estimated costs are included in Figure 14, based on data from previous Arup confidential projects.

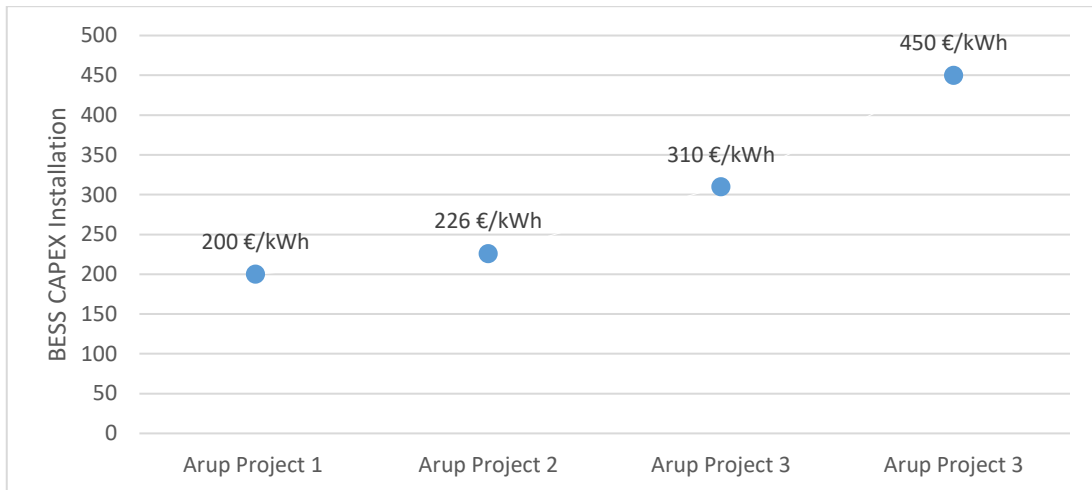


Figure 14.- Total CAPEX for lithium-ion installations for projects within Europe (excludes grid connection and transformer cost)

Operational and maintenance is a key cost which should also be considered. Benchmark data for battery installations other than lithium-ion is limited due to a limited number of commercial projects globally. The operations and maintenance of an energy storage installation includes monitoring and control, maintenance, safety, and environmental considerations.

Using information from a range of previous lithium-ion battery projects in the UK, OPEX costs have been reviewed to allow the calculation of a benchmark. These figures may vary depending on economies of scale. The estimated annual operation and maintenance cost for a battery installation is expected to be within the range 14.5 – 18.5 €/kWh.

LIST OF REFERENCES

- Arup. (2019). *Five Minute Guide Electricity Storage Technologies*. Retrieved from <https://www.arup.com/perspectives/publications/research/section/five-minute-guide-to-electricity-storage>
- BloombergNEF. (2023, 04 23). *BloombergNEF*. Retrieved from <https://www.bnef.com/insights/31023/view>
- BloombergNEF. (2023, 04 23). *Energy Storage Assets*. Retrieved from BloombergNEF: <https://www.bnef.com/storage-assets>
- BloombergNEF. (2023, 04). *GIGA Buffalo Solar Wind Energy Storage Project*. Retrieved from <https://www.bnef.com/storage-assets/15987>
- BloombergNEF. (n.d.). *Battery Price Sensitivity & Builder* . Retrieved from <https://www.bnef.com/interactive-datasets/2d5d59acd900002d?tab=Battery%20price%20sensitivity>
- Cubes, G. (2022). *Why Lithium is Taking Over Stationary Storage*. Retrieved from <https://greencubes.com/in-the-news/why-lithium-is-taking-over-stationary-energy-storage/#:~:text=Figure%20%3A%20The%20main%20two,density%20matters%20nothing%20beats%20NMC>.
- EnergiGune. (2021). *GIGAFACTORÍAS: UNA GRAN APUESTA DE EUROPA PARA SU RECUPERACIÓN A TRAVÉS DEL DESARROLLO DE FÁBRICAS DE BATERÍAS*. Retrieved from <https://cicenergigune.com/es/blog/gigafactorias-apuesta-europa-recuperacion-fabrica-baterias>
- Insulators, N. (2023). *About NAS Batteries*. Retrieved from <https://www.ngk-insulators.com/en/product/nas-about.html#:~:text=NAS%20battery%20has%20a%20calendar,long%20life%20can%20be%20expected>.
- Lazard. (2018). *Levelised Cost of Energy and Levelized Cost of Storage 2018*. Retrieved from <https://www.lazard.com/research-insights/levelized-cost-of-energy-and-levelized-cost-of-storage-2018/>
- Leach, G. (2023, April). *BloombergNEF Company Profiles: European Battery Manufacturers* . Retrieved from <https://www.bnef.com/insights/30981/view>
- Nsitem. (2023, April). *BloombergNEF, 2022 European Energy Storage Market Overview* . Retrieved from <https://www.bnef.com/insights/28999/view>
- Power. (2020). *Flow Batteries: Energy Storage Option for a Variety of Uses*. Retrieved from <https://www.powermag.com/flow-batteries-energy-storage-option-for-a-variety-of-uses/#:~:text=With%20life%20spans%20reaching%20up,storage%20technologies%20on%20the%20market>.
- ScienceDirect. (2021). *Sodium Nickel Chloride*. Retrieved from <https://www.sciencedirect.com/topics/engineering/sodium-nickel-chloride#:~:text=The%20roundtrip%20efficiency%2C%20energy%20density,%2C%20and%2015%20years%2C%20respectively>.